In presenting the dissertation as a partial fulfillment of the requirements for an advanced degree from the Georgia Institute of Technology, I agree that the Library of the Institute shall make it available for inspection and circulation in accordance with its regulations governing materials of this type. I agree that permission to copy from, or to publish from, this dissertation may be granted by the professor under whose direction it was written, or, in his absence, by the Dean of the Graduate Division when such copying or publication is solely for scholarly purposes and does not involve potential financial gain. It is understood that any copying from, or publication of, this dissertation which involves potential financial gain will not be allowed without written permission.

7/25/68

STRESS CORROSION CRACKING
OF AUSTENITIC STAINLESS STEELS

A THESIS

Presented to

The Faculty of the Division of Graduate

Studies and Research

by

Miroslav Marek

In Partial Fulfillment

of the Requirements for the Degree

Doctor of Philosophy

in the School of Chemical Engineering

Georgia Institute of Technology

December, 1970

STRESS CORROSION CRACKING

OF AUSTENITIC STAINLESS STEELS

Approved:

Chairman

Date approved by Chairman: 11/30/70

ACKNOWLEDGMENTS

I wish to express my sincere appreciation to Dr. Robert F. Hochman, my thesis advisor, for his confidence, encouragement, and patience during the course of this work. I owe him also a special debt of gratitude for making my graduate study at Georgia Institute of Technology possible. Appreciation is also extended to Dr. Helen E. Grenga for helpful comments and discussion of the results, and to Dr. Edgar A. Starke, Jr., for reviewing this work and for his help and encouragement during my graduate study.

I also wish to thank Mr. James L. Hubbard of the Engineering Experiment Station, whose excellent work on the scanning electron microscope was vital to this thesis, and Mr. James W. Johnson for his analytical work. To Mr. Charles R. Blackwood of the Chemical Engineering workshop I wish to express my appreciation for willingly and skillfully turning my numerous designs into reality.

To my fellow graduate student and friend, Bob Lukat, I extend my special thanks for answering my countless questions about English usage and for his advice in preparing the manuscript. Mrs. Joyce Williams deserves my sincere thanks for efficient and careful typing.

I gratefully acknowledge the support of the Texaco Corporation Fellowship which has allowed me to pursue this work. I also wish to acknowledge the ARPA Corrosion Coupling Program, ARPA Order 878, and The National Institute of Dental Research Training Grant, DE-00127, whose partial support in areas of related interest assisted greatly in the

work presented here.

My parents have my deep gratitude for making my education possible and for encouraging my efforts for further accomplishment.

Finally, I wish to thank my wife, Anna, for her love, patience and encouragement during the long years of graduate study and during the work on this thesis.

TABLE OF CONTENTS

TABLE OF CONTENTS (Continued)

LIST OF TABLES

LIST OF FIGURES

LIST OF FIGURES (Continued)

LIST OF FIGURES (Continued)

LIST OF FIGURES (Concluded)

CHAPTER I

SUMMARY AND INTRODUCTION

Summary

Crystallography, morphology, and kinetics of stress-corrosion cracking in austenitic stainless steels exposed to boiling, aqueous, 45 per cent magnesium chloride solution were studied on single crystal specimens of a type 316 stainless steel. Notched specimens of selected orientations were stressed in bending, using a self-relieving loading system. The variations of load during crack propagation were recorded and analyzed to obtain a relation between the crack propagation rate and other parameters. A single-surface analysis of crack traces on the specimen sides and a two-surface trace analysis on sections through flat regions of fracture surfaces were used in the determination of the crystallographic orientation of the cracking plane. Fracture surface topography and corrosion attack on slip steps were examined in a scanning electron microscope.

Anodic behavior of the single crystal in the boiling magnesium chloride solution was also investigated. Potentiodynamic polarization curves for several selected crystal faces were recorded and analyzed.

The results of the crystallographic analysis show that the stress-corrosion cracks propagated on {210} oriented crystal planes. After an initial period the cracks in each specimen studied propagated at a constant rate, independent of crack length and nominal stress. The average

crack propagation rate in the constant-rate period was 0.121 mm/hour.

Scanning electron micrographs are presented showing typical fracture surface features and evidence of corrosion attack on slip steps. It is shown that the cracks may be initiated by the surface attack but that they do not follow the slip planes.

The anodic polarization experiments showed crystallographic-dependent behavior of the surfaces, the over-voltages being in the order $\eta_{\{210\}}<\eta_{\{110\}}$, $\eta_{\{211\}}<\eta_{\{100\}}$. The overpotentials on the {111} face were close to those on the {110} and {211} faces. No differences in the open-circuit potentials of various crystal faces were detected. The polarization curves converged to a limiting current density of approximately 0.15 amps/cm^2.

Models of stress-corrosion cracking mechanisms are discussed in view of the results obtained. It is concluded that the evidence introduced does not fit the present dissolution models. The models involving hydrogen as critical species and the stress-sorption model seem to be in best accord with the findings.

Introduction

The phenomena of stress corrosion cracking have been known since the 19th century and intensively studied in the last 30 years. A vast amount of experimental data has been gathered and analyzed. Yet, despite all the research effort and voluminous literature, there is little consensus on the subject of the mechanism by which stress corrosion occurs. The understanding of the mechanism is, however, the prerequisite for an efficient prevention of this dangerous form of

corrosion.

Various definitions of stress corrosion cracking have been proposed. It seems now that the least restrictive, such as "a failure by cracking under combined action of corrosion and stress" (1) fit best the variety of observed phenomena.

There are several characteristics that seem to be common to the entire field of stress corrosion of metals:

1. Only specific environments cause cracking in a given material, in other words, stress corrosion cracking occurs only in specific material-environment systems.
2. Pure metals are rarely susceptible to stress corrosion cracking, if at all.
3. An effective tensile component of the stress must be present for cracking to occur.
4. Cracking in a given system may be either exclusively transgranular, or intergranular, or both.

Some of the best known stress corrosion systems are brasses in ammoniacal media, aluminum alloys in sea water, stainless steels in chloride environments, mild steels in caustic solutions, and titanium alloys in a variety of media. However, the total number of systems in which stress corrosion has been observed is considerably larger. Most of them have been listed by Logan (2).

The transgranular stress corrosion cracking of austenitic stainless steels in chloride environments in probably the most widely studied area in the field of stress corrosion. It is also the one in which the

greatest diversity of opinions exists. This work was undertaken as an effort to examine some of the least understood, and at the same time very important parameters of cracking in this system. The main effort was directed to the investigation of the crystallography of cracking, which is intimately related to the mechanism. The recent availability of single crystals of stainless steel and the development of modern research techniques such as the scanning electron microscope made a fresh approach to this controversial subject possible. The design of the experiments allowed a limited study of kinetics of crack propagation, which is also one of the parameters suffering from lack of reliable data.

Finally, in view of the strong possibility that dissolution plays an important role in the cracking, it was considered pertinent to make a short study of anodic polarization on various crystal faces of the material studied, since no such data have been reported. The objective was to find if differences in anodic behavior exist between various faces in this system and, if so, to correlate these differences with the stress corrosion behavior.

In the following chapter the models of stress corrosion in general and of stress corrosion in this system in particular are briefly discussed. Because of the large amount of literature on this subject only the principal works have been referenced. The literature on crystallography of cracking and on the kinetics of crack propagation is reviewed in detail. The review of published anodic polarization data is limited to reports on this system and to some pertinent data on the crystallographic dependent anodic behavior in some other systems.

In the discussion of the experimental results of this work both the specific significance and the general implications of the data will be considered. It is hoped that this contribution may stimulate some critical experiments which are acutely needed if the long-standing controversy is to be resolved.

CHAPTER II

REVIEW OF THE LITERATURE

Models of the Mechanisms of Stress Corrosion Cracking

Many models have been introduced in the last 30 years in attempts to explain and describe the mechanism of stress corrosion cracking (SCC). Recently many scientists have reached the conclusion that no single model can explain all observed phenomena in all known systems (3). According to this view several models may be correct if applied to different systems. It is also apparent that several mechanisms may contribute to cracking in any given case. In systems exhibiting an induction period before the onset of cracking different mechanisms may operate in the induction and propagation periods.

The majority of the models proposed thus far may be classified broadly into two groups, depending on whether the advancement of the crack is described as a process of dissolution or as mechanical separation. In the former case the main role of the stress or strain is the one of localizing the dissolution process to the crack tip and eventually enhancing the dissolution process itself. In the group of mechanical models the stress has the principal role of advancing the crack. The environment may play a variety of roles, such as providing the embrittling species, lowering the surface energy, forming a brittle phase by a reaction with the material, etc. Dissolution itself may have an important supporting part in the mechanical models, such as to affect the solution

chemistry or to remove the obstacles to fracture.

The following is a short review of the best known models with the emphasis on cracking in metallic materials.

Dissolution Models

a. Dissolution along a Predetermined Path. Dix (4) presented this idea in 1940, describing stress corrosion as an accelerated selective corrosion along a path determined by microscopic structural heterogeneities. The model, at first limited to intergranular cracking, was later generalized (5) to include transgranular cracking and the predetermined path was generalized to any path of lower resistance to corrosion.

b. Dissolution Due to Film Rupture. The idea that the exposure of a bare metal surface when a protective surface film is ruptured would lead to rapid localized attack was mentioned by Dix (4) and the model was developed by Logan (6). The surface film involved may be a passive film, an oxide film, a layer enriched by selective dissolution or redeposition, etc.

c. Mechanochemical Anodic Dissolution. Hoar and Hines (7) suggested that dissolution was enhanced by the disarray of the metal at the yielding tip of the crack. Hoar and West (8) presented experimental evidence and theoretical analysis of the mechanism.

d. Dissolution at Dislocations. Tromans and Nutting (9), noting a frequent correlation between the occurrence of planar arrays of dislocations and the susceptibility to stress corrosion cracking, suggested that both the initiation and the propagation of cracks was due to accelerated dissolution at dislocations which produced a series of microcracks

that were then linked by plastic tearing.

e. Dissolution of Phases Forming at the Crack Tip. The model explains cracking by dissolution of highly anodic phases forming at the crack tip, the transformation being induced by the specific conditions at the tip. Edeleanu (10) and Vaughan et al (11) advocated this model for stainless steels.

Mechanical Models

a. Brittle Fracture Assisted by Electrochemical Action. Keating (12) proposed a model of discontinuous crack propagation in which brittle facture is triggered by electrochemical dissolution of obstacles. In order to explain cracking in normally ductile materials Forty (13) suggested that an embrittled zone, produced in a reaction with the environment, makes possible the initiation of the cracks, which then extend into the substrate. The rate of yielding in the susceptible materials must be slow enough to prevent relief of stresses at the tip of the crack. When the crack is halted, usually at slip bands, it must be reinitiated by further chemical action. Edeleanu (14) reported experimental evidence for this mode of propagation.

Nielsen (15) examined corrosion products forming in stress corrosion cracks and suggested that the wedging action of these products, combined with other stresses, triggers spontaneous crack extension. Pickering, Beck and Fontana (16) presented experimental evidence for the wedging action of corrosion products. In their model cracking is discontinuous on the atomic scale, being interrupted by periods of a build-up of elastic strain energy as the corrosion products grow.

b. Brittle Film Fracture. In this model the crack propagates by

fracture of a brittle surface layer or phase and is arrested when it enters the metal. A new film forms on the exposed surface until it attains a critical thickness and fractures again. The model is derived from the Forty's formulation (13), leaving out the extension of the crack in the substrate. It was developed by Forty and Humble (17) and by McEvily and Bond (18). The model is well supported by evidence for the system of brass in tarnishing solutions and indications are that it may be applicable to systems with similar characteristics.

c. Stress-sorption Cracking. Adsorption of specific species under specific conditions of potential and chemistry at the crack tip is supposed to weaken the bonds at the crack tip and thus reduce the stress required for breaking the bonds and thus advancing the crack. This is equivalent to lowering the surface energy of the newly forming crack surfaces. The idea was applied to stress corrosion of metals by Uhlig (19, 20) and Coleman et al (21).

d. The Tunnel Model. A mechanism consisting of corrosion tunneling followed and accompanied by mechanical tearing of the walls between the tunnels was proposed by Swann and Pickering (22). The propagation of the cracks is thus a combination of separate chemical and mechanical actions.

e. Hydrogen Embrittlement. Similarly to hydrogen embrittlement of high strength steels, stress corrosion cracking is supposed to result from embrittlement of a zone in front of the crack tip due to absorption of hydrogen into the lattice, or by the formation of brittle phases at the crack tip. The model was applied to SCC by Evans (23) and Edeleanu (24). Powell and Scully (25) advocated this model for the system of

alpha-titanium in aqueous sodium chloride.

Stress Corrosion Cracking of Austenitic Stainless Steels in Hot Aqueous Chloride Solutions

Boiling, concentrated, aqueous magnesium chloride solution has been widely used in testing the susceptibility of austenitic stainless steels and other iron-chromium-nickel alloys to SCC. At a sufficient stress level all standard austenitic stainless steels crack, relatively quickly, with little or no general corrosion (26). It is generally assumed that cracking in this solution is basically similar to cracking in other, more practical chloride environments, such as hot water containing small amounts of inorganic chlorides, although little has been done to prove this. The majority of data on SCC of austenitic stainless steels has been gathered in tests with this solution boiling at 154°C.

General Features

The following general features of SCC in this system have been observed:

a. Cracking is primarily transgranular (2). Evidence of partly intergranular failures in type 304 steel has been reported (27), but transgranular crack propagation is obviously predominant.

b. An induction period is often observed before the onset of cracking (7, 28, 29). This period is probably stress-dependent (30, 29), although some reports were made to the contrary (7, 31).

c. Cracking can be stopped by cathodic polarization (32). A critical potential can be found, cracking occuring only at potentials more noble than the critical value (33, 34).

d. Cracking is temperature-dependent, the rate increasing with increasing temperature (35).

e. Susceptibility to SCC decreases with increasing nickel content, as shown by Copson (36). Numerous studies have been made on the effects of various other compositional changes, as reviewed recently by Latanision and Staehle (37). The complexity of the system and lack of standard criteria makes it difficult to draw reliable conclusions.

Almost all models of SCC suggested for any system have been advocated in attempts to explain SCC in austenitic stainless steels. Many models have been originally proposed for this system. At present there is still no general agreement on the mechanism.

Dissolution Models

The basis of any dissolution model is that an electrochemical cell is set up between the crack tip and other surfaces, the material at the tip being anodically dissolved. To account for the observed crack propagation rates in stainless steels it was estimated that current densities of up to two amperes per square centimeter must be possible at the tip of the crack (38). Hoar and Hines (7, 39) concluded from potential measurements that the advancing edge of the crack is polarized by only a few milivolts. The anodic polarization data for unstrained electrodes (8, 40), on the other hand, show that such high current densities are possible only at overpotentials of several hundred millivolts.

To overcome the discrepancy Hoar and West (8) suggested that the activation overpotential at the crack tip is reduced by yielding and that the concentration overpotential is eliminated by the flow of the electrolyte to the tip of the crack. Hoar and West (8) and Hoar and

Scully (41) presented results of polarization measurements on strained wires that showed the "mechanochemical effect" of reduced activation overpotential and the effect of solution flow. The materials not susceptible to SCC did not exhibit similar large reductions of the activation overpotential. West (42) made experiments on the flow of electrolyte in propagating crevices and concluded that the flow to the edge of the crack was sufficient to reduce the concentration overpotential.

Hoar and West (8) and Hoar (43) attempted to explain the mechanochemical effect by an analysis of the kinetics of anodic dissolution on a disarrayed surface. Hoar (43) concluded that the major effect is the increase in the number of active sites. The absence of a significant effect on non-susceptible materials was attributed to differences in the number, distribution, and mobility of defects (44). Recently Despic, Raicheff, and Bockris (45) confirmed the existence of a slight mechanochemical effect on pure FCC metals and a much larger effect on BCC metals, and analyzed it in terms of increased activity at the edges of slip steps and high index planes, double layer charging of the newly exposed material, and increased surface roughness. Materials susceptible to SCC were not examined.

Since the presence or absence of a protective film or noble surface layer on stainless steels in magnesium chloride is still a matter of dispute, the possibility that the large mechano-chemical effect in this system is related to the rupture and repair of such a film cannot be excluded (46).

The applicability of models based on the dissolution of unprotected metal after the rupture of a surface film depends also on whether

any such film exists in this system. The existence of a passive film was denied by Hoar and Hines (7) and Barnartt and Van Rooyen (40). The formation of a nickel enriched film, suggested by Latanision and Staehle (37), has not been experimentally proven.

A different approach to the question of increased activity at the crack tip was taken by Tromans and Nutting (9) in their model of cracking due to dissolution at dislocations. Since the calculated energy difference between a dislocation and the defect-free matrix results in negligible difference in the electrochemical potential (19), segregation of solute atoms to dislocations was thought to be responsible for the high activity. However, the correlation between the susceptibility to SCC and the coplanarity of dislocations, which is an inherent feature of this model, has been recently disputed (47). No new data or quantitative analysis supporting the model have been reported.

Several variations have been proposed of models involving dissolution of phases forming at the tip of the crack. Since the phase is supposed to form under the specific conditions of strain and chemistry at the crack tip, and to be completely dissolved during cracking, the difficulty of providing direct experimental evidence is obvious. The theory that strain-induced martensite is responsible (10) has been strongly criticized (48, 49). Vaughan et al (11) reported that they found a preferentially dissolving phase, which they identified as a hydride, in cathodically hydrogenated austenitic steel. More recently Holzworth and Louthan (50) reported hydrogen-induced austenite-martensite transformation in normally stable austenitic steel. Apart from preferential dissolution, hydrogen-induced phases may cause cracking by

mechanisms falling in the category of hydrogen embrittlement. Other aspects of the question of hydrogen as a critical species will be reviewed in the discussion of that model.

Mechanical Models

The mechanical models face the basic difficulty of explaining how cracks can propagate in a seemingly brittle manner in a very ductile material, in which yielding is likely to relieve stresses at the crack tip and blunt the crack.

The only mechanical model that does not have to deal with this problem is the tunnel model in which plastic tearing of the ductile walls between the corrosion tunnels is part of the mechanism (22). Tunneling in stainless steels has been observed by several workers (51, 52, 53, 54). Dean et al (55) found correlation between the susceptibility of alloys to cracking and the incidence of tunneling. On the other hand, McCollough and Scully (55) and Armijo and Wilde (53) found tunneling even in the environments that do not cause SCC. No experimental evidence has been found that fracture surfaces in stainless steels, stress corroded in magnesium chloride solutions, were formed by tunneling and tearing of walls. The only clear evidence of this mode of crack propagation was presented by Harston and Scully (56) who studied the system of stainless steel in 5N H_2SO_4 + 0.5N NaCl. In magnesium chloride solutions the cracks appear to advance on a linear front (37, 57).

The model of brittle film fracture has not been advocated for this system because of the lack of positive evidence that any pertinent film forms and because fractography has not revealed features consistent with this model.

The "classical" mechanical model, as proposed by Keating (12) and developed by Forty (13) has not, in this system, been supported by reliable experimental evidence. Various general suggestions for the possible reasons for a restricted dislocation movement that have been made by Forty (58) may be applicable to these materials, but evidence that a sufficient hardening effect exists in austenitic Fe-Cr-Ni alloys is lacking. There is an equal lack of evidence of embrittlement necessary for the initiation of the cracks. The model predicts a discontinuous mode of crack propagation. Neither an unambiguous direct evidence nor a systematic fractographic evidence of this mode of propagation has been found.

A specific form of embrittlement, usually treated as a special model, is hydrogen embrittlement. The loss of ductility may be due to absorption of hydrogen in the lattice, hydrogen-induced formation of brittle phases, embrittlement of strain-induced phases, etc. In SCC hydrogen is presumably evolving in a cathodic reaction inside the crack. Bubbles of gas have been observed emerging from cracking stainless steel specimens in boiling magnesium chloride (40). Whiteman and Troiano (59) and Shively et al (60) showed that thin sections of austenitic steels can be embrittled by severe cathodic charging.

The usual argument against any model involving hydrogen as critical species in this system is that cathodic polarization, which favors the hydrogen reaction, impedes cracking. Hoar (38) also argued that hydrogen-ion reduction is thermodynamically impossible unless acidity is very high, a condition he considered unlikely in this system. Rhodes (61) argued that hydrogen reaction inside the crack is made possible by the very high acidity near the crack tip resulting from anodic

oxidation. Cathodic polarization, by slowing the anodic reaction, reduces the acidity and thus impedes cracking. An evidence that the solution near the crack tip in stress-corroding stainless steel is highly acidic has been reported (27).

Stress-sorption cracking in this system has been advocated mainly by Uhlig and his co-workers (33, 34). Evidence in favor of the mechanism was also presented by Coleman et al (21), who studied the grain-size dependence of stress-corrosion cracking stress in a type 304 stainless steel and in a Mg-Al alloy. Using the Petch-Stroh relationship, which contains a surface-energy term, they calculated the effective surface energies associated with fracture in the presence of the stress-corroding environment. The calculated value for stainless steel was an order of magnitude lower than the estimated surface energy of this material with respect to its vapors. This interpretation of the data was questioned by Pugh et al (46).

There is evidence that adsorption of Cl^- ions is potential dependent (62, 63), which could explain the potential dependence of stress corrosion. The ability of some anions to displace the adsorbed Cl^- ions (62) has been interpreted as the reason for the effect of some stress-corrosion inhibitors (33). The specificity of chemisorption is thought to explain the specificity of environments causing cracking (20). The reason for the difference between damaging and non-damaging species has not been explained. The model suffers from lack of evidence linking more directly adsorption with stress-corrosion.

Crystallography of Trangranular Stress Corrosion Cracking in Alloys with Cubic Lattices

Orientation of transgranular cracks has been one of the most puzzling aspects of stress corrosion cracking. Whether cracks follow a definitive crystallographic path and, if they do, which family of planes is preferred has been subject to speculations and investigations. To date positive conclusions have not been reached. The following review of published reports is limited to cracking in body and face centered cubic alloys.

Studies on Polycrystalline Samples

In 1956 Logan and Sherman (64) reported using two-surface trace analysis to determine orientation of cracks in large-grained type 304 and 304L stainless steel specimens cracked in boiling NaCl-NH_4NO_2 solution. The reported results from preliminary studies of four grains did not show any preferred crystallographic orientation of cracking. The same method was used by Logan on beta brass cracked in ammonia (65). The results from 18 grains containing 47 transgranular cracks show random orientation of cracks. No cracks observed were oriented close to lowest index planes ({111}, {100}, {110}).

Leu and Helle (66) investigated cracking of 18 Cr - 8 Ni and 25 Cr - 20 Ni steels in hot, aqueous chloride solutions. Surfaces of specimens were examined by optical microscopy. The authors found that slip lines were attacked and that cracks originated in areas of heavy attack. They concluded that "the cracks lie in a plane perpendicular to the highest tensile stress and do not proceed along crystallographic planes".

Nielsen (15) presented electron micrographs of oxide replicas from fracture surfaces of a type 316 stainless steel cracked in boiling $MgCl_2$ solution. The micrographs showed a faceted surface indicating a crystallographic nature of fracture. Nielsen expressed the belief, based on examination of many similar micrographs, that "fracture or cleavage occurs preferentially on the {111} planes during stress corrosion cracking".

Hines and Hugill (67) presented the results of an extensive study of the morphology of stress corrosion cracks in austenitic Cr-Ni stainless steel wires exposed to boiling 42 per cent $MgCl_2$. They reported that cracks inside the grains were roughly straight and usually showed some deviation from the general direction and occasionally exhibited marked change in direction of crack propagation when crossing a grain boundary. In a number of cases cracks changed direction when crossing a twin band in such a way that the final direction was parallel to the original one. This evidence indicated a crystallographic nature of cracking. In an attempt to find the orientation the authors compared the distribution of the angles between the traces of cracks with the theoretical distribution which would be obtained if the cracks followed either {100}, {110} or {111} planes. They found that the observations did not fit the distributions of either of the lowest index planes and concluded that "stress corrosion cracks in austenite do not, in general, follow a single crystallographic plane over long distances". They mentioned that the observed numerous small changes of direction would be possible if the cracks followed planes of higher order, but considered it improbable "in the absence of a reasonable physical explanation".

Nielsen's work on corrosion tunneling (51) in type 304 stainless steel stressed in boiling $MgCl_2$ solution showed the crystallographic nature of the tunnels which form in rows along surface traces of the {111} slip planes and branch in the same planes at angles which were believed to correspond to <110> directions. Oreintation of the tunnels with respect to the ultimate fracture surface was not definitely established but the angles observed seemed to indicate a {110} fracture plane rather than {111}.

Scully and Hoar (68) studied morphology of stress corrosion cracks in an 18 Cr - 8 Ni steel stressed in boiling $MgCl_2$ solution. Visual observations and sectioning of cracked specimens did not reveal any macroscopical crystallographic orientation. Cracks were initiated along the directions of maximum shear strain.

Louthan (69) used both optical and electron microscopy to study the effect of exposure of types 304 and 304L stainless steels to chloride solutions. Both bulk stressed samples and thin foils were exposed to the corrosive media. He found preferential attack along the traces of {111} planes and reported that cracks often changed direction at grain boundaries. Incipient cracks were aligned within $\pm$ 2 degrees of the {111} traces.

Tromans and Nutting (9) used electron microscopy in an extensive study of crack initiation in single phase copper alloys and 18 Cr - 10 Ni austenitic stainless steel. Cu - Zn, Cu - Al, Cu - P and Cu - Zn - Al alloys were stress corroded in ammoniacal and sulfur dioxide environments, and the stainless steel in boiling magnesium chloride solution. The experimental methods consisted of stress corrosion of thin metal foils,

controlled thinning of bulk stress-corroded specimens and carbon replication of stress corroded surfaces. Orientations of the grains were determined by selected area diffraction technique, and the single-surface trace analysis of crack orientations was conducted. In all cases the plane of initiated cracks was within five degrees of the (111) pole. A few experiments were made on Cu - 30 Zn specimens in which cracks propagated through depths of at least one grain diameter. The traces of cracks "ran more or less parallel to {111} traces," but an insufficient number of different zones and foils prevented positive identification.

Logan (70) presented a picture of a stress corrosion crack in a type 304 stainless steel cracked in a chloride solution. The geometric pattern formed by the crack suggested propagation on low index crystallographic planes. In his book Stress Corrosion Cracking of Metals (2) Logan concluded for austenitic stainless steels exposed to chloride solutions, that "present information and ideas would indicate that cracking occurs predominantly upon {111} slip planes with a crack shifting from one plane to a parallel plane when its path is blocked by an inclusion, grain boundary or other obstruction". He also presented a picture from unpublished work by Logan and McBee at the National Bureau of Standards showing a section through a crack and noted that "cracking was not associated with evidence of slip but rather crossed these deformation lines at a large angle".

Ronquist (52) made a study of the initial stages of stress corrosion cracking of two 18 Cr - 11 Ni stainless steels in chlorine gas. Corrosion products from tunnels were extracted on plastic replicas. He found sites of preferential attack along traces of slip planes.

Lehtinen (71) made foils for transmission electron microscopy from bulk specimens of a stress-corroded 18 Cr - 11 Ni stainless steel and observed dislocation structure around the crack. He presented a picture showing a crack running at an angle of 30 degrees from <111>.

Smith and Staehle (72) presented further evidence of the crystallographic nature of crack propagation by showing a picture of mirror-image changes of direction of a crack through twin bands in a 20 Cr - 15 Ni steel stress-corroded in 1 weight per cent NaCl, and a criss-cross pattern of cracking in a type 310 stainless steel exposed to a boiling $MgCl_2$ solution.

Recently Harston and Scully (56) studied stress corrosion cracking of type 304 stainless steel in 5N H_2SO_4 + 0.5N NaCl at room temperature using scanning electron microscopy. They found that fracture resulted partly from tunneling across grains. On a free surface, rows of pits producing parallel tunnels into the metal formed along the slip lines. Some extremely flat fracture planes observed in large grain size material were thought to be formed either from extremely fine tunnels or by even front dissolution. In some specimens the angular relationship of slip markings indicated a {111} fracture plane, and in one specimen the angle between mutually inclined flat fracture planes was close to the angle between two intersecting {111} planes. In many fractographs, however, tunnel formation appeared to be noncrystallographic.

Studies on Single Crystals

As early as in 1942 Wassermann (73) reported a stress corrosion cracking test on a Cu - 36 Zn cylindrical single crystal stressed in moist ammonia atmosphere. Orientation relationships were not specified.

Cracks were generally normal to the tensile axis and no identifiable crystallographic fracture plane was found. Cracks were initiated on surface traces of slip planes.

Skorchelletti and Titova (74) reported stress corrosion tests on six single crystal specimens of Cu - 28 to 31 Zn, partially immersed in ammonia solution and stressed in tension. In all cases rupture occurred at the solution - air boundary. The time to failure varied widely from sample to sample. This was attributed to differences in orientation, which was not specified.

Bakish and Robertson (75) studied initial stages of stress corrosion cracking of Cu_3Au single crystals loaded in tension and exposed to ferric chloride. The 11 samples were randomly oriented. The cracks were initiated mostly on slip clusters and the traces of incipient cracks on the free surfaces were normal to the axis of tension. The authors concluded that the initial crack growth is independent of crystallography.

Later Bakish (76) prepared several thin single crystal slices of Cu_3Au of various orientations, immersed them for one month in a 2 per cent aqueous solution of $FeCl_3$ and then, subsequent to the immersion, stressed them in bending. The specimens bent normal to the {110} plane cracked in a brittle manner. The fracture surfaces indicated that cleavage took place and Laue back reflection photographs showed very little deformation of the surfaces.

In 1959 Edeleanu (14) reported results of visual observations at high magnifications, including still and motion photography, of the propagation of cracks in single crystals of a 70 - 30 alpha brass in ammonia. The cracks, as observed on the free surfaces, propagated in a

direction "more or less at right angles to the applied stress". They also tended to follow roughly a trace of a possible, but inactive, slip plane. The picture show cracks propagating at high angles to the traces of active slip planes.

In a discussion to the Hines and Hugill's paper (67) in the 1959 Symposium on Physical Metallurgy of Stress Corrosion Fracture, Denhard reported results of an investigation of orientation of cracks in large-grain 18 Cr - 11 Ni alloys and single and bicrystals of alpha brass. No crystallographic correlation was found by measurements of crack directions in two planes, but examination of fine leading edges led to a conclusion that "cracks tend to proceed on the {111} planes in those crystals oriented to give lowest stress for plastic deformation". Denhard suggested that "cracks are composed of steplike segments which tend to follow the major slip planes but which compositely appear normal to applied stress".

In 1961 Reed and Paxton (77) reported results of an extensive study of stress corrosion cracking of 20Cr - 20Ni, 20 Cr - 12 Ni and type 304 stainless steel single crystals. Crystals were machined into flat tensile specimens of various, arbitrary orientations, and loaded in tension in boiling aqueous 42 per cent $MgCl_2$. The orientation of crack surfaces was determined by the two-surface trace analysis. The plane of cracking in the 20 Cr - 20 Ni steel was positively identified as the {100} plane. The cracks in 20 Cr - 12 Ni and type 304 steels were "roughly normal to tensile axis and unrelated to any crystallographic plane over long distances". Poles of four planes were shown, neither of them being close to either (111) or (001) orientation. The microscopic examination

showed that fracture surfaces of the 20 Cr - 20 Ni specimens were predominantly crystallographic ({100} orientation) over the entire area. Fracture surfaces of the 304 type crystals appeared to be made of small faces less than one micron in size. A picture of a crack in a 20 Cr - 20 Ni crystal changing direction when crossing a twin boundary in a recrystallized region was also presented.

Kinetics of Propagation of Stress Corrosion Cracks in Austenitic Stainless Steels

There is a lack of reliable data on the kinetics of propagation of stress corrosion cracks and on the relation between stress and the propagation rate. In a vast majority of stress corrosion studies the criterion of time to failure was used which obliterates the distinction between incubation and propagation periods. The variety in specimen sizes, geometries and ways of loading has contributed to the difficulty of comparing and analyzing data from different laboratories.

There are several reasons why the true speed of crack advancement was seldom investigated and never accurately measured. Tests aimed at the time to failure may be simple, inexpensive, and require little attention. Extensive metallographic examination or sophisticated instrumentation are required to detect the onset of cracking. Accurate monitoring of crack penetration is difficult, especially when more than one crack propagates.

Most methods used for determination of the crack length, such as metallography, deformation analysis, or resistance measurement, suffer from the inherent defficiency that the depth of penetration (or reduction

of specimen cross-section) is determined, which may be significantly different from the actual length of the path of the crack because of the many deviations from the average direction of propagation. If cracking proceeds discontinuously, as predicted by some models, then methods such as metallography yield only average values which may have little meaning.

Investigation of the effect of stress on the rate of crack propagation is further complicated by the usual branching and multiplicity of cracks and by changes in the magnitude of applied stress during penetration. In constant load tests the nominal stress increases with increasing crack depth. The stress concentration due to the notch effect of the crack is superimposed on the nominal stress and yielding almost certainly occurs. In constant deformation tests the nominal stress changes in an uncontrolled manner and these tests are generally least amenable to crack length monitoring. Moreover, the magnitude of the initial nominal stress is usually uncertain. No tests at constant stress have been reported.

The propagation rates of stress corrosion cracks in austenitic stainless steels have been mostly estimated. Edeleanu (10) reported that some of the cracks in 18 Cr - 10 Ni steels penetrated at rates greater than 10 mm per hour. Hoar and Hines (7), working on small diameter wires of various 18 Cr - 8 Ni steels, followed both changes in potential and extension of samples in order to distinguish between the propagation and incubation periods. They estimated that cracks propagated at 0.5 to 3.0 mm per hour and they found little variation of the rate with applied stress. Hines (29) using similar techniques on thicker wires reported that the average rate of propagation was in the range of 1.0

to 4 mm per hour.

Staehle et al (78) estimated that cracks propagated at rates between 0.067 and 0.2 mm per hour in type 347 steel cracked in chlorides containing water at 400°F. They used self-relieving specimens stressed in bending.

Eckel (28) studied the depth of the deepest crack in six commercial grade austentic steels as a function of exposure time. Self-relieving U-bend specimens were used, stresses were not determined, and crack depths were examined metallographically. A straight line relationship was obtained by plotting maximum crack depth as a function of the logarithm of exposure time. By extrapolation to zero crack length the propagation period was distinguished from incubation. The data presented show that the average rate of crack propagation was between 0.015 and 0.8 mm per hour. Propagation rates as calculated from the relationship decreased sharply with penetration depth. This was attributed to the self-relieving effect.

Hawkes et al (79) studied the effect of applied stress on cracking of types 304, 309 and 316 wires, both annealed and cold-worked, stressed in tension by constant load. Cracks occurred in the material exposed above the liquid-vapor interface of the magnesium chloride solution. The depth of crack penetration, determined metallographically, decreased with increasing stress, while crack density increased. The average speed of crack propagation was between 0.05 and 0.125 mm per hour.

Kraft et al (80) used similar techniques in an investigation of SCC of type 302 and 316 annealed steel wires. They found average propagation rates of 0.179 and 0.649 mm per hour in wires stressed to 10,000

psi and 20,000 psi, respectively. In a follow-up investigation on cold-worked type 302 wires Greeley et al (81) found the rates to be nearly independent of the applied stress. The average rate varied from 0.061 to 0.20 mm per hour. Specimens cold-worked 10 per cent exhibited highest propagation rates. In both investigations the cracking occurred above the liquid-vapor interface.

Many attempts have been made to find the threshold stress - the stress below which SCC will not occur (7, 78, 80, 82). A wide range of stresses was found and even data indicating that no threshold exists were reported (83). It is likely that instances of a low threshold stress can be attributed to the presence of residual stresses (80).

Pertinent Anodic Polarization Studies

Anodic polarization data for polycrystalline austenitic stainless steels in boiling magnesium chloride solutions have been reported by Barnartt and Van Rooyen (40), Hoar and West (8), Smialowski and Rychcik (84) and Uhlig and Cook (33). These published results are summarized in Figure 1. The positions of the curves on the potential scale must be considered only approximate because of the uncertain junction potentials, and temperature and concentration effects (8). Only Barnartt and Van Rooyen (40) reported making corrections for IR drops in the specimens and solutions.

The two curves reported by Hoar and West (8) show the effect of the solution flow. In the "stationary" solution the only stirring was that due to boiling. The other curve was obtained in a test with a solution flowing at a rate of 30 cm/sec. Still higher flows did not

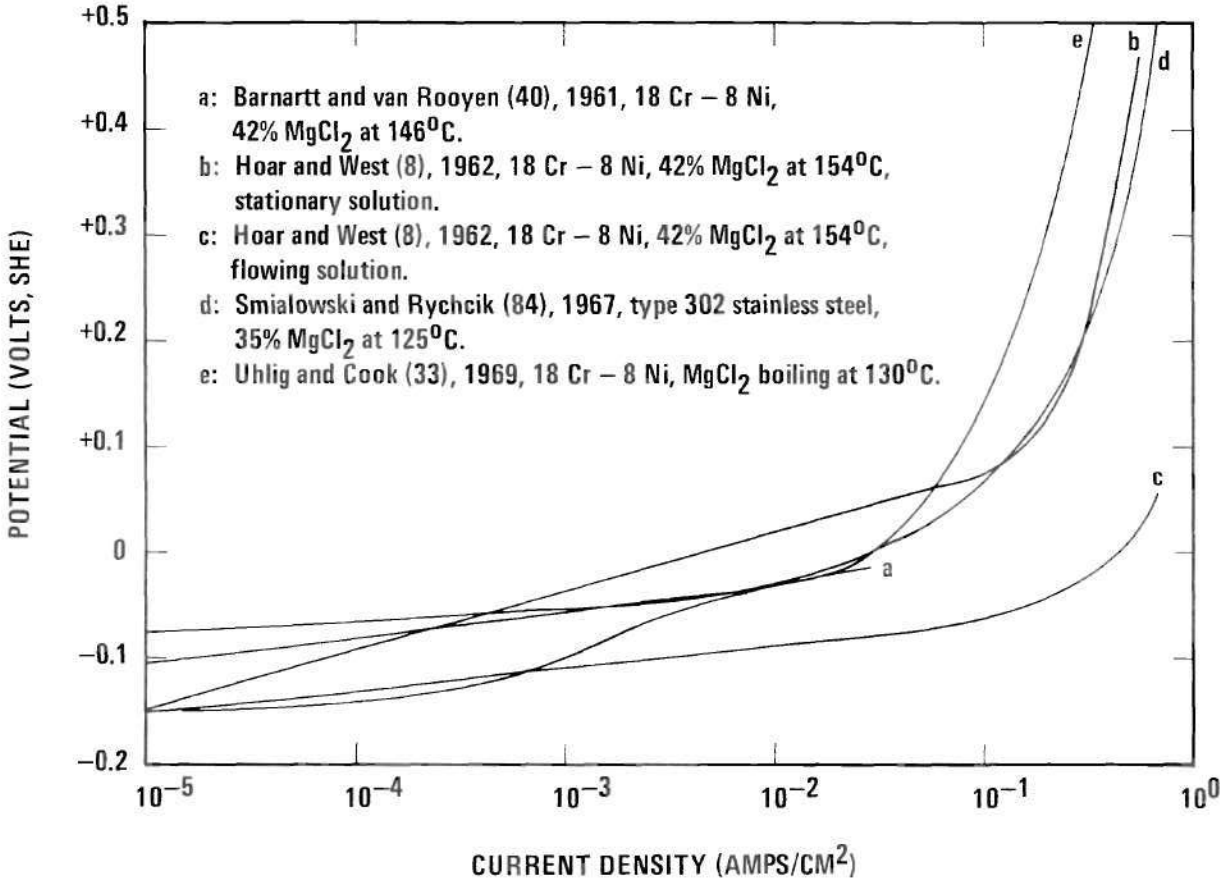

Figure 1. Summary of Published Anodic Polarization Data for Stainless Steels in Hot Magnesium Chloride Solutions.

produce significantly different results. No stirring, other than that due to biling, was apparently used in the experiments of Barnartt and Van Rooyen (40) and Smialowski and Rychcik (84). Uhlig and Cook (33) did not specify the experimental conditions.

The results in Figure 1 show that current densities are limited to less than one ampere per square centimeter even at relatively high noble potentials and that there is no indication of passivation. Even Hoar and West's results with solution flowing at high rate show a definite convergence to a limiting current density, despite the author's assertion that "such flow rates abolish concentration polarization almost entirely at all current densities used". The difference of slope between the curves obtained in stationary and flowing solutions, interpreted as concentration polarization at low current densities, was attributed to hydroxyl-ion impoverishment rather than to metal-ion accumulation or chloride ion impoverishment.

No anodic polarization studies on single crystals of austenitic iron-chromium-nickel alloys have been reported. A study of general corrosion of single crystals of a 20 Cr - 20 Ni steel in boiling nitric acid, reported by Leggett and Paxton (85), showed the weight loss to be independent of crystallographic orientation. Only corrosion on lowest-index faces was investigated.

In other systems polarization experiments indicated that significant differences in the kinetics of anodic behavior between various crystallographic faces exist. In 1959 Piontelli et al (86) presented results of an extensive study of the behavior of single crystals of Pb, Cd, Sn, Ag, Cu, and Ni as electrodes in various solutions. They

used galvanostatic pulse techniques to determine the overvoltages as functions of current densities. Morphology of surfaces was also studied. Anodic overvoltages on copper in perchlorate solution increased in the order $\eta(110)<\eta(111)<\eta(100)$. Nickel electrodes exhibited only minor differences between anodic behavior on different faces.

Bertocci (87) measured anodic and cathodic overvoltages as functions of current densities on copper faces parallel to {100}, {110}, {111}, and {321} planes in chloride solutions containing cuprous ions. The overvoltages for the {100} electrodes were significantly higher than for any other orientation. The {321} oriented electrodes exhibited lowest overvoltages, but differences were minor between orientations other than {100}. Similar results were obtained recently by Jenkins (88) in a study of galvanostatic overpotential transients on copper single crystals in a solution of cupric perchlorate.

In systems exhibiting an active-passive transition, crystallographic dependent behavior may also exist. Mauvais et al (89) detected differences in passivation behavior of low-index faces of nickel in 1N H_2SO_4. Current densities in the passive region decreased in the order $i_{\{100\}}>i_{\{110\}}>i_{\{111\}}$, while critical current densities for passivation increased in the same order.

CHAPTER III

EXPERIMENTAL WORK

Materials

Specimens

All specimens used in the course of this work were machined from one large single crystal of austenitic stainess steel. The crystal was obtained from Aremco Products, Inc., where it had been grown by the Bridgman technique. The crystal in the as-received condition is depicted in Figure 2, which also shows the major dimensions. Only about three quarters of the crystal could be utilized because of the porosity at the larger end.

The as-received crystal was encapsulated in a quartz tube filled with 99.99 per cent helium and homogenized in a furnace for five days at 1250^{o}C. In order to prevent a collapse of the tube the initial pressure of helium was adjusted to a value that led to approximately atmospheric pressure at the homogenizing temperature. After the five days the temperature was lowered to 1050^{o}C and held for one day. The crystal was then quenched by breaking the quartz envelope under water.

The homogenized crystal was analyzed for major alloying elements and interstitial impurities. The results are in Table 1. The orientation of the major axis was determined by back-reflection Laue technique and found to be close to <111> direction.

(a)

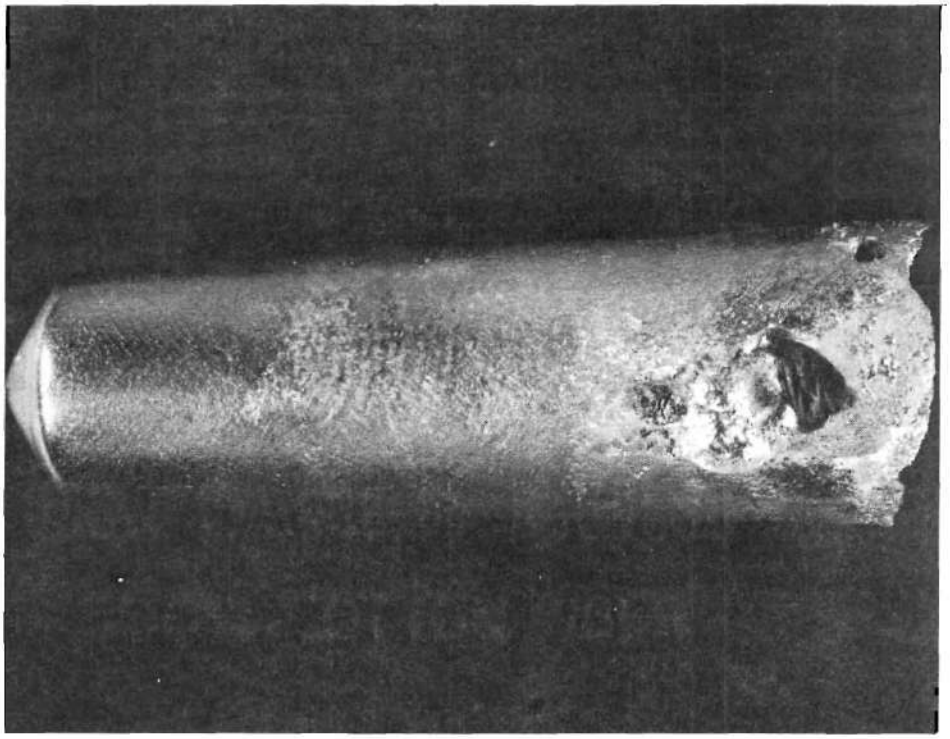

(b)

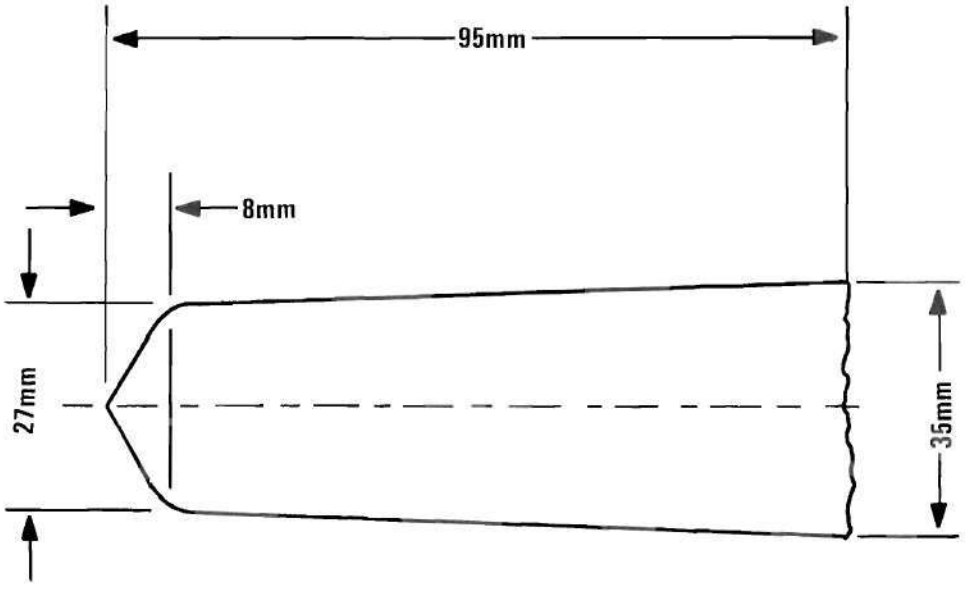

Figure 2. Single Crystal of Stainless Steel: (a) As Received, (b) Dimension.

Table 1. Alloy Composition

Element	Cr	Ni	Mo	C	N	Fe
Weight Per cent	16.21	13.69	2.86	0.022	0.032	Balance

All machining operations, except for the cutting of the notches in the specimens for stress corrosion testing, were done on a SERVOMET SMD spark machine in order to prevent structural changes. The general procedure in machining a surface to the desired orientation was as follows: the piece of the crystal to be machined was fixed on a two-circle meter which was then set on a specially designed Laue back-reflection camera (film size 5 x 5 inches). Figure 3 shows the goniometer and the camera attached to the Siemens KRISTALLOFLEX II X-ray machine which served as the X-ray source. The developed Laue photograph was analyzed, the goniometer was adjusted to the desired orientation and this was checked by taking another Laue picture. When the desired orientation was achieved the goniometer was set on the table of the SERVOMET spark machine and the crystal was planed using a rotating brass wheel as a tool. The relative positions of the tool and the goniometer had been carefully adjusted to make sure that the machined surface was exactly parallel to the desired crystallographic plane.

Other machining operations used in producing the desired shapes of the specimens were spark-cutting with a wire-slicer or with a brass tool, and turning on a spark-lathe.

Three sets of specimens were machined from the original crystal:

A. Three tensile specimens for the determination of the critical

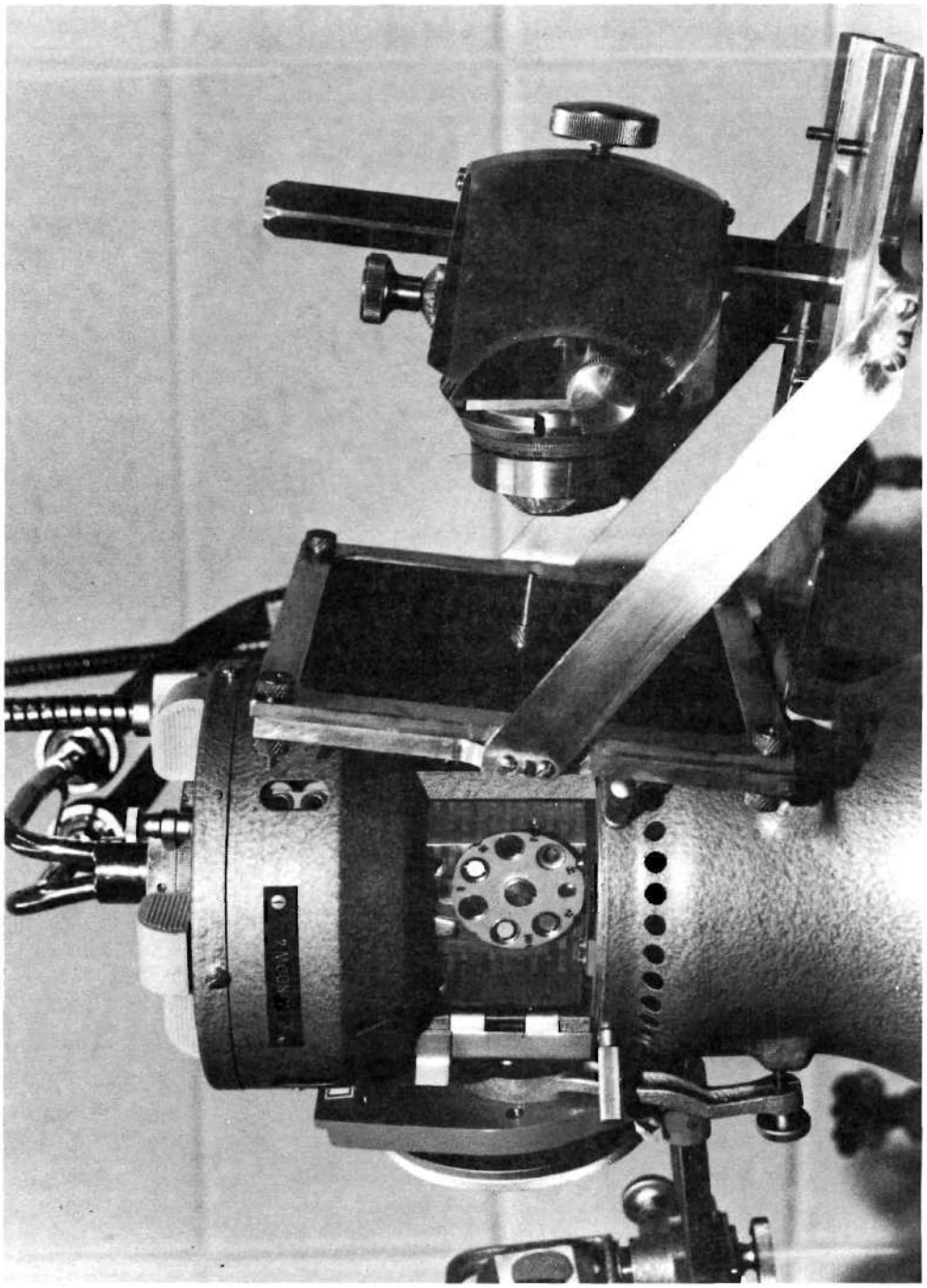

Figure 3. Goniometer and Back Reflection Laue Camera on the KRISTAL-LOFLEX II X-ray Machine.

resolved shear stress.

B. Seventeen prismatic specimens for stress corrosion tests.

C. Five disk-shaped specimens for the anodic polarization study.

Tensile Specimens. The shape and dimensions of the tensile specimens are shown in Figure 4a. The specimens were spark-machined from different parts of the original crystal. Because of the informative nature of the tensile tests no specific orientations were sought. After spark-machining the specimens were diamond-polished and heavily electro-etched in 10 per cent aqueous ammonium persulfate solution. The orientations, determined by back-reflection Laue technique, are shown in Figure 4b.

Specimens for Stress Corrosion Tests. The shape and dimensions of the specimens are shown in Figure 5a. Figure 5b shows the actual specimens in the pre-test and post-test conditions. The entire shape, except for the notch, was spark-machined. After the preliminary cutting the surfaces were spark-planed to the desired orientations. The maximum final deviation allowed was two degrees. The final spark-machining of the sides (the ends were only cut and in some cases not machined at all) was done simultaneously on all 17 specimens. Spark-planing in this stage was conducted at progressively lower intensities of the spark and finished at the lowest setting. To remove the final sparked surface layer the specimens were lightly diamond-polished and electro-etched in a 10 per cent aqueous ammonium perchlorate solution. This solution, used on polycrystalline materials, reveals grain boundaries and slip traces. On well-annealed single crystal surfaces the dissolution is uniform. This step served also as a final check that there were no grain boundaries in the

(a)

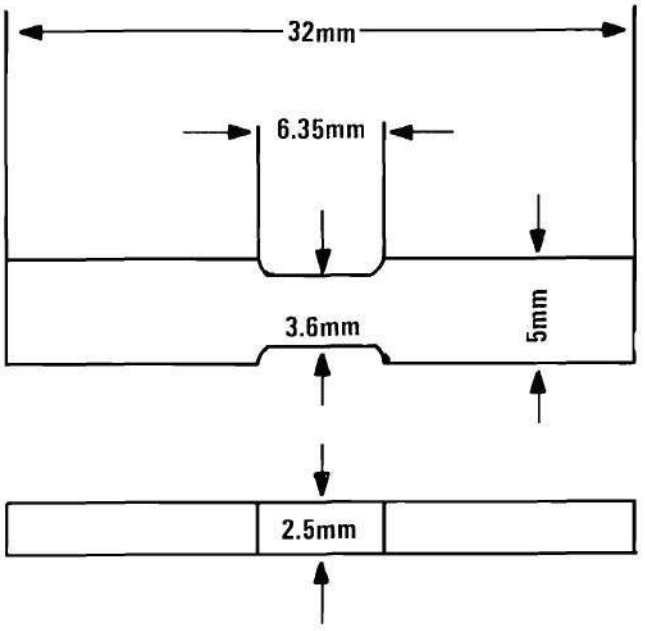

(b)

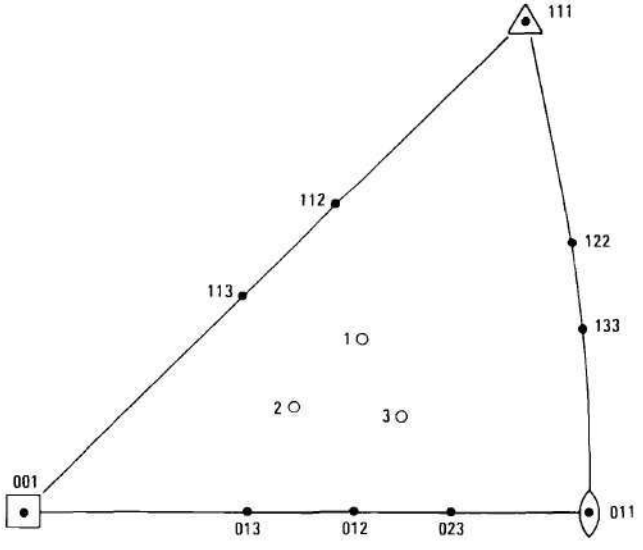

Figure 4. Single Crystal Tensile Specimens: (a) Dimensions, (b) Orientations of Tensile Axes of the Three Specimens.

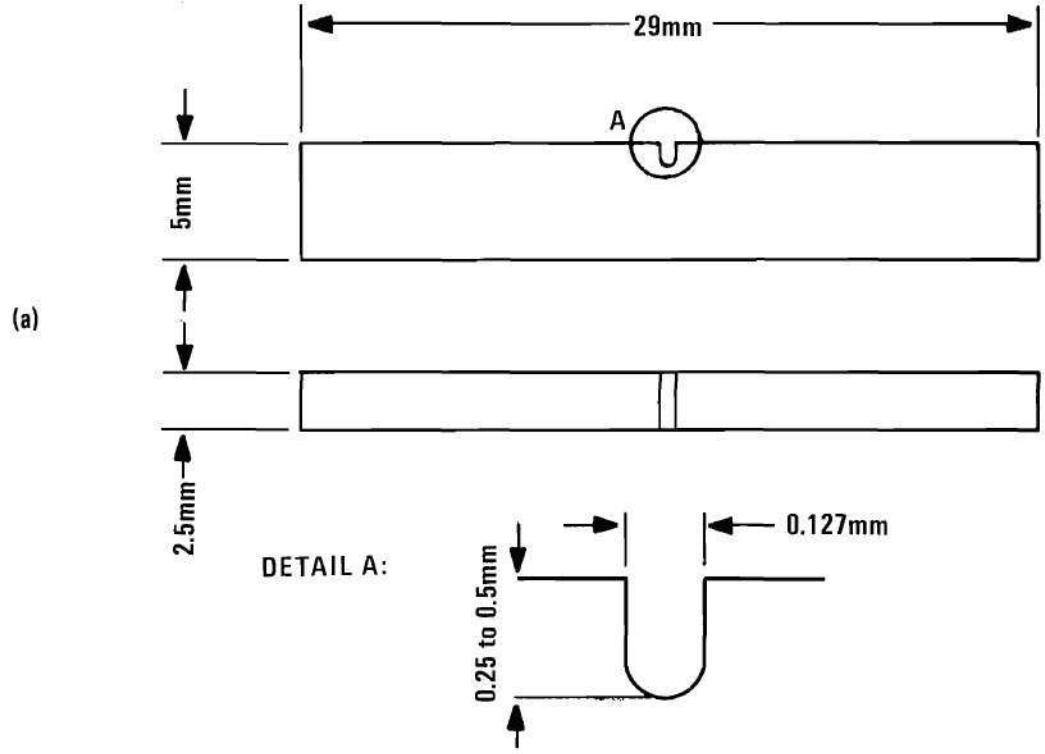

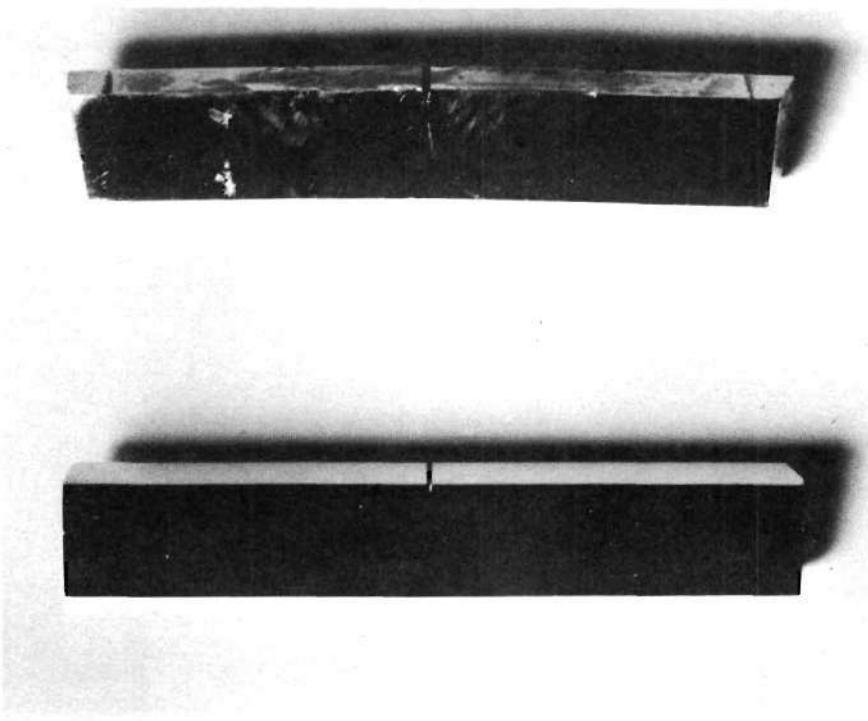

Figure 5. Single Crystal Specimens for Stress Corrosion Testing: (a) Dimensions, (b) Actual Specimens in the Post-test and Pre-test Conditions.

critical areas and that the strain-hardened surface layer was completely removed. The polishing and electro-etching operations were performed on all 17 specimens simultaneously. The specimens were affixed to a brass block using a conductive, acetone-soluble glue, and strips of stainless steel of the same thickness were affixed around to prevent rounding of edges.

As the final machining operation the notches were cut on a wire-saw using a wire of five thousands of an inch in diameter. This produced notches with well defined, finely abraded surfaces. The depths of the notches, however, could not be kept to close tolerances and varied between 0.25 and 0.5 mm. Specimens X1, X2, X3, and X4 were not notched.

Of the 17 specimens prepared 13 were machined to selected orientations. The choice of orientations was limited by the orientation of the original crystal and by the effort to make the most of the available material. Four specimens of chance orientations (X1 to X4) were prepared from the fringe parts. All orientations are listed in Table 2. In order to reduce the ambiguity of the trace analysis specific indices (not just family indices) are listed and later used in the analysis of experimental data.

All important dimensions of the specimens are presented in Table 4 in the Appendix.

Specimens for Polarization Studies. Specimens of the {100}, {110}, {111}, and {211} orientations of the studied faces were originally prepared. A {210} oriented specimen was added in the later stages of the investigation.

All specimens were machined from the same piece of the original

Table 2. Orientations of Specimens for Stress Corrosion Testing.

Specimen	Stress Axis	Wide Side	Narrow Side
X1, X2, X3	ND	ND	ND
X4	[023]	$(\bar{1}\bar{3}\ \bar{3}\ 2)$	$(1\bar{3}2)$
A1, A2, A3	$[1\bar{1}0]$	$(11\bar{1})$	(112)
B1, B2, B3, B4	$[11\bar{1}]$	$(1\bar{1}0)$	(112)
C1, C2, C3	$[11\bar{1}]$	(112)	$(1\bar{1}0)$
E1, E2, E3	$[1\bar{1}0]$	(112)	$(11\bar{1})$

ND . . . . Not Determined

crystal in order to minimize a possibility of variation in composition. After preliminary cutting slabs of selected orientations were machined by spark-planing. By using a longer film-to-specimen distance (60 mm) in the Laue camera and by careful adjustment of all parts, the maximum final deviation from the desired orientation was less than 30 angular minutes.

A disk approximately 13 mm in diameter was then cut from each slab using a tubular spark-cutting tool. All four of the original specimens were then machined simultaneously to a diameter of 12.7 mm on a spark-lathe. The {210} oriented specimen was later machined in the same way.

All specimens (four in the first part and five in the second part of the investigation) were then inserted into holes in a stainless steel disc, the faces in-plane with its surface, and affixed from behind with a conductive glue. The surface of the disc, including the faces of the specimens, was then lightly spark-planed, lightly diamond-polished and electro-etched in a 10 per cent aqueous ammonium persulfate solution. After the polishing the specimens were removed from the disc, cleaned, and stored in a dessicator.

Tensile Properties of the Alloy

The three tensile specimens were tested in an INSTRON Model TTDL testing machine. Tests were made at room temperature. Because of the small size of the specimens no extensometer was used and the load-elongation diagram was obtained as a relation between measured load and the displacement of the grips. The rate of displacement was 0.02 inches per minute.

No yield drops were observed. The load-elongation curves passed

smoothly from the elastic range into a constant load range when yielding began. The tests were terminated at approximately 3 per cent of plastic strain at which stage the Luders' band had not yet filled the gage length. The critical resolved shear stress was calculated from the load in the constant load region, the cross-sectional area and the parameters of the orientation. The data and results are presented in Table 3 of the Appendix.

Testing Solutions

Both the stress corrosion tests and the polarization studies were made using a boiling, aqueous solution of magnesium chloride. The boiling point was 155°C which corresponds to a concentration of 45 weight per cent of $MgCl_2$ according to most recent data (90).

The solution for stress corrosion tests was prepared from purified magnesium chloride (Fisher chemical M-31) by adjusting the boiling point to 155°C by adding distilled water. This was done in a 4000 ml flask equipped with a reflux condenser. Four thousand ml of the solution were prepared and this was used in all tests. The solutions used in the first four tests were returned to the flask. In the remaining 13 tests the solutions were discarded after each experiment. The stock solution was kept in the flask in which it was prepared at a temperature slightly above the melting point to prevent solidification.

The solution for the polarization studies was prepared in exactly the same way, but a higher grade chemical (Fisher Chemical M-33, certified A.C.S.) was used. Approximately 3200 ml of the solution were

prepared. It was discarded after each experiment.

Stress Corrosion Cracking Experiments

Instrumentation and Equipment

The experiments were conducted in the device shown in Figure 6 and Figure 7. The solution was in a Pyrex beaker with a ground glass top. Heating was provided by a hot plate. The hot plate with the beaker could be raised or lowered by means of a scissor-jack. In the upper position the top of the beaker was sealed by means of a teflon ring against a specimen holder made of sintered alumina. The ceramic holder was in the form of a thick flange with the two protrusions holding the specimen projecting inside of the beaker*. A thermometer graduated in $0.2^{\circ}C$, a reflux condenser, and a teflon guide for the load-carrying rod pass through the holes in the ceramic flange.

The specimen support and geometry of loading are shown in Figure 8. The specimen is placed in a slit in the two protrusions of the ceramic holder and is supported on two polished alumina rods 2.38 mm in diameter, spaced 25.4 mm apart. The load is applied by means of a small prismatic alumina piece which fits loosely between the protrusions and which is provided with two alumina rods similar to the supports, contacting the specimen at a spacing of 8 mm. Four point loading is thus achieved producing a state of pure bending between the two central loading rods. The load is carried to the prismatic piece by a polished alumina rod 6.35 mm in diameter which passes through a teflon guide and seal, which is inserted in the central hole in the ceramic flange. An

*The ceramic holder was made by slip casting and sintering at the High Temperature Materials Branch of Georgia Institute of Technology.

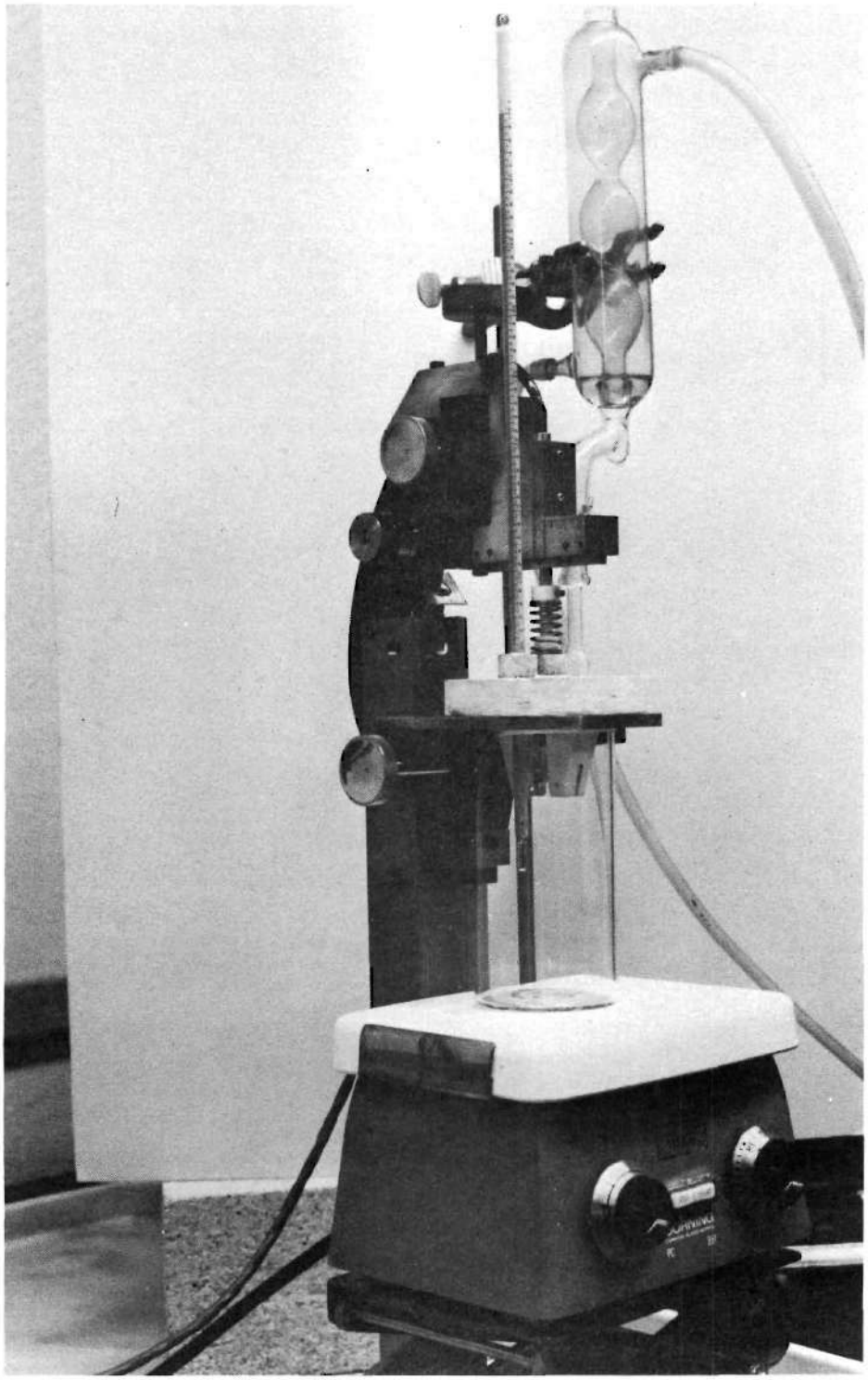

Figure 6. Device for Stress Corrosion Testing of Single Crystal Specimens.

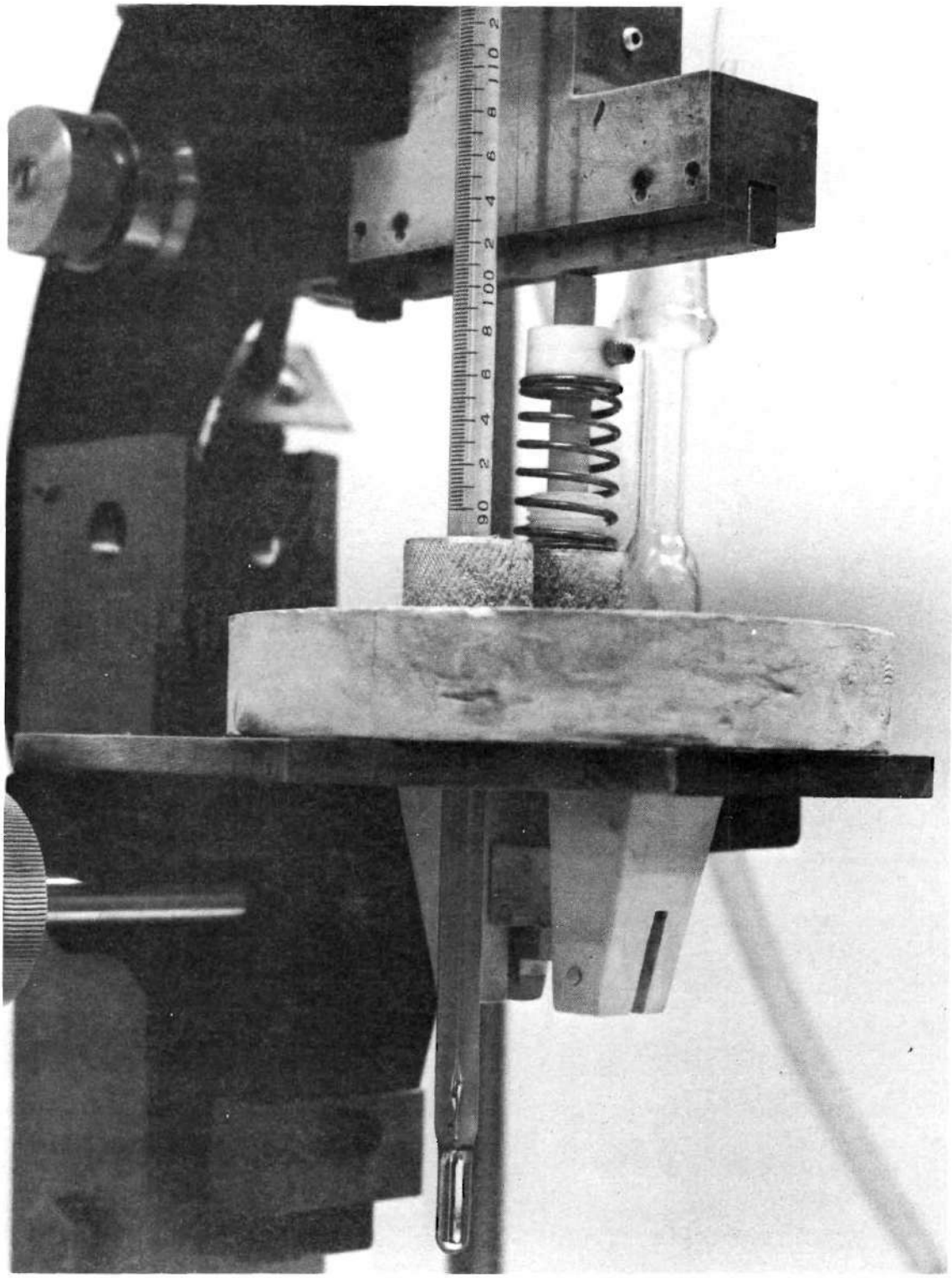

Figure 7. Device for Stress Corrosion Testing of Single Crystal Specimens: Detail of Specimen Support and Loading.

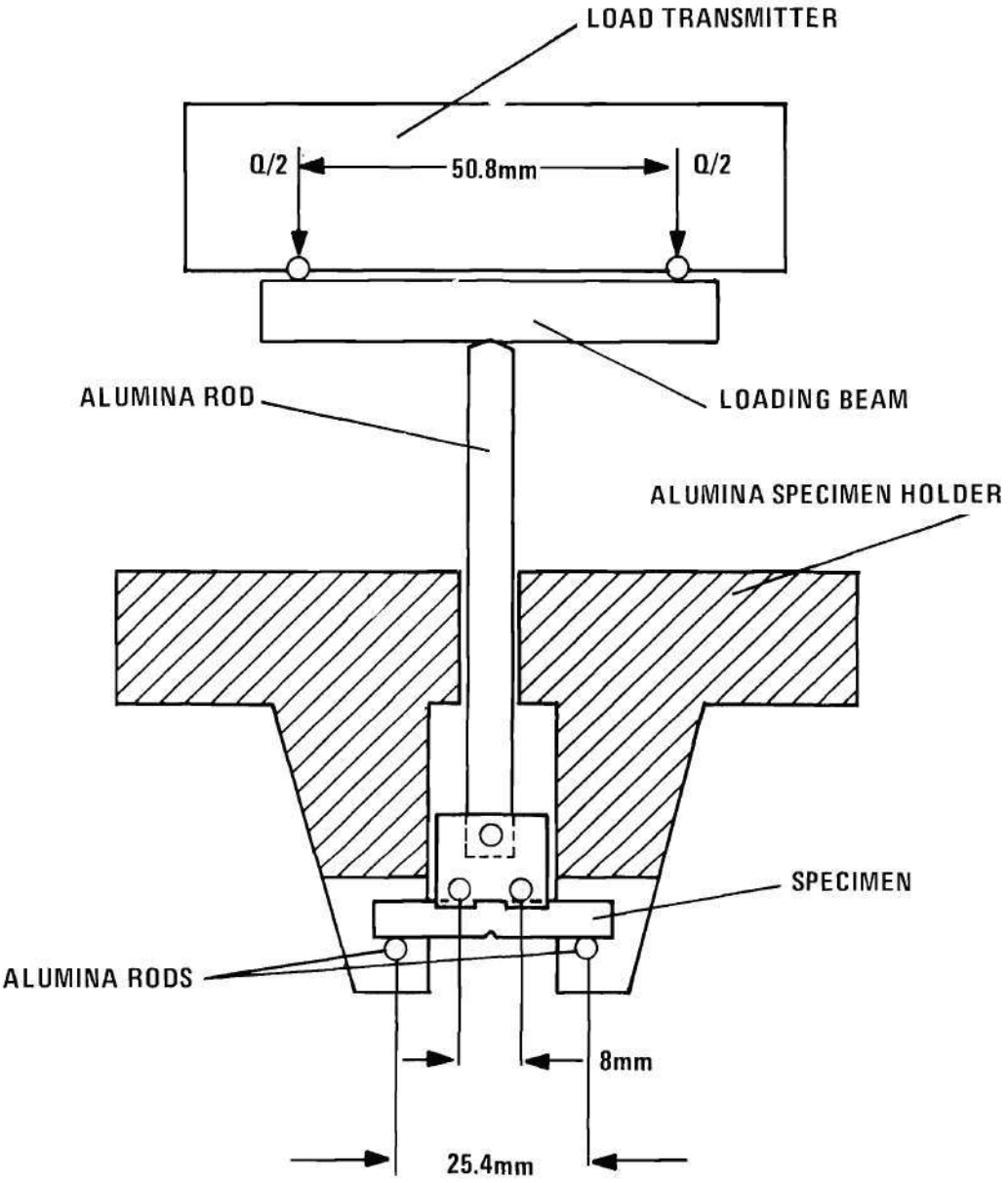

Figure 8. Geometry of Loading in Stress Corrosion Tests.

alumina pin connects the rod with the loading piece in order to allow a certain amount of tilt and thus ensure symmetrical loading.

The upper end of the alumina rod has a knife edge in contact with the loading beam made of high-strength steel. The beam is three-point loaded, the load being applied through a brass part with two steel pins (load transmitter). This part slides in a guide in the upper part of a cast-iron frame (adapted from a table microscope); to the lower part of this frame the ceramic flange is rigidly affixed. The actual loading is done by turning a screw in the frame which pushes on a hard-steel insert in the load transmitter.

A linear-displacement differential transformer transducer (DAYTRONIC Model DS 100) is placed inside the load transmitter and contacts the loading beam in the center, on the side opposite to the alumina rod. The transducer detects the deflection of the loading beam which is proportional to the load. This same load is automatically applied to the specimen. A DAYTRONIC Model 300D transducer-amplifier provided excitation to the transducer and amplification of the signal. The output from the transducer-amplifier was fed into a Honeywell ELEKTRONIK 194 strip chart recorder. The loading beam was calibrated in a special fixture using dead weights. The sensitivity of the transducer-amplifier-recorder system was adjusted to give approximately one inch on chart per 10 pounds of load. The exact values were read from the calibration chart.

The loading system is partly self-relieving. When the specimen deflects the load decreases because the deflection of the loading beam is reduced. The initial deflection of the specimen during loading is automatically compensated, but any further deflection during the test

reduces the load. When a crack forms the cross-section decreases and deflection tends to increase. This reduces the load, which in turn reduces somewhat the deflection of the specimen, and a new equilibrium is established. The nominal stress thus varies less than in constant-load tests. A true constant-stress condition cannot be achieved, however. The self-relieving effect increases with increasing rigidity of the loading beam. Noise and sensitivity of the amplifier-transducer system become limiting factors together with the stability of the loading device. As a practical compromise a beam with a deflection-load characteristic of 4.5×10^{-5} cm/kg was selected in these tests. The nominal stress increased during cracking to about 2.75 times the initial value in the case of longest cracks. Figure 9 shows a comparison between the nominal stresses in the system described and in a constant-load test.

Experimental Procedure

The following procedure was adopted and strictly maintained in all stress corrosion tests:

1. The beaker and the ceramic holder were pre-heated in order to prevent thermal cracking and to speed up the establishment of thermal equilibrium. The transducer-amplifier and the recorder were turned on to warm up.
2. The selected specimen was re-electropolished for one minute in a 10 per cent ammonium persulfate solution, washed in distilled water and immediately inserted in the ceramic holder.
3. The beaker was filled with 300 ml of the hot magnesium chloride solution. The jack was raised to seal the beaker and the solution was heated to boiling. The boiling point was adjusted, if necessary, to $155 \pm 0.2^{\circ}C$ by adding small amounts of distilled water through the reflux condenser.

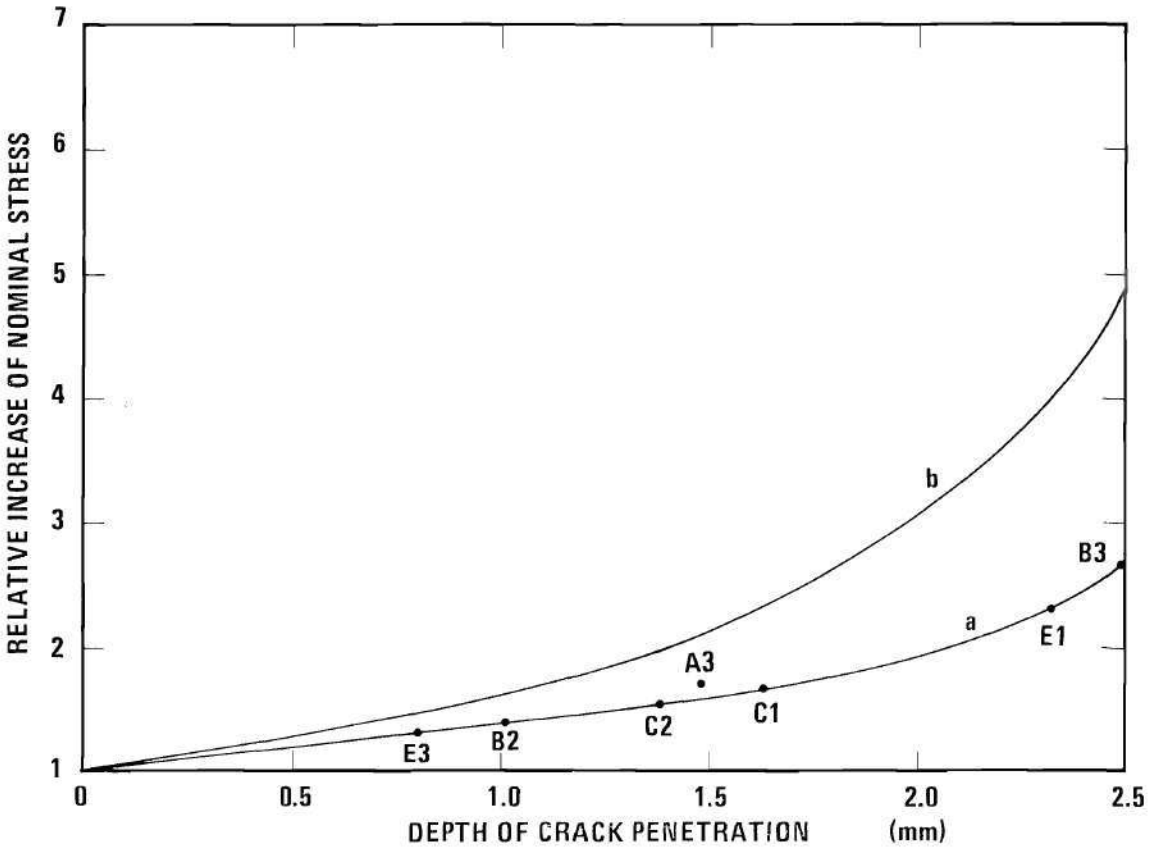

Figure 9. Variation of Nominal Stress with Crack Penetration: Curve (a) for the Loading System Used in this Work, Curve (b)for a Constant Load Test.

The heating and adjustment of the boiling point took approximately 10 minutes.

4. Since the transducer was found to be somewhat affected by temperature variations a period of 30 minutes was allowed to establish thermal equilibrium before loading. The recorder was started to monitor the variations in the transducer-amplifier signal.

5. After the 30 minutes the pen of the recorder was adjusted to zero line and load was applied by turning the loading screw, thus moving the pen on the chart to the level selected according to calculations and the calibration curve. Chart speeds of 50 or 100 minutes per inch of chart were used.

7. The test was terminated when the crack reached the desired length. Visual observation as well as evaluation of the recorded variations of load were used to estimate the crack length. The load was removed, the solution discarded and the specimen removed, washed in distilled water and dried.

8. Surfaces of the specimens showing crack traces were photographed on a VICKERS 55 microscope at 25x magnification. The angles between the crack traces and the edges of the specimen, as well as the lengths of the crack traces, were measured on the photographs.

9. On most specimens a cut was made with a spark-slicer from the side opposite to the notch to the immediate vicinity of the crack edge. The specimen was then mechanically broken. Another cut was made to make the specimen length suitable for examination in the scanning electron microscope. Fracture surfaces were examined under an optical stereo-

microscope and in a scanning electron microscope, Cambridge STEREOSCAN Mark II.

The following variations of the general procedure were carried out in special experiments.

One test (specimen E2) was interrupted in the period of crack propagation, and cracking was re-initiated at a lower load.

Several specimens were examined in the scanning electron microscope before they were broken in order to study the surface attack.

On some specimens further sectioning by spark planing was carried out as described in the chapter on results.

Anodic Polarization Experiments

Instrumentation and Equipment

The potentiodynamic determination of anodic polarization curves on various crystal faces was carried out using the electrolytic cell shown in Figure 10 and Figure 11. The complete set-up is shown in Figure 12. The cell is basically a beaker with a ground flange top. A specimen holder and a platinum counter-electrode are inserted in the two taper ground joints in the lower part. A glass ball ground joint in the upper part permits insertion of a remote reference junction with a porous ceramic tip. The tip can be positioned close to any point on the specimen surface. The salt bridge consists of the remote reference junction filled with magnesium chloride, a small beaker with saturated KCl solution, and a cotton string connecting the two. A standard saturated calomel electrode is placed in the beaker.

The glass lid of the cell has taper ground joints for a thermometer, a reflux condenser and a reservoir of distilled water. The lid had been

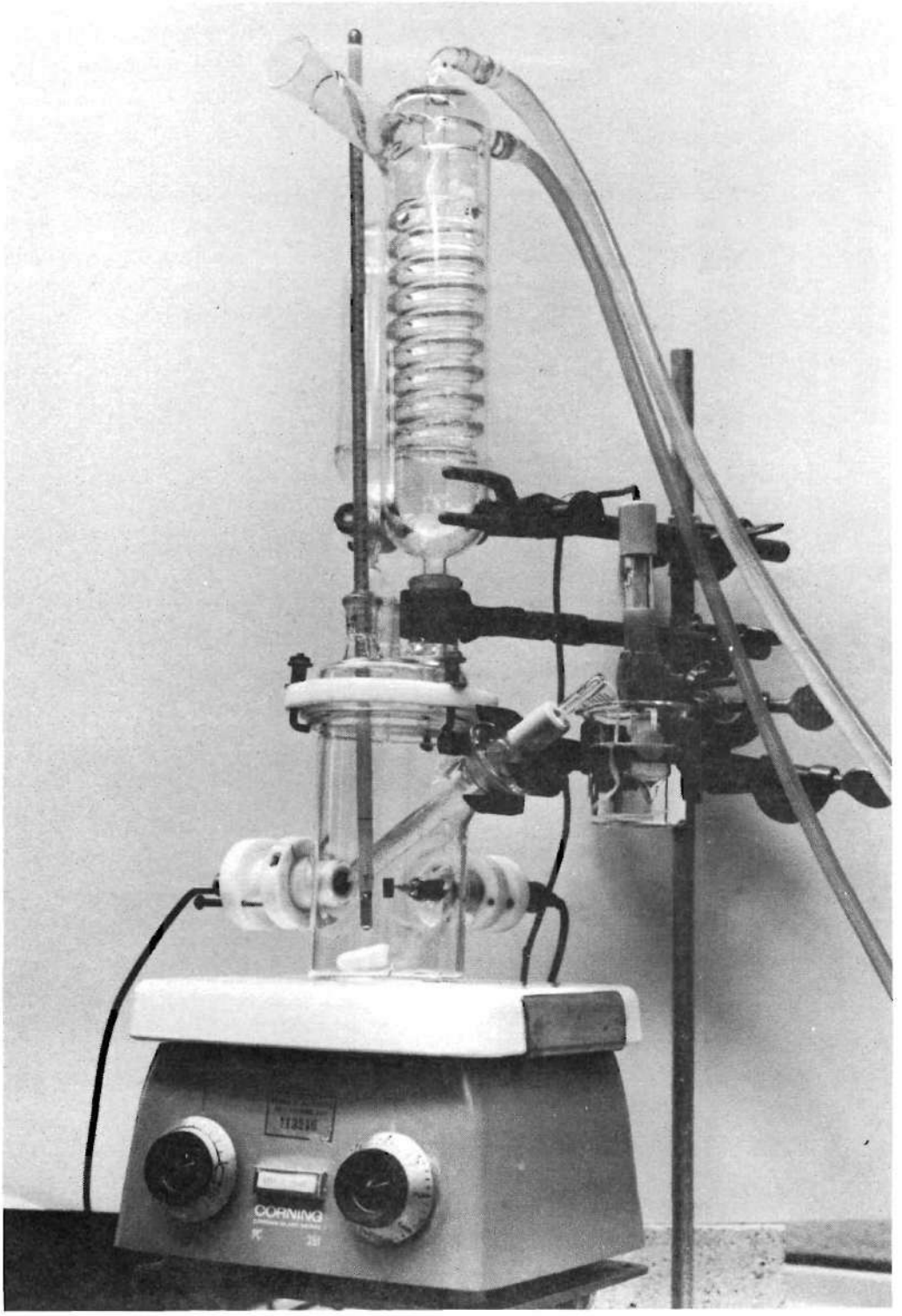

Figure 10. Electrolytic Cell for Anodic Polarization Experiments.

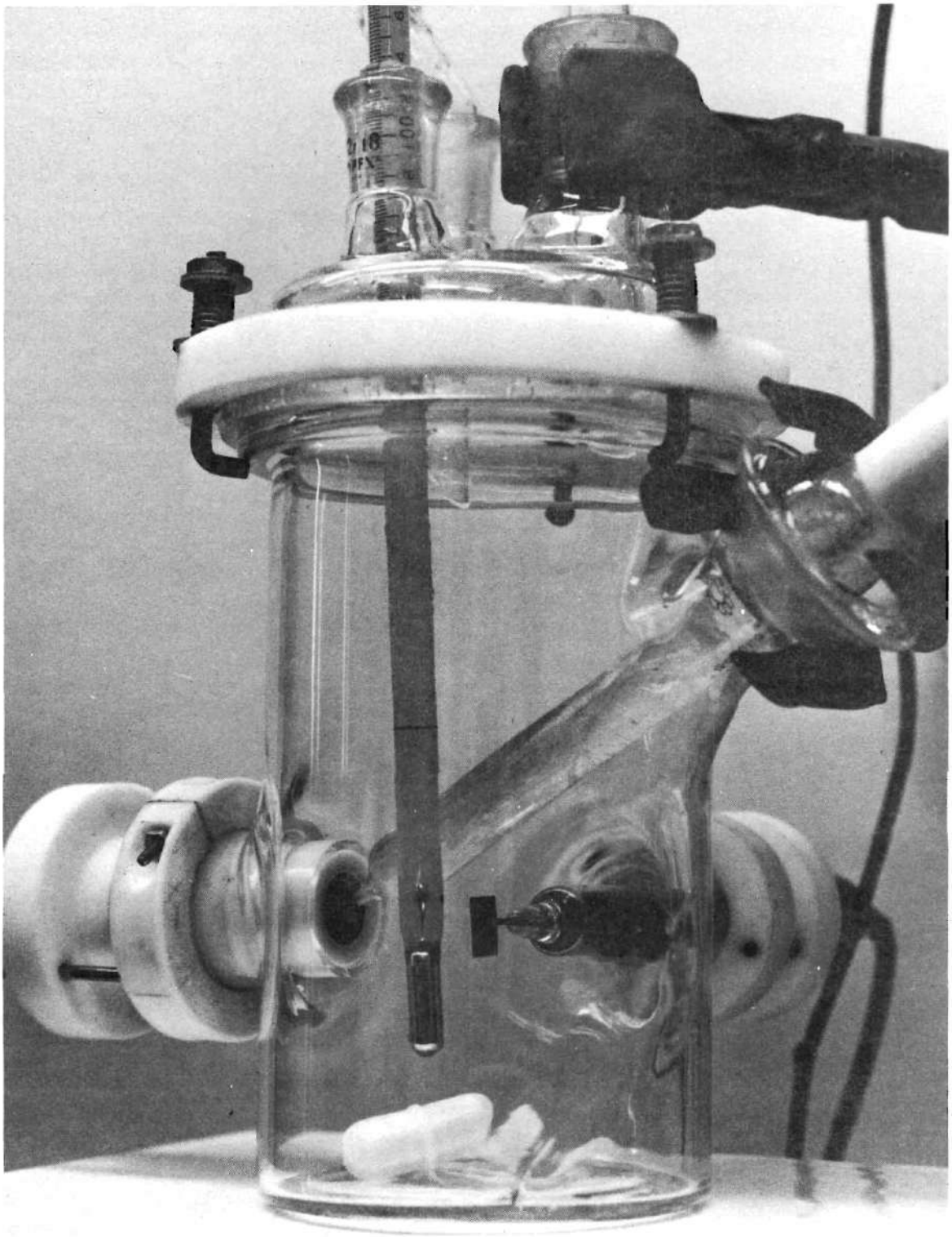

Figure 11. Electrolytic Cell for Anodic Polarization Experiments: Detail of Arrangement of Electrodes.

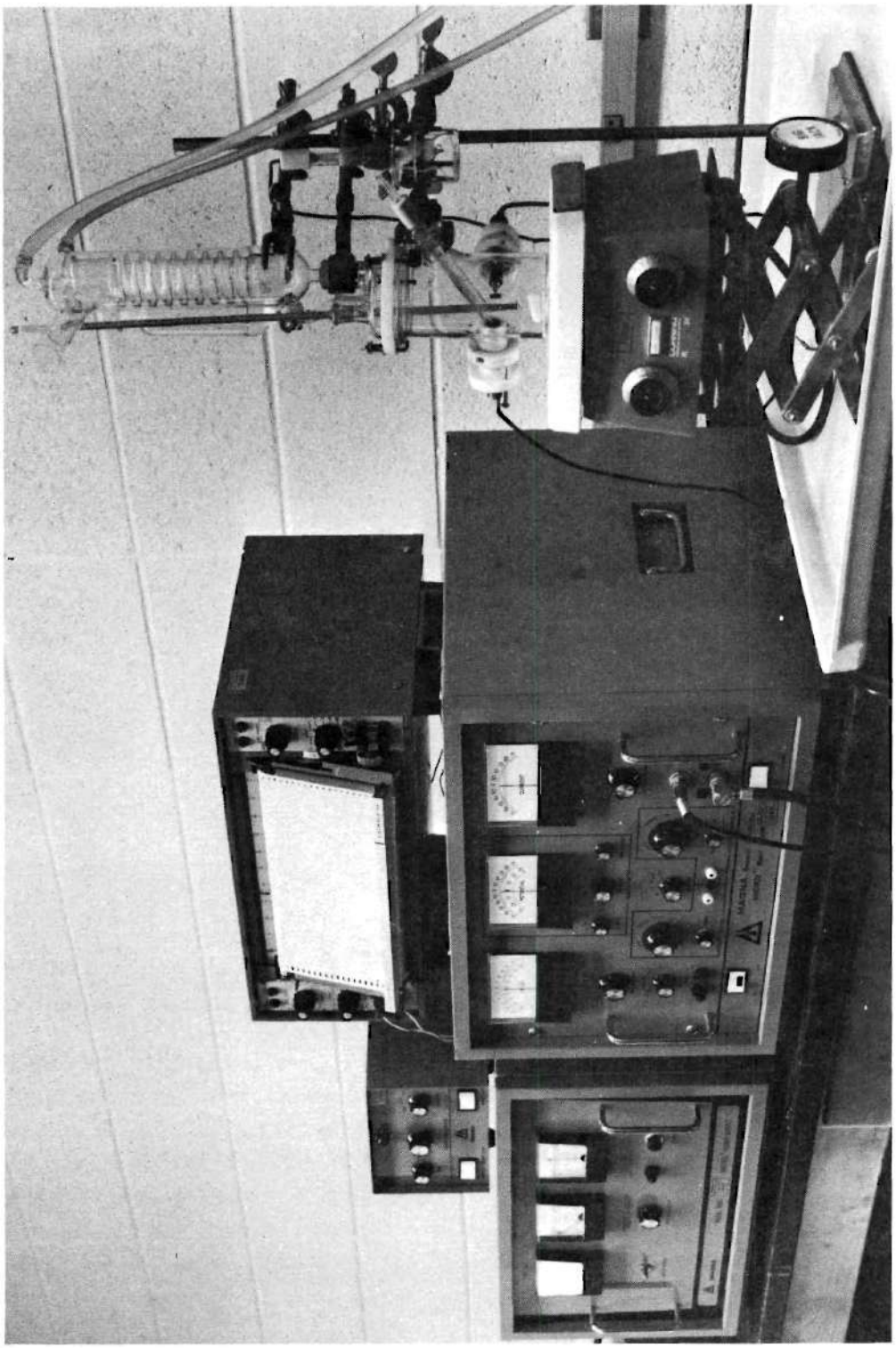

Figure 12. Anodic Polarization Set-up.

ground flush with the beaker flange and during the test it is secured by means of a teflon ring with three spring-loaded clips.

The specimen holder is made of Teflon and fits into one of the taper joints on the beaker. The drawing in Figure 13 shows the general design of the holder. A cylindrical specimen 12.7 mm in diameter can be inserted in the tight hole in the holder. A coil spring pushes the specimen against a lip at the end of the hole and also makes electrical connection with the brass stopper to which a lead from the potentiostat is connected. A quartz ring is slipped on the front end of the holder. When the teflon holder is heated up at the beginning of the test it expands and safely seals the specimen, compressing it under the ring.

The potentiostat used was ANOTROL Model 4700 M Research Potentiostat made by Magna Corporation, with a linear scanning accessory, Model 4510. Since an X-Y recorder was not available at the time of the tests a strip chart recorder, a Honeywell ELECTRONIK 194, was used to record the polarization curves. The current output from the potentiostat was fed to the input of the recorder which was synchronized with the scanning unit, so that the time scale served as a potential scale. A four-digit millivoltmeter, CIMRON Model 6453, with an input resistance of more than 10^9 ohms, was connected directly across the reference and working electrodes, making possible a very accurate determination of relative potentials.

Experimental Procedure

The following procedure was adopted and strictly maintained in all polarization experiments:

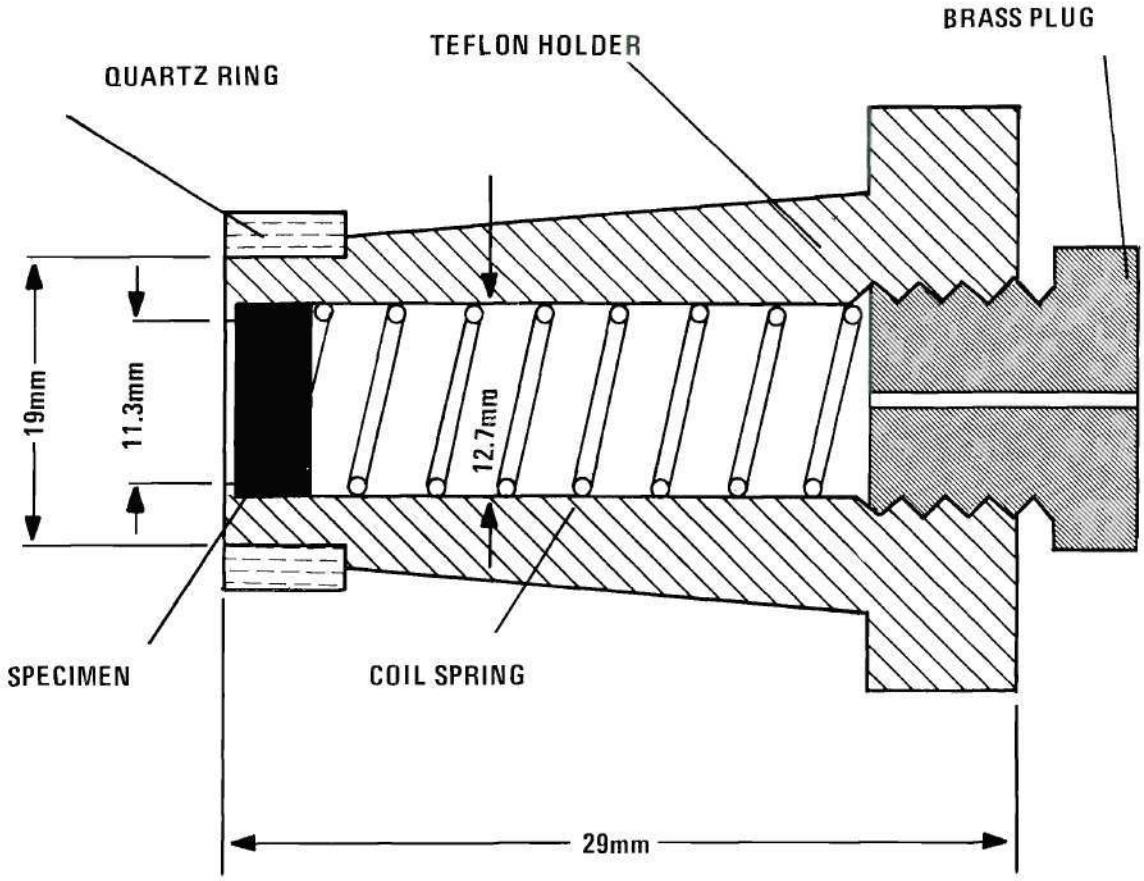

Figure 13. Specimen Holder for Anodic Polarization Experiments in Hot Magnesium Chloride Solutions.

1. The electrolytic cell, except for the specimen holder, was pre-heated by means of the hot plate. The potentiostat and the recorder were turned on, warmed up and balanced.

2. A selected specimen was taken from the dessicator, inserted in the holder and re-electropolished for one minute in a 10 per cent aqueous ammonium persulfate solution.

3. In the first series (the four original specimens) the tests were made on specimens in the electro-etched condition. In the following two series (five specimens each) the specimens were cathodically activated in 3N HCl at 50 ma/cm^2 for one minute following electro-etching.

4. The holder with the specimen was washed in distilled water, inserted in the port on the beaker and secured. The beaker was filled with 200 ml of the hot magnesium chloride solution. The hot plate with the beaker were raised by means of the scissor-jack, the lid was secured and the solution was brought to boiling. The boiling point was adjusted, if necessary, to 155 $\pm$ 0.2°C by adding small amounts of distilled water from the reservoir. It took approximately 5 minutes to bring the solution to boiling and to adjust the boiling point. A total time of exactly 15 minutes was allowed between filling the beaker and starting the polarization experiment.

5. The open circuit potential was measured with the digital mil meter. The average value during the last minute of the waiting period was taken as the corrosion potential.

6. The recorder was started and the potential scan was initiated from a potential of -0.400 V relative to the standard saturated calomel electrode. The potential was switched to the operating mode when the

scan reached the corrosion potential. The current range was switched in steps during the test, starting with the range of 10^{-4} amperes full scale and switching to a higher decade each time the current reached the full scale value. The scan was terminated at various potentials and currents, as described in the following chapter.

7. Different rates of potential change were used in each of the three series. In the first series the rate was 160 mV per minute, in the second series 100 mV per minute, in the third series 50 mV per minute.

8. The procedure was repeated with each specimen in the set. Then the specimens were inserted in the stainless steel disc and the preparation procedure was repeated, starting with the spark planing of the surfaces. Each specimen was tested three times, except for the {210} orientation which was tested twice.

CHAPTER IV

RESULTS

Stress Corrosion Cracking Experiments

Crystallography of Cracking

Examination of the crack traces on the sides of the specimens showed them to be mostly straight but the directions varied with the orientation of the specimen. Figures 14a, b, 15a, b and 16a, b show the similarity of cracking in specimens of same orientation.

The angles between the crack trace directions and the long edges of the specimens were determined from the optical micrographs. Since the orientations of the surfaces were known, these measurements made a further analysis possible. The slip lines, clearly visible on many surfaces, were used as an additional reference. The results are presented in Table 5 of the Appendix together with other crystallographic data.

A single-surface trace analysis was made as a first step in the determination of the preferred plane of cracking. The results are summarized in Figure 17.

Although the results indicate a high probability that the orientation of the cracking plane is close to {210}, they were not considered completely satisfactory for the following reasons:

a. A single-surface trace analysis gives ambiguous results. The surface trace is an axis of a zone and the poles of all planes of this zone lie on a line that crosses several basic triangles in the sterographic

Figure 14. Traces of Stress Corrosion Cracks on Sides of Single Crystal Specimens; $(1\bar{1}0)$ Surface: (a) Specimen B3 (Magnification 50x).

Figure 14. (continued) Traces of Stress Corrosion Cracks on Sides of Single Crystal Specimens; $(1\bar{1}0)$ Surface: (b) Specimen B4 (Magnification 50x).

(a)

(b)

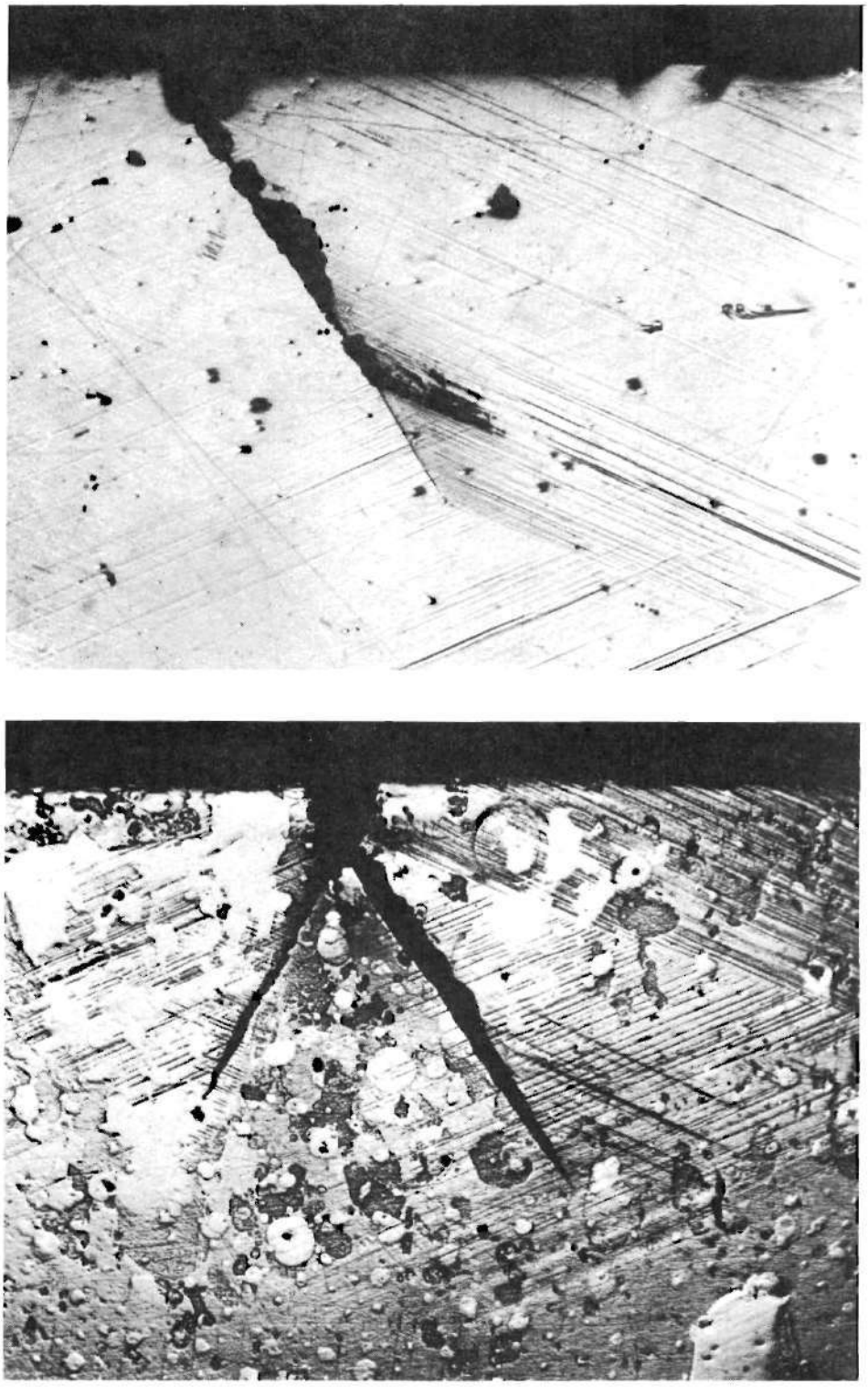

Figure 15. Traces of Stress Corrosion Cracks on Sides of Single Crystal Specimens; (112) Surface: (a) Specimen C1, (b) Specimen C2 (Magnification of both 33x).

(a)

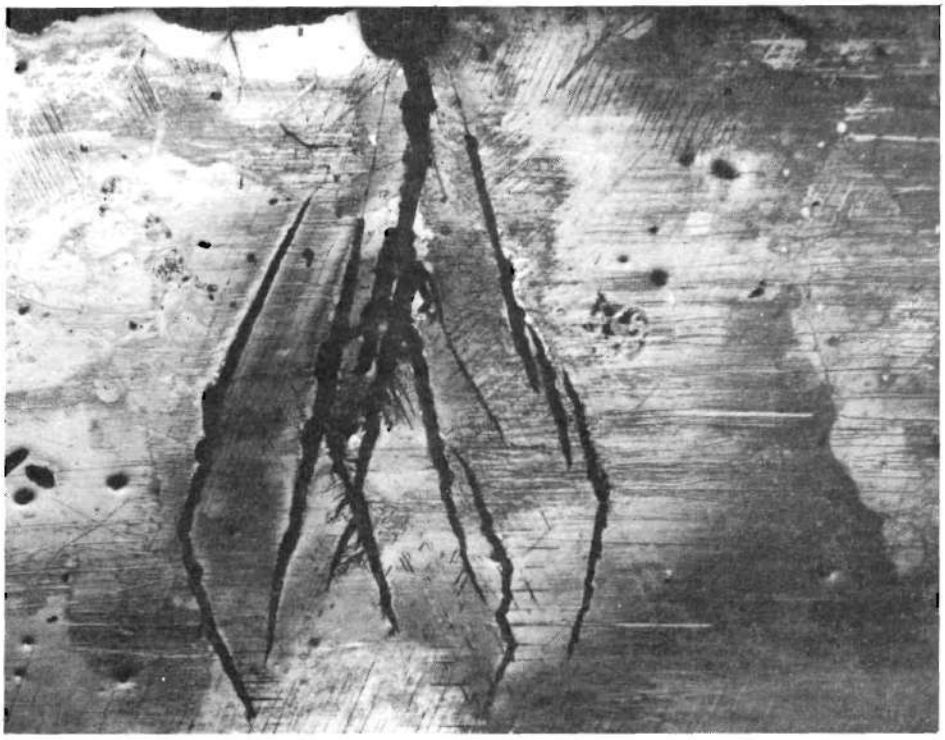

(b)

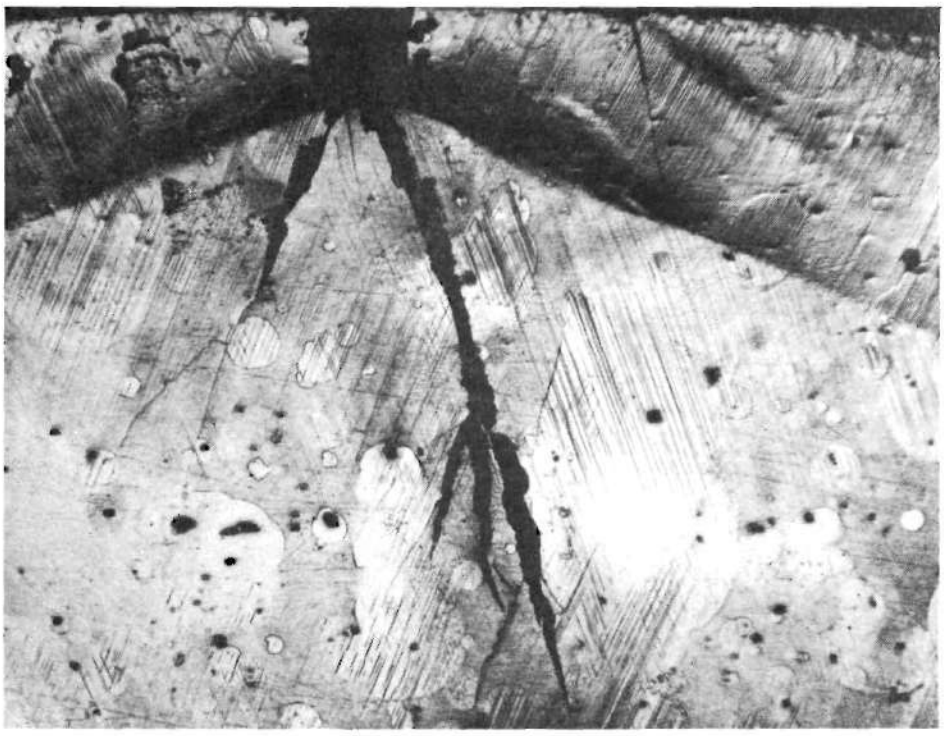

Figure 16. Traces of Stress Corrosion Cracks on Sides of Single Crystal Specimens; (112) Surface: (a) Specimen E1, (b) Specimen E2 (Magnification of both 33x).

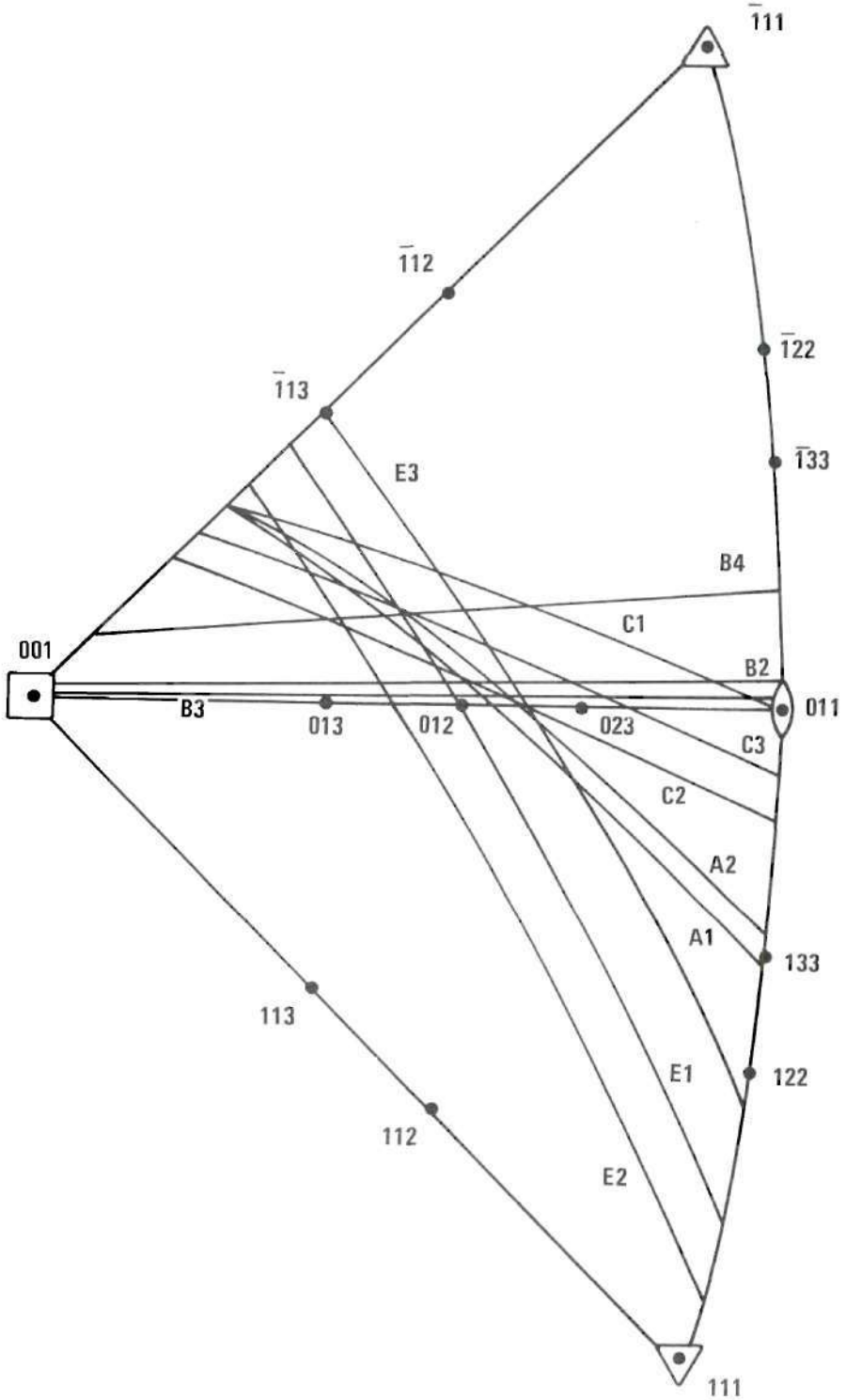

Figure 17. Summary of Results of the Single-surface Trace Analysis.

projection. If all these lines were transposed into a single triangle the picture would not be clear and some of the information would be meaningless. The lines shown in the two triangles in Figure 17 were selected on the basis of an assumption that the crack is unlikely to run at a sharp angle to the direction of the highest tensile stress. b. The lines in Figure 17 do not intersect in one point or very close to one point so that an exact identification would be subject to doubt. c. In view of the observed localized corrosion effects on the free surfaces the traces of the cracks may be affected by processes with crystallographic dependence different from that of the crack propagation.

In order to overcome these uncertainties a positive identification by means of a reliable two-surface trace analysis was sought, to be conducted not on original external surfaces but on sections intersecting flat areas of the fracture surfaces. Four specimens made such an analysis possible. These were specimen A2 and three specimens of the B series.

In the specimen A2 the crack propagated partly at an angle to the notch, as shown in Figure 18a, and the fracture surface in that area was smooth. The specimens B2, B3, and B4 all cracked in a similar geometry with relatively smooth and flat surfaces in areas far from the notches and from the sides. Figure 18b shows a section parallel to the (112) plane (the narrow side of the specimen) before the specimen B2 was broken. In Figure 19a a low-magnification scanning electron picture of the specimen B3 is presented, representative of the mode of cracking in all three specimens of the B series. The flatness of the fracture surfaces in the central area is shown later in Figure 28b.

(a)

(b)

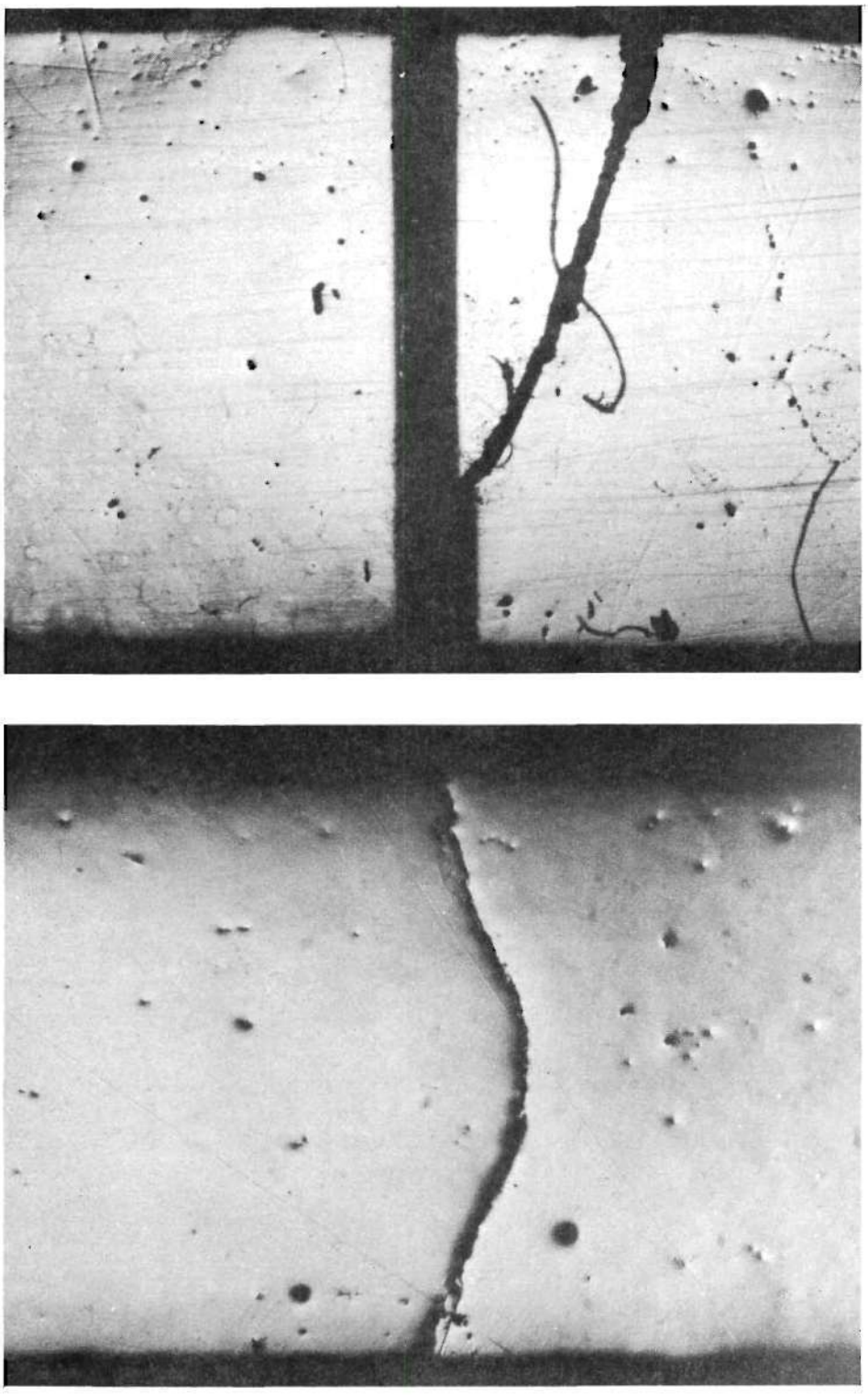

Figure 18. Traces of Stress Corrosion Cracks: (a) Notched Side of Specimen A2, (112) Surface, (b) Section Parallel to the Notched Side of Specimen B2, (112) Surface (Magnification of both 36x).

(a)

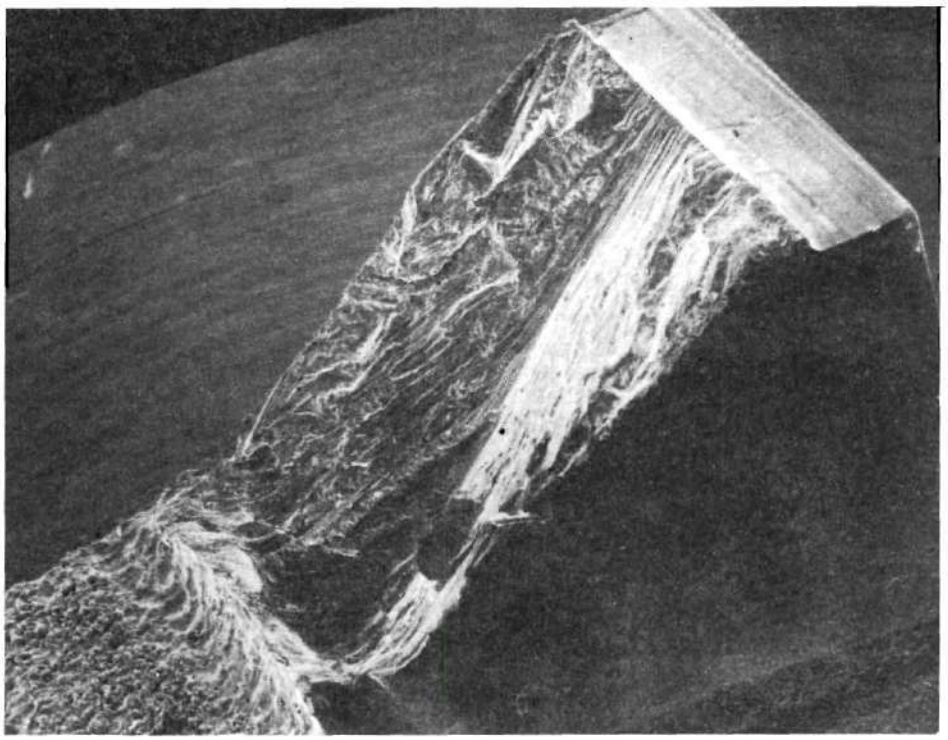

(b)

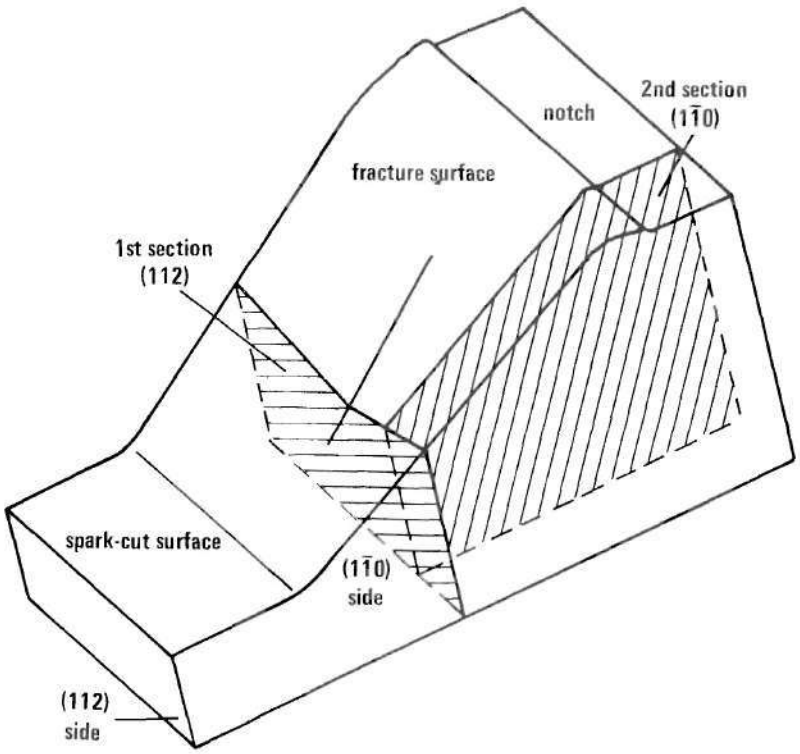

Figure 19. Morphology of Cracking in Specimens of the B-series: (a) Scanning Electron Micrograph of the Fracture Surface of Specimen B3, (b) Sectioning for a Two-surface Trace Analysis.

The above mentioned specimens were spark-planed parallel to the original surfaces to such a depth that the cuts intersected the most representative flat areas of the fracture surfaces. The way the specimen B3 was sectioned (and similarly specimens B2 and B4) is depicted in a drawing in Figure 19b. The drawing is oriented similarly to the specimen in Figure 19a in order to make an interpretation of the features easier. Two such sections are shown in Figure 20. The results of the two-surface trace analysis on the above mentioned four specimens and on the specimen X4 (traces on external surfaces) are presented in Table 6 of the Appendix and in Figure 21. All points are within 5 degrees of the (012) pole.

Special attention was given to the specimens of the C-series. Despite the close similarity with the specimens of the B-series the fracture surfaces were not flat and the traces of cracks on the sides corresponded in some cases more closely to traces of {110} planes than to traces of {210} planes.

Since the direction of the highest tensile stress in specimens of the C and B series is <111>, two sets of planes of the {210} family are subjected to the same highest tensile stress. In the chosen reference system these planes have indices (120), (210), ($\bar{1}$02), (0$\bar{1}$2), and (20$\bar{1}$), (02$\bar{1}$). Their traces on the (112) surface of the sides of the C-series specimens make angles of $67^{\circ}48'$ and $50^{\circ}46'$ respectively. The traces of cracks, making angles between 52 and 59°, thus run in between the traces of the two sets of {210} planes. This suggests that the crack might alternate between the two equivalent orientations. A high magnification optical micrograph of the fine end of the crack trace on the side of the specimen C1, shown in Figure 22, seems to support this idea. It shows

(a)

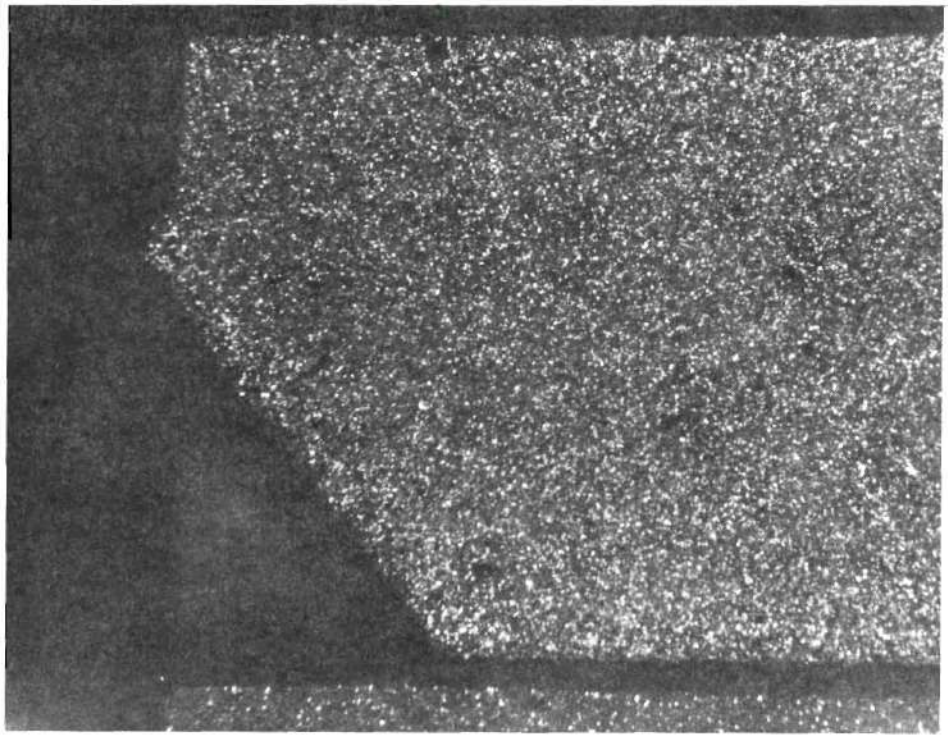

(b)

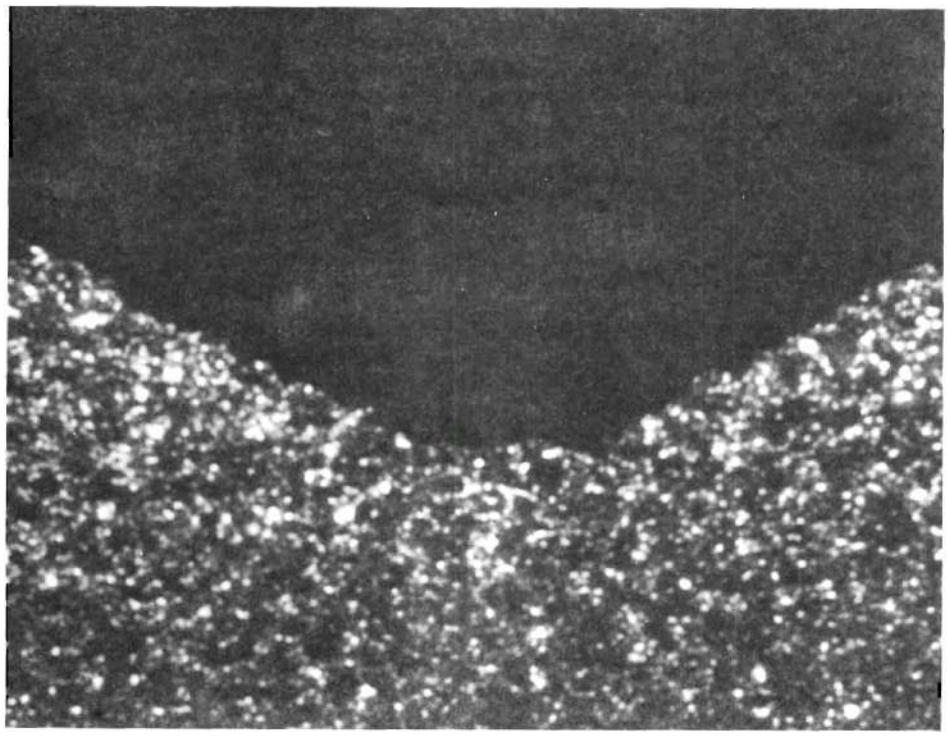

Figure 20. Micrographs of Spark-planed Sections; Specimen B3:
(a) Section Parallel to (110) (Magnification 48x),
(b) Section Parallel to (112) (Magnification 100x).

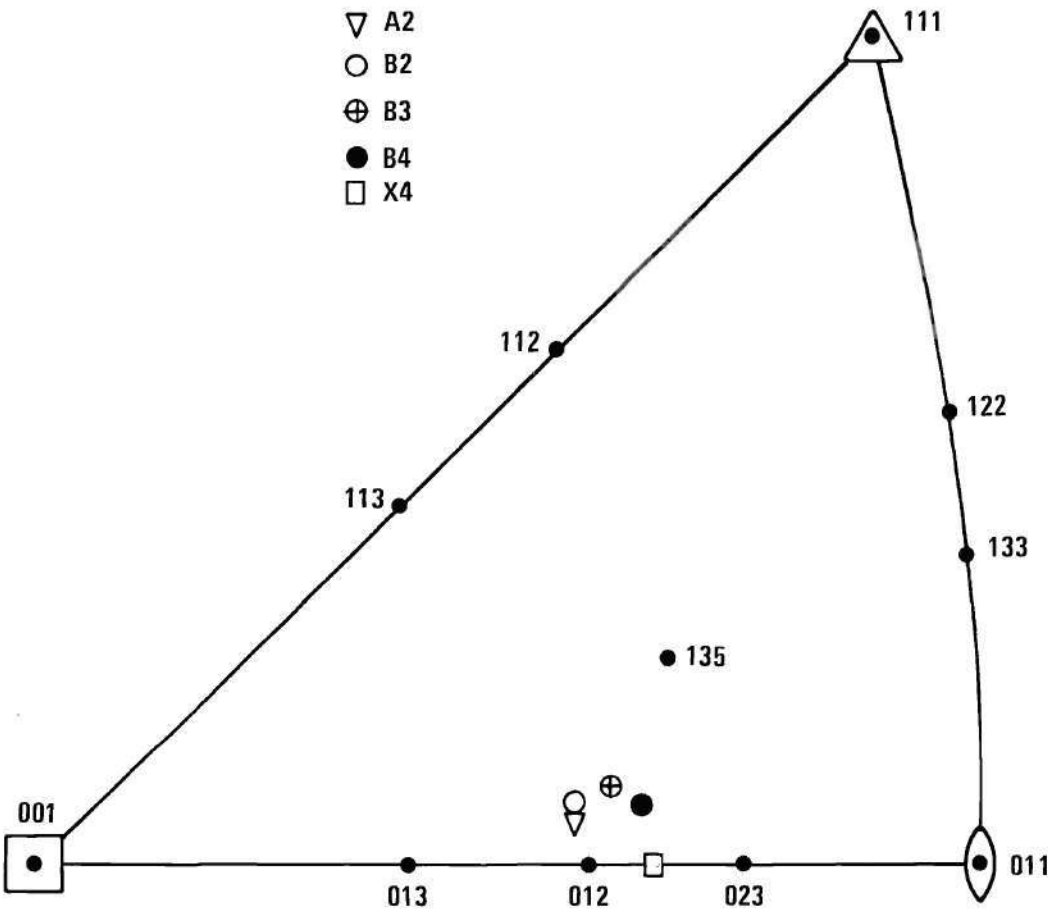

Figure 21. Summary of Results of the Two-Surface Trace Analysis.

Figure 22. End of Crack Trace on the (112) Side of Specimen C1; Optical Micrograph (Surface lightly polished and etched, Magnification 2,200x).

that the trace is made of short segments, directions of many of them being consistent with the direction of the traces of {210} planes.

To examine this further, fractography and sectioning of the specimen C2 was carried out. The electron scanning micrograph of a typical area of the fracture surface, presented in Figure 23a, shows ridges running approximately in the direction of crack propagation. A cut parallel to the $(13\bar{1})$ orientation, which is close to perpendicular to the general orientation of the fracture surface, was made by spark-planing and the profile was examined in the electron scanning microscope. The micrograph of the profile in Figure 23b shows that the directions of the traces of the sides of the ridges are consistent with the $(20\bar{1})$ and $(\bar{1}02)$ orientations. Since only a single-surface trace analysis was possible in this case the results are only tentative.

Fractography

Macroscopically most fracture surfaces were rough but often exhibited symmetrical features. A frequently observed feature was a stepped surface, such as shown in Figure 24 and 28a. Steps of this kind, with edges running roughly in the general direction of crack propagation, were most frequent in the regions where cracking started, near the roots of the notches.

Large flat and relatively smooth surface areas were observed on specimens of the B series (see Figure 19a) and on specimens A2, X1 and X4. Small flat areas were common. The fracture surface of the specimen X4 is shown in Figure 25.

A characteristic feature on specimens X2 and X3 was a highly diversified fracture surface, as shown in Figure 26.

(a)

(b)

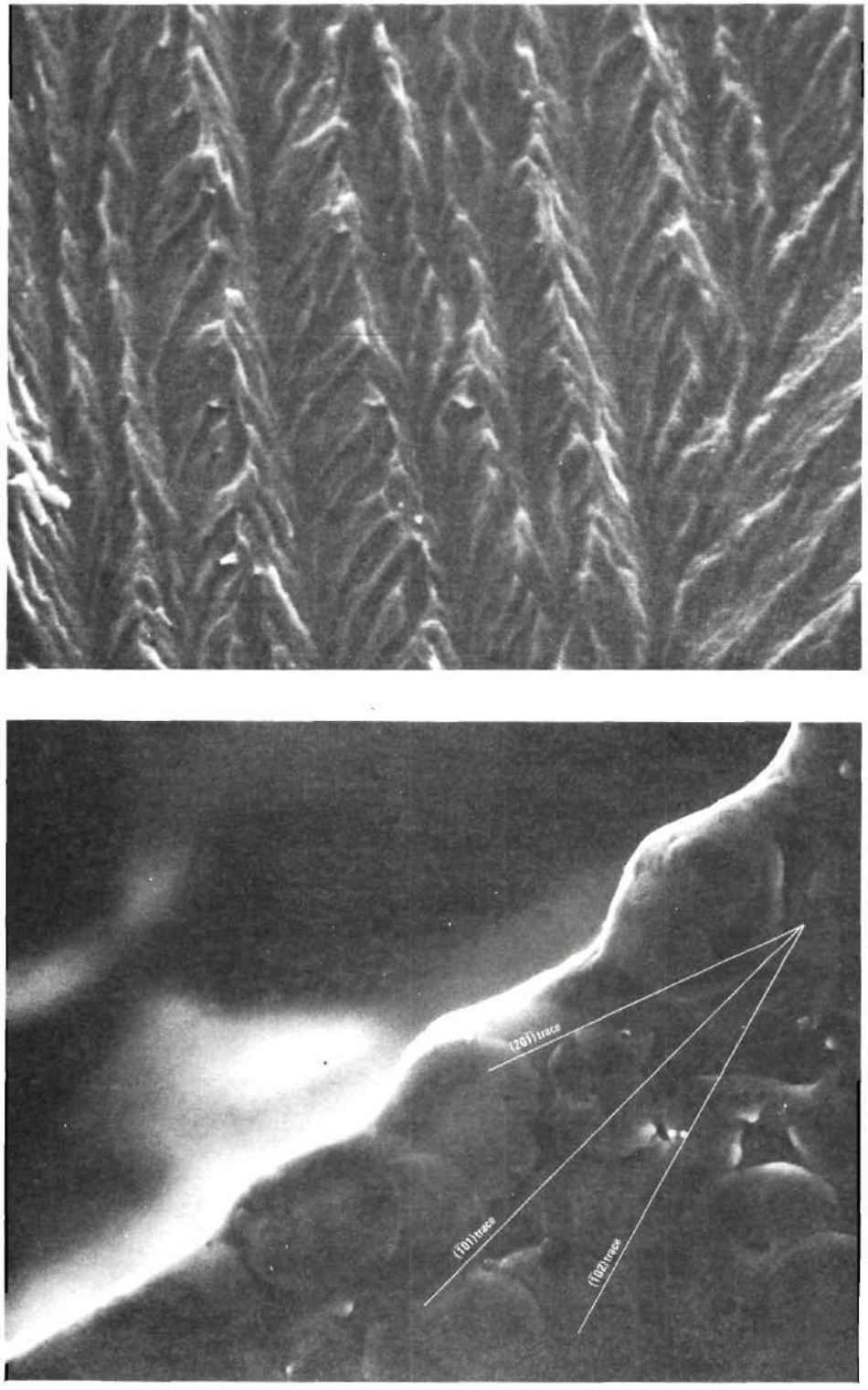

Figure 23. Ridges on the Fracture Surface of Specimen C2; (a) Scanning Electron Micrograph of the Surface (Magnification 1,150x), (b) Traces of the Walls of the Ridges on a Section (Magnification 2,900x).

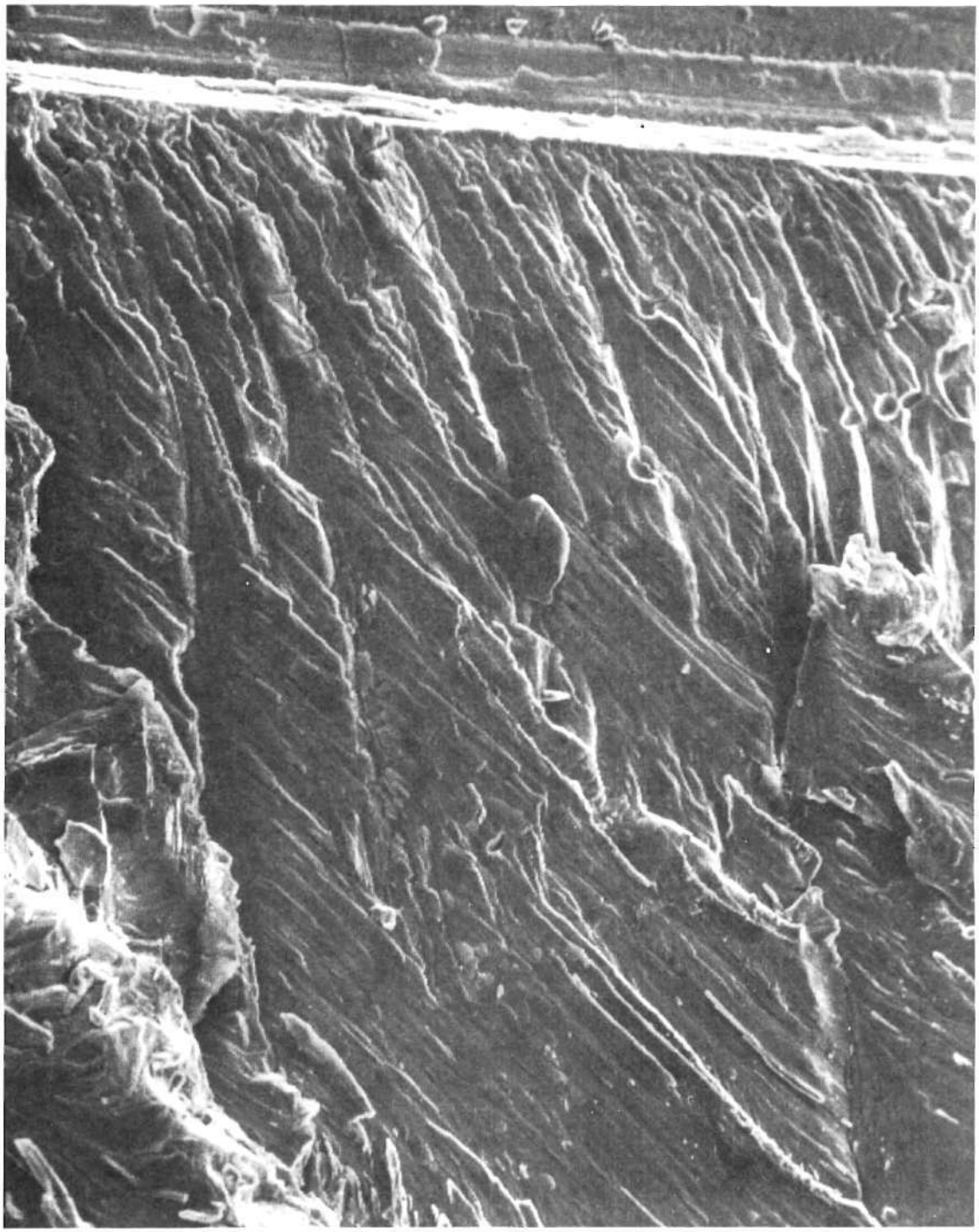

Figure 24. Fracture Surface of the Specimen A2; Stepped surface. Scanning Electron Micrograph (Magnification 250x).

Figure 25. Fracture Surface of the Specimen X4. Scanning Electron Micrograph (Magnification 500x).

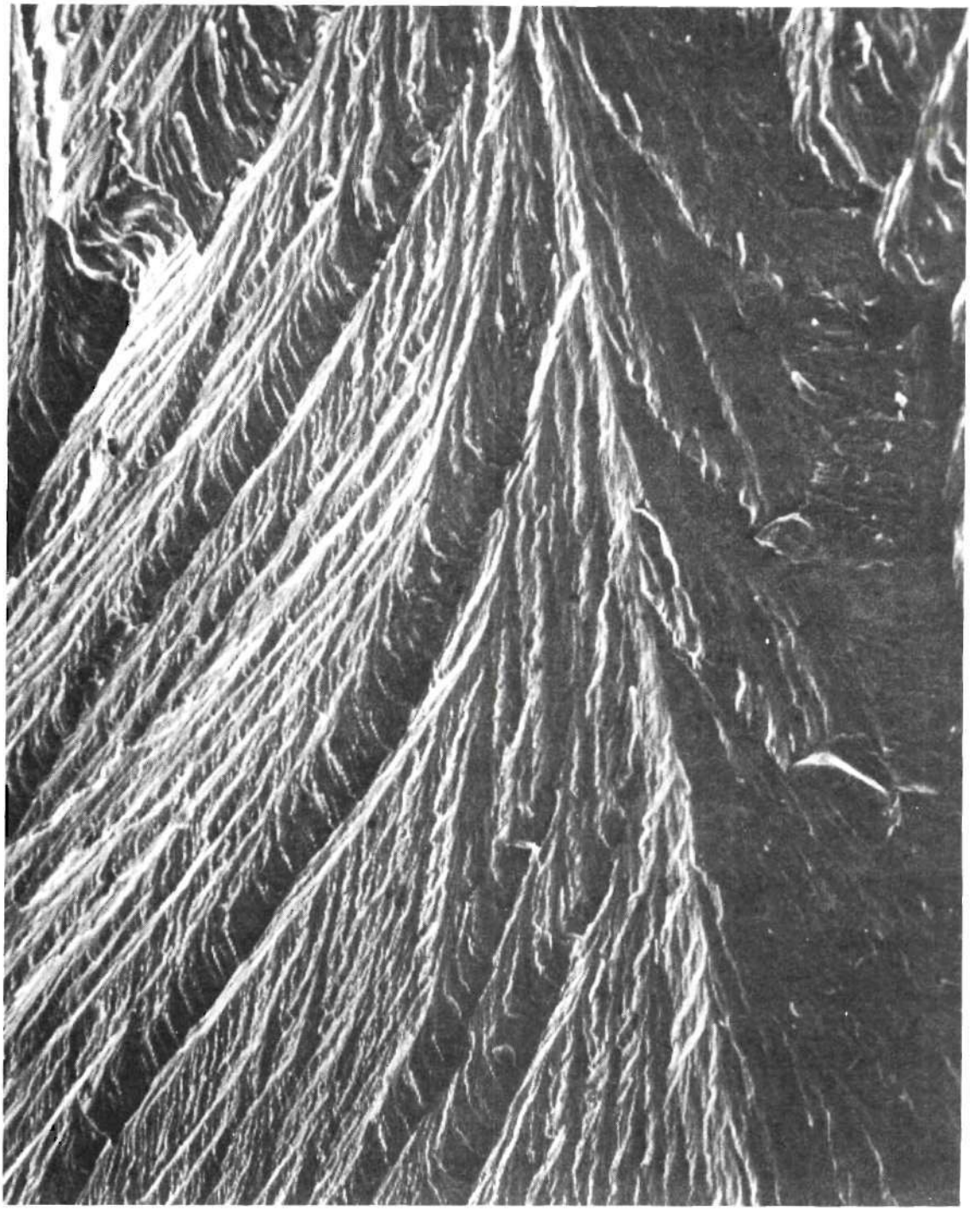

Figure 26. Fracture Surface of the Specimen X3. Scanning Electron Micrograph (Magnification 500x).

At higher magnifications several typical surface features were observed. On very smooth surfaces, such as shown in Figure 27a, two kinds of surface marks could be seen. The directions of the marks running parallel to the lines labeled a 1 and a 2 in Figure 27a were found to be consistent with directions of traces of active slip planes. Ridges observed on another area of the fracture surface of the same specimen, shown in Figure 27b, also seemed to correspond to slip traces, but on a much rougher scale. Figure 27b also shows a pronounced macroscopic crystallographic feature of the topography of cracking.

In Figure 27a other marks can also be seen as fine, shallow ridges running approximately in the general direction of crack propagation (parallel to a line labeled b). They can be seen in more detail in Figure 33 and also in Figure 32b. They were observed frequently on relatively smooth surfaces, always running in the general direction of crack propagation.

Large, macroscopically flat fracture surfaces on specimens of the B series consisted of smooth, flat regions bound by low, irregular steps, as shown in Figure 28b. Examination at high magnification did not reveal any details. In areas closer to the specimen sides the surfaces were less smooth, as shown in Figure 29. This appearance was frequent on all specimens.

On specimens of the A and E series the fracture surfaces, as observed at high magnifications, had either a feather-like appearance, as shown in Figure 30a, or exhibited sharp-edged striations, as shown in Figure 30b and in more detail in Figure 31.

Specimens of the C series exhibited many ridged areas, as shown

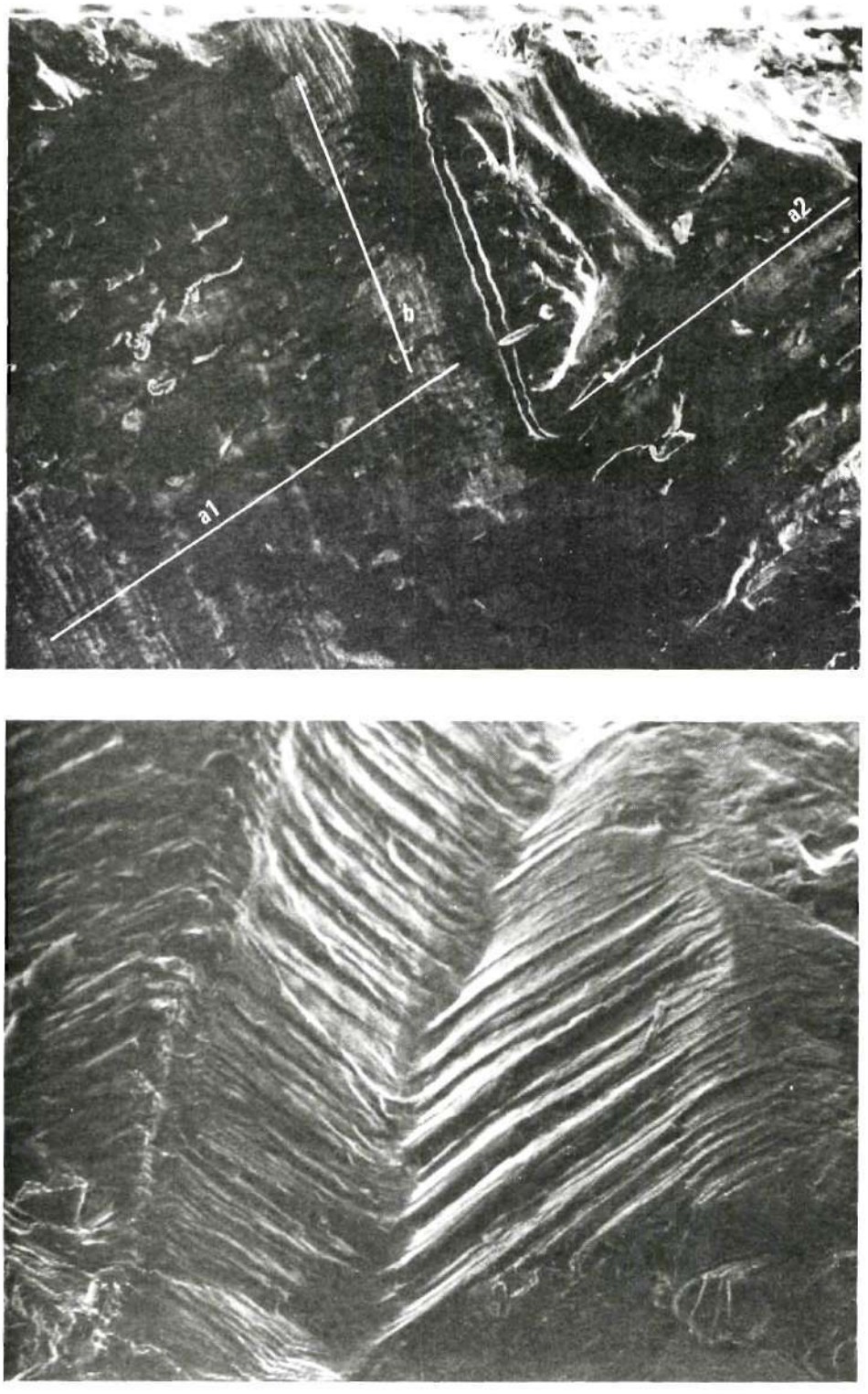

Figure 27. Fracture Surface of the Specimen X1. Scanning Electron Micrographs: (a) Area with a Grain Boundary Trace (Magnification 320x), (b) Crystallographic Feature (Magnification 240x).

(a)

(b)

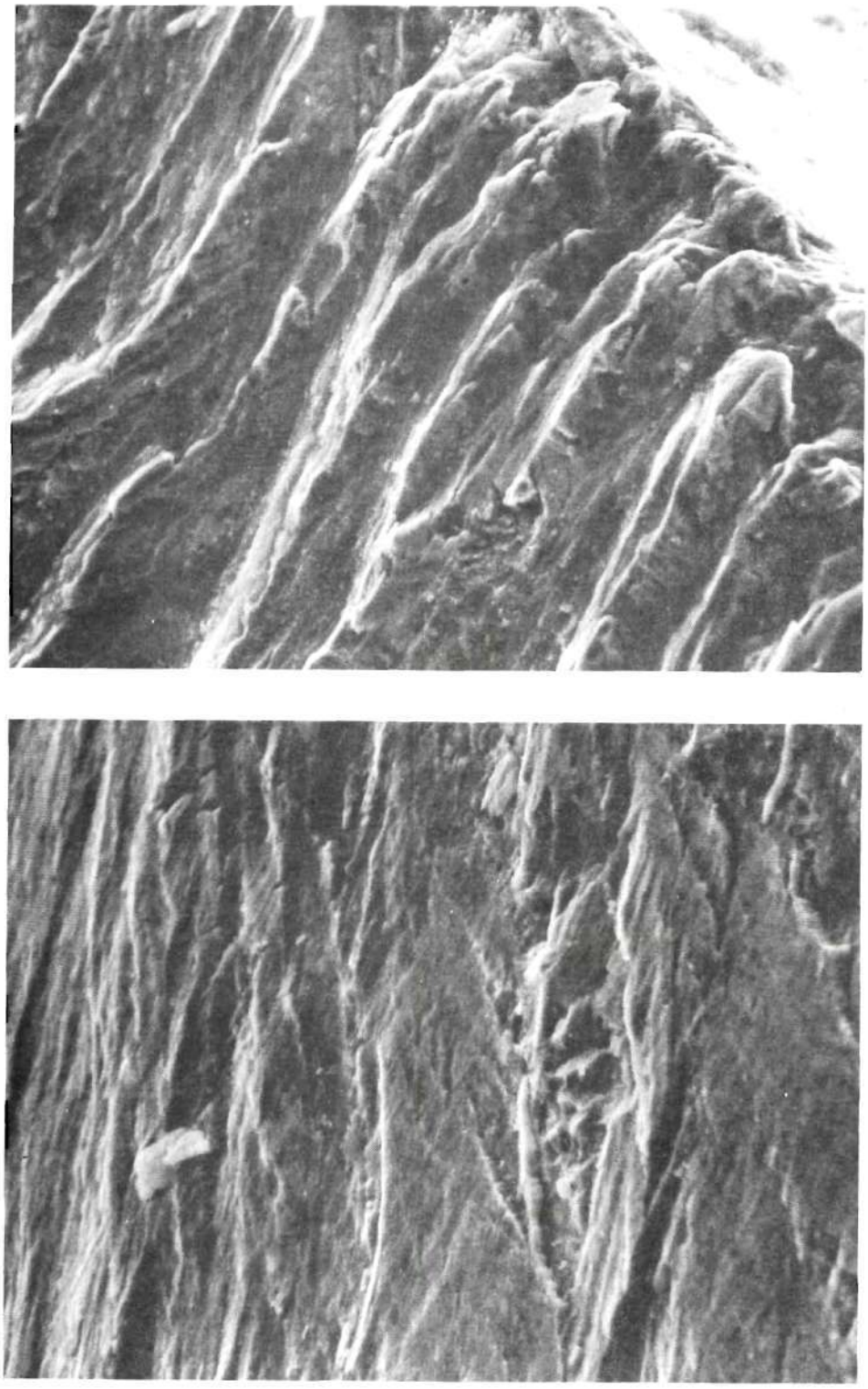

Figure 28. Fracture Surface of the Specimen B3. Scanning Electron Micrographs: (a) Area at the Notch (Magnification 1,650x), (b) Area Distant from the Notch (Magnification 2,000x).

Figure 29. Typical Fracture Surface Features: Cleavage-like Surface (Specimen B3). Scanning Electron Micrograph (Magnification 3,000x).

(a)

(b)

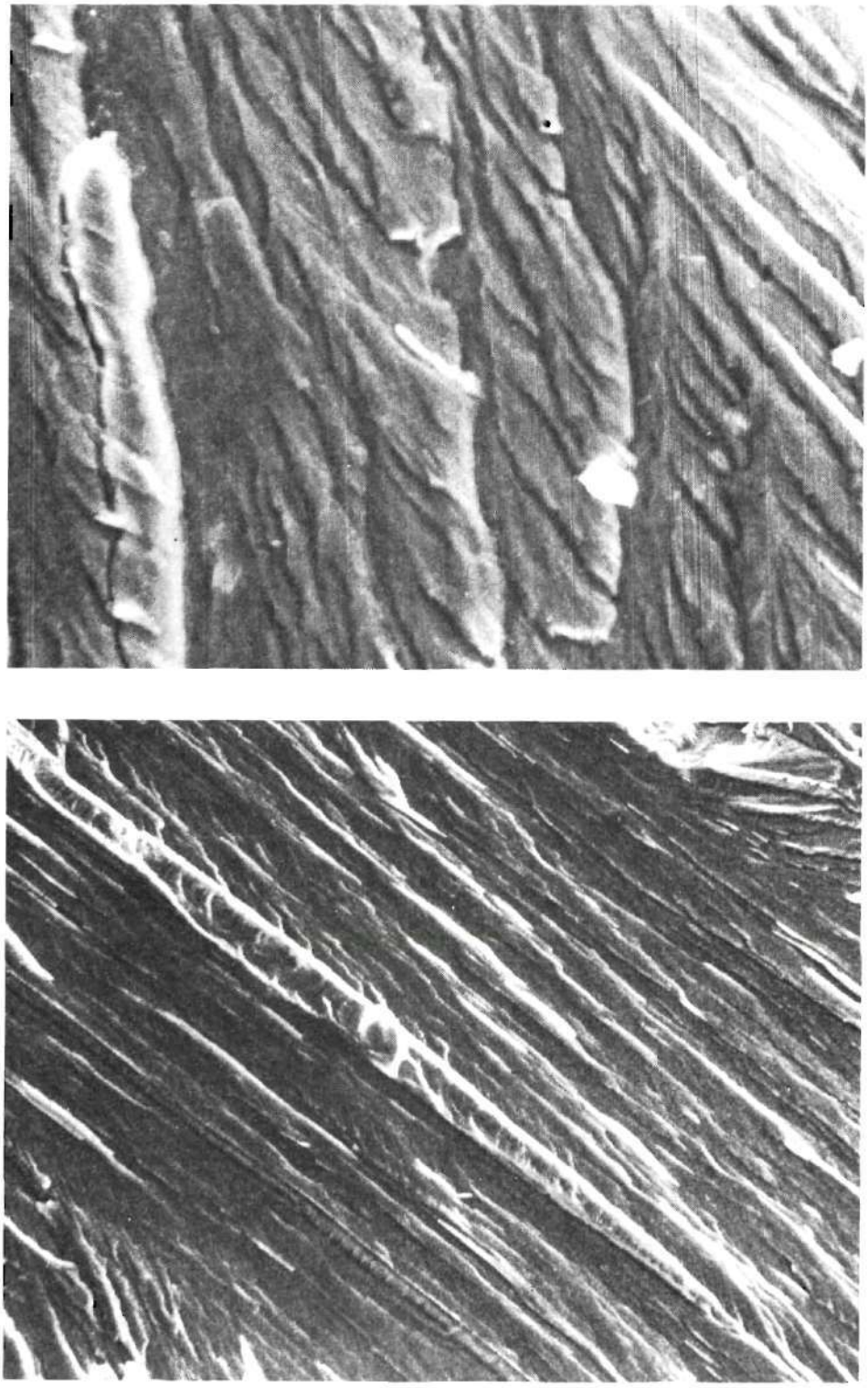

Figure 30. Typical Fracture Surface Features. Scanning Electron Micrographs: (a) Feathery Surface, Specimen A2 (Magnification 2,100x), (b) Striations, Specimen A1 (Magnification 1,000x).

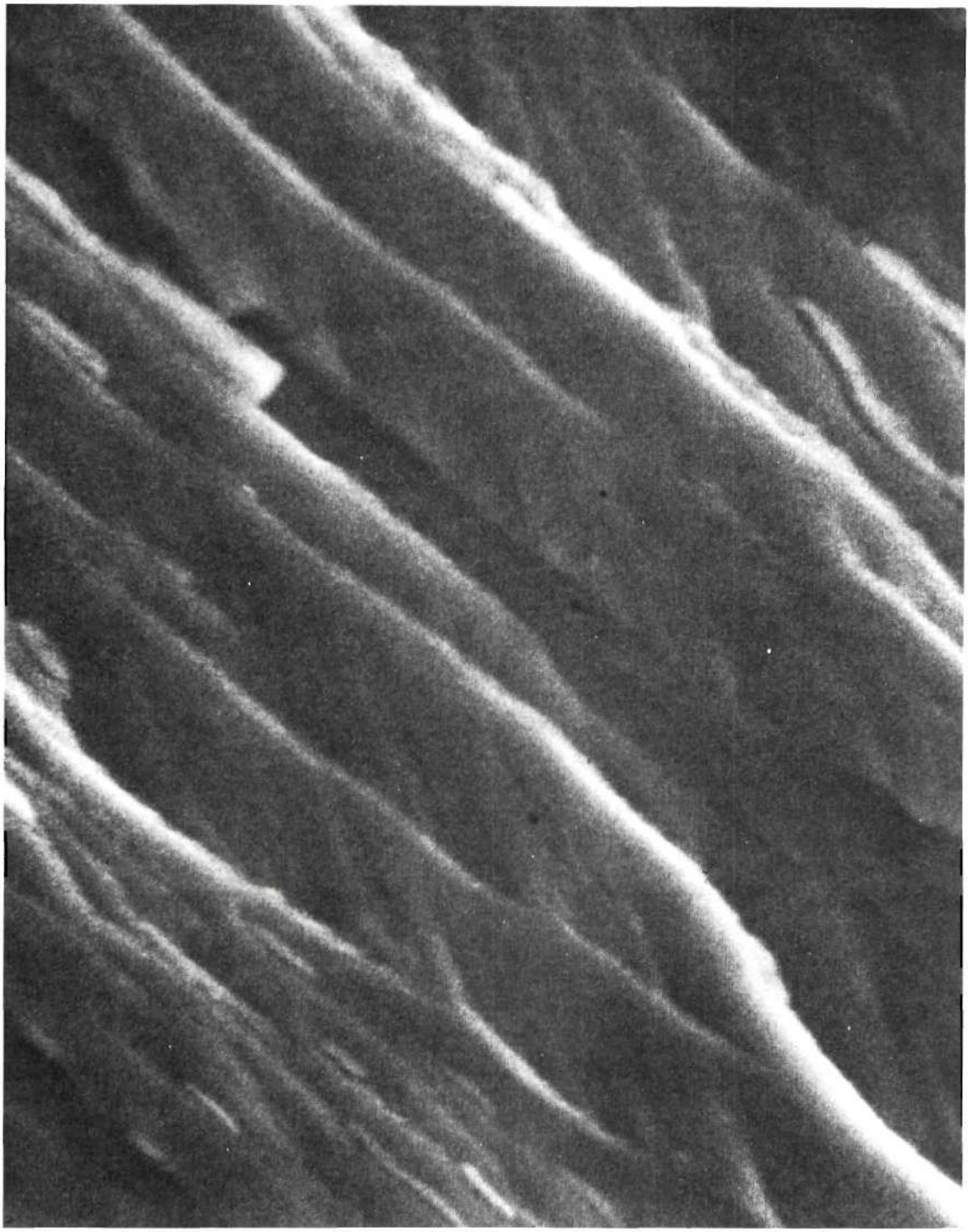

Figure 31. Typical Fracture Surface Features: Striations at High Magnification, Specimen A1. Scanning Electron Micrograph (Magnification 12,600x).

earlier in Figure 23. A large number of steps, with edges roughly perpendicular to the general direction of crack propagation, were found as shown in Figure 32. Surface areas similar to those found in specimens of the other series were also observed.

Specimen X1 was unique among all the tested specimens in that a grain boundary ran through the cracked region. In Figure 27a the boundary trace can be seen running roughly in the vertical direction on the fracture surface. A subcrack that developed on the boundary is shown in detail in Figure 33. The surface is partly covered with a film of corrosion products.

Other Observations

Morphology of Cracking. In all notched specimens cracks were initiated at the roots of the notches and propagated from there, except for the specimen A2 in which the crack deviated from the notch. In the unnotched specimens several cracks were usually initiated along the region of highest stress.

In some of the notched specimens a single crack developed (see Figure 15a), in others two symmetrical cracks (see Figure 15b) were found, and still other specimens exhibited more extensive branching (see Figure 14a, b, and 16a). This information is included in Table 5 in the Appendix.

Very short cracks branching from the main cracks, as for example in Figure 14a, were usually limited to the surface zone and did not penetrate the specimen laterally. (Subcracks initiated inside the specimens were also observed.) They were, however, real subcracks, branching from other cracks and exhibiting pronounced crystallographic dependence. On

(a)

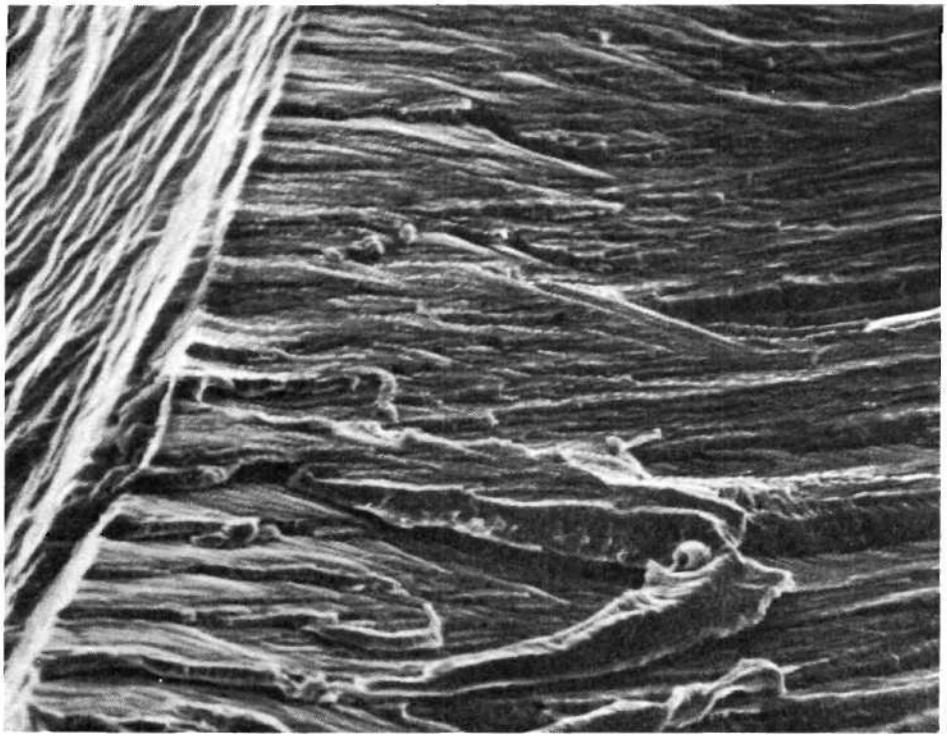

(b)

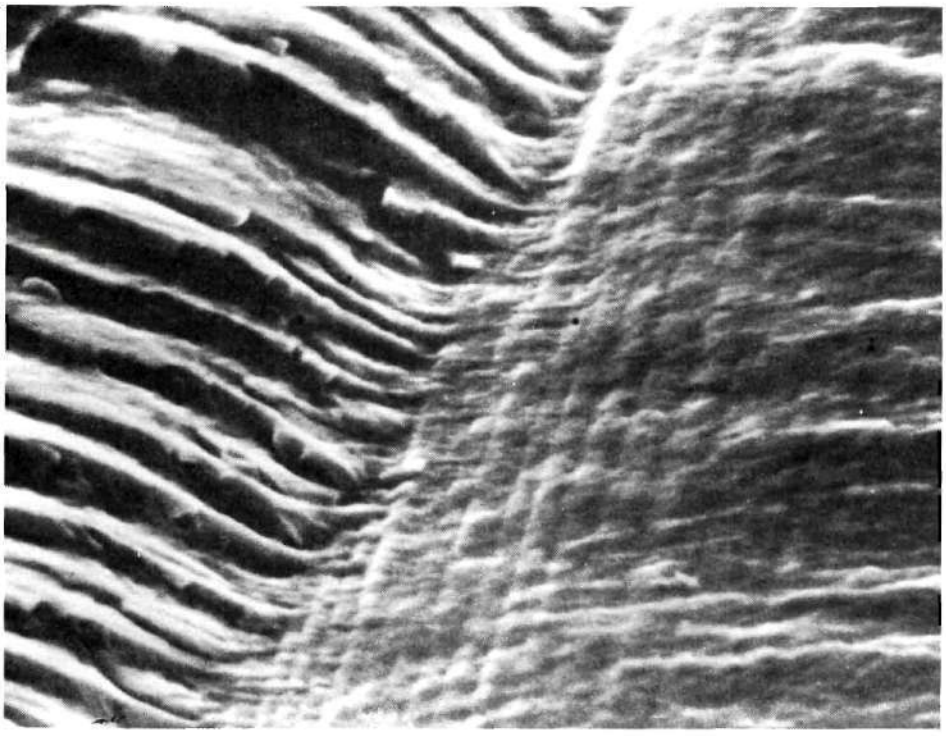

Figure 32. Typical Fracture Surface Features. Scanning Electron Micrographs: (a) Steps, Specimen C2 (Magnification 1,200x), (b) Steps and Grooves, Specimen C2 (Magnification 7,600x).

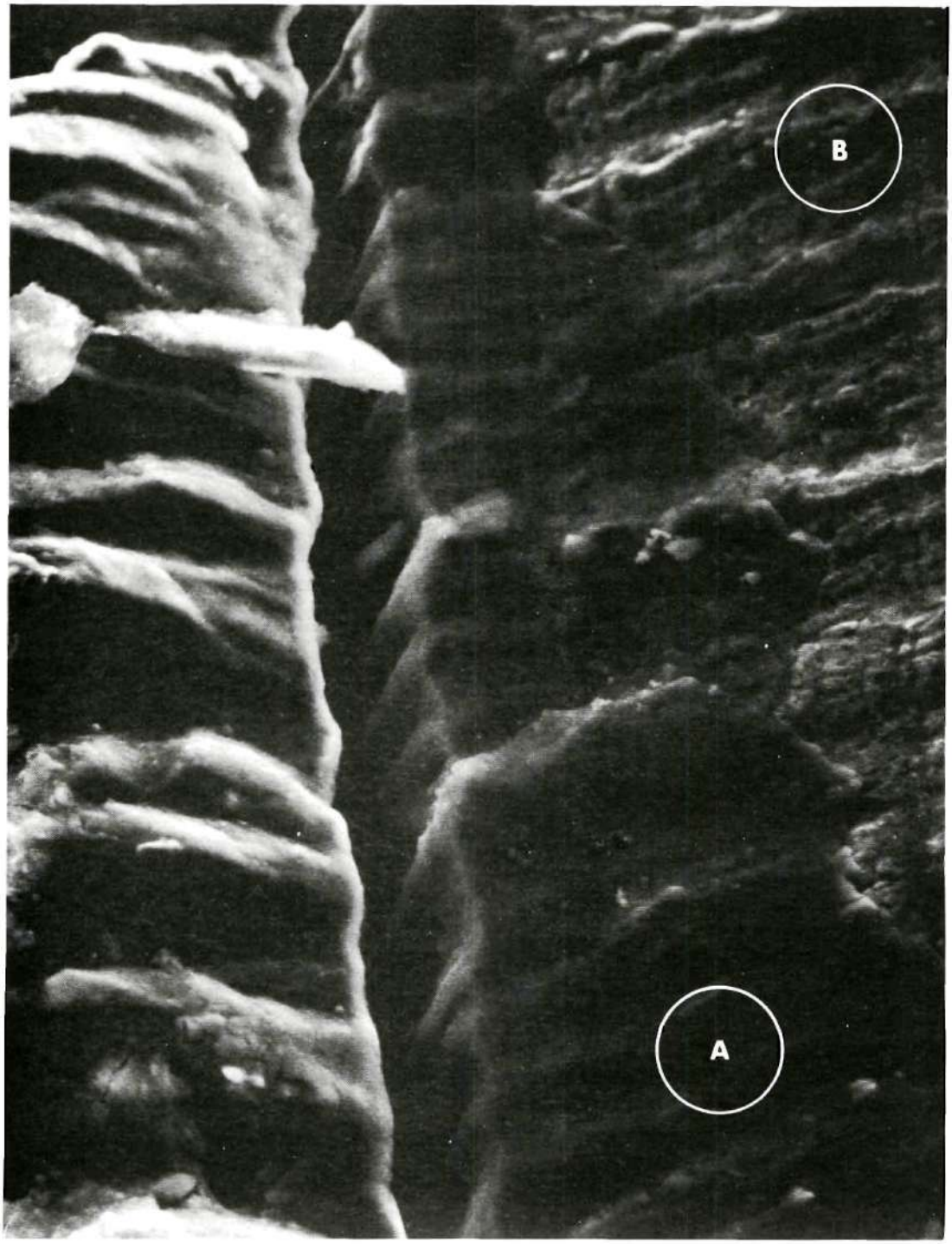

Figure 33. Subcrack on Grain Boundary in Specimen X1. Scanning Electron Micrograph (Magnification 2,670x; Circles labeled A and B indicate the areas where a non-dispersive X-ray analysis was performed).

the other hand, cracks not connected with those propagating from the notch were also observed on the surfaces. These were obviously initiated on the side surfaces and did not penetrate to a great depth. An example is presented in Figure 34 which shows the side of the specimen B2 after the test and after removing surface layers to a depth of 0.10 mm and 0.20 mm. These surface cracks were less strongly crystallographic, if at all.

Surface Attack. An attack on slip steps was evident on most specimens. Scanning electron micrographs in Figure 35 show the details of the attack.

The edges of the crack surfaces on the sides of the specimens were also severely corroded. The appearance of the crack traces, as in Figures 14 to 16, is greatly affected by this attack. Actually the majority of observed cracks were hairline cracks after propagating a short distance from the notch, except in cases when a high load was applied and opened the cracks.

Corrosion Products. In the course of the scanning electron microscopy of fracture surfaces an attempt was made to investigate the composition of the corrosion product film adhering to the fracture surfaces in a few areas. A non-dispersive X-ray analysis was made subsequently on the surface covered with the film (labeled A in Figure 33), and on the neighboring bare metal surface (labeled B in Figure 33). The same collecting times and electrical parameters were used in both tests. The resulting two curves are shown in Figure 36. The analysis is semi-quantitative, the comparison of the heights of corresponding peaks being an approximate measure of the differences in the concentration of the elements. The comparison shows that iron and nickel are present in

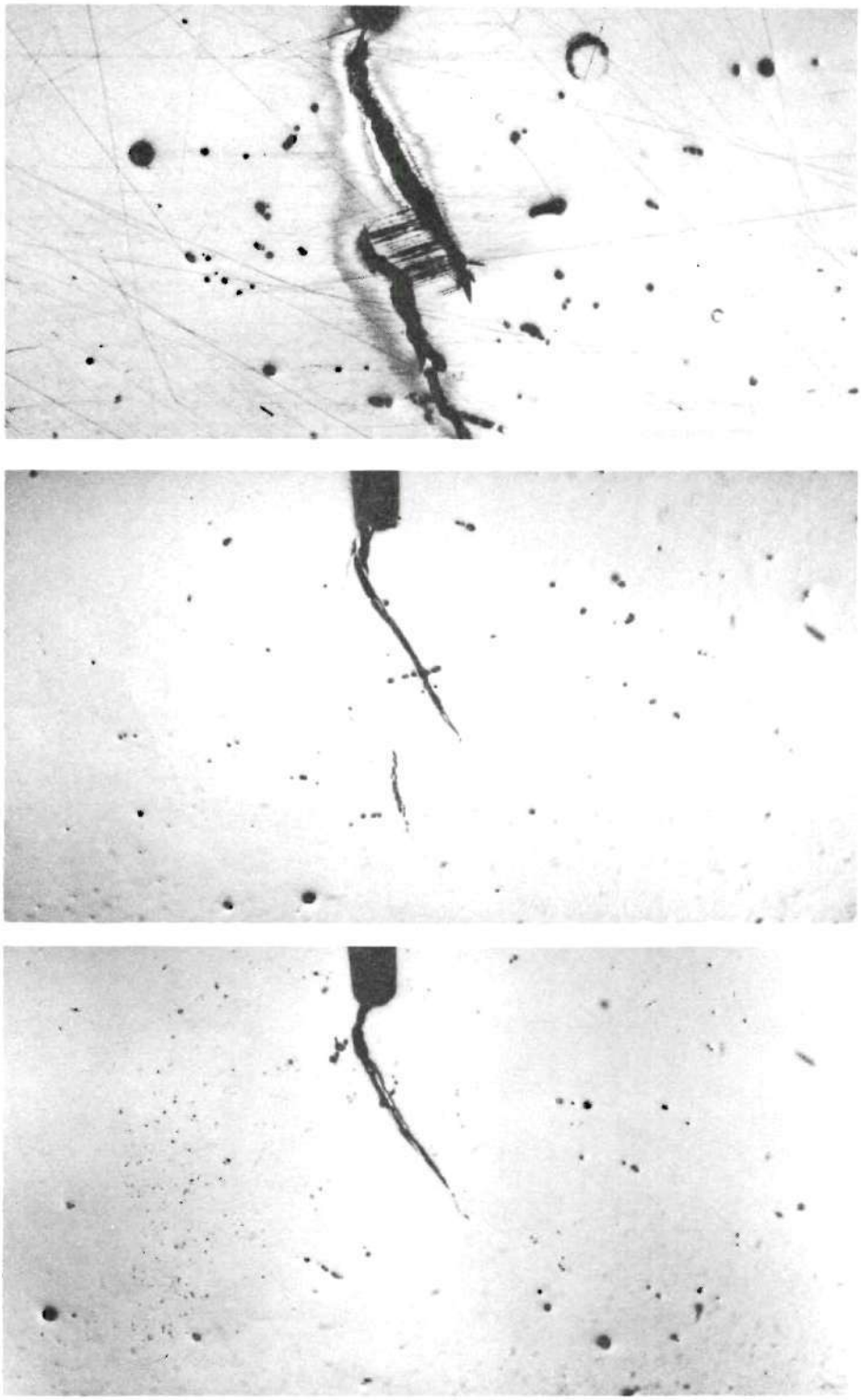

(a)

(b)

(c)

Figure 34. Crack Traces on Specimen B2: (a) Surface of a Side after the Test, (b) and (c) Same side after Grinding off 0.10 and 0.20 mm, respectively.

(a)

(b)

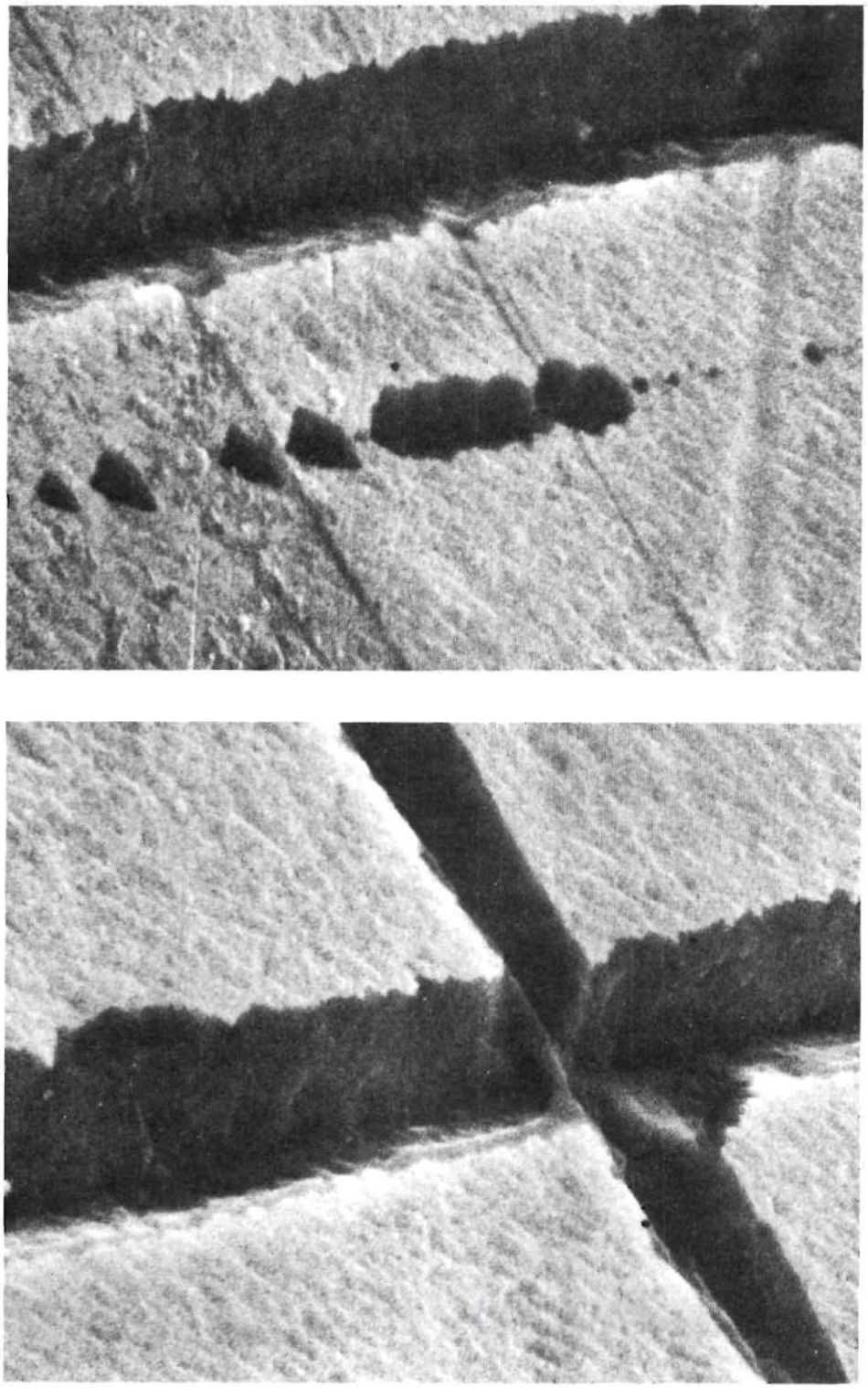

Figure 35. Corrosion Attack on Slip Steps; Specimen X2. Scanning Electron Micrographs (Magnification of both 11,500x).

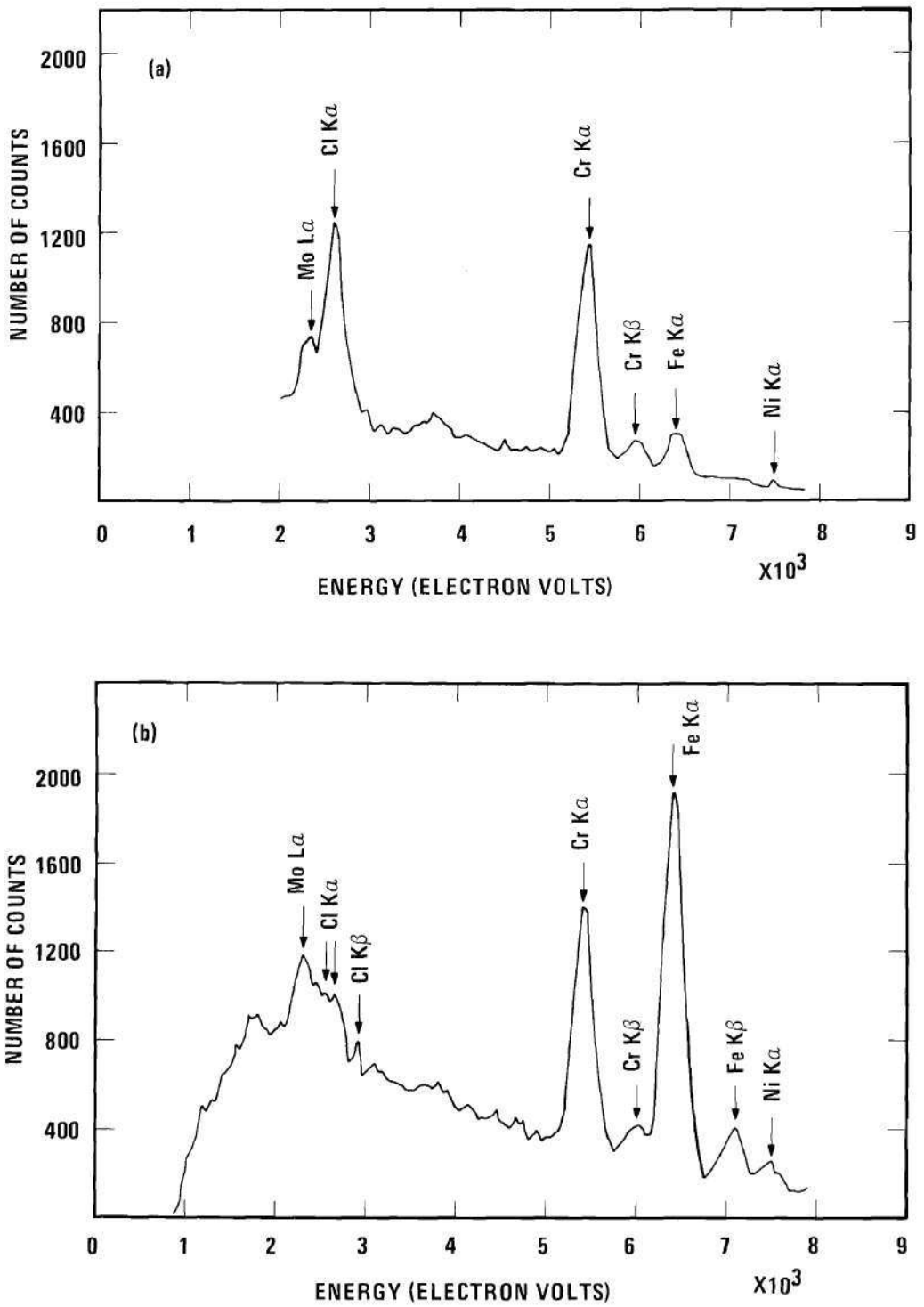

Figure 36. Results of a Non-dispersive X-ray Analysis on the Fracture Surface of Specimen X1 (Graph (a) for surface covered with corrosion products, graph (b) for bare surface).

considerably lower quantities in the corrosion product than in the substrate, despite the fact that some contribution to the emission from the substrate may be expected. Unfortunately it is difficult to estimate the effect that an eventual enrichment of the surface layer of the metal by some elements might have on the analysis. A microprobe analysis, which has a similar depth of penetration, did not show any systematic differences between freshly prepared surfaces and fracture facets.

A microprobe analysis of a corrosion product extracted from inside of one of the deep pits in specimen B1 after a 200 hour exposure to the testing solution was made. The only metallic element found was chromium.

Kinetics of Crack Propagation

An analysis of crack propagation kinetics was made possible by the monitoring of load variations during the tests. First the time when propagation started, i.e. the end of the induction period, had to be accurately determined. This was accomplished by plotting the logarithm of the rate of load change against the logarithm of time. The onset of crack propagation was marked by a sharp change of the slope of the plot.

Then a relation, F, between the relative change of load and the crack length was found empirically by plotting the data obtained at the end of each test, as shown in Figure 37. The relation is of the form

$$\frac{Q_o - Q}{Q_o} = F\,(l_c . \sin \alpha)$$

where Q_o is the load at the end of the induction period,

Q is the load at time t,

l_c is the average crack length at time t,

α is the angle between the trace of the crack on the side of the specimen and the edge.

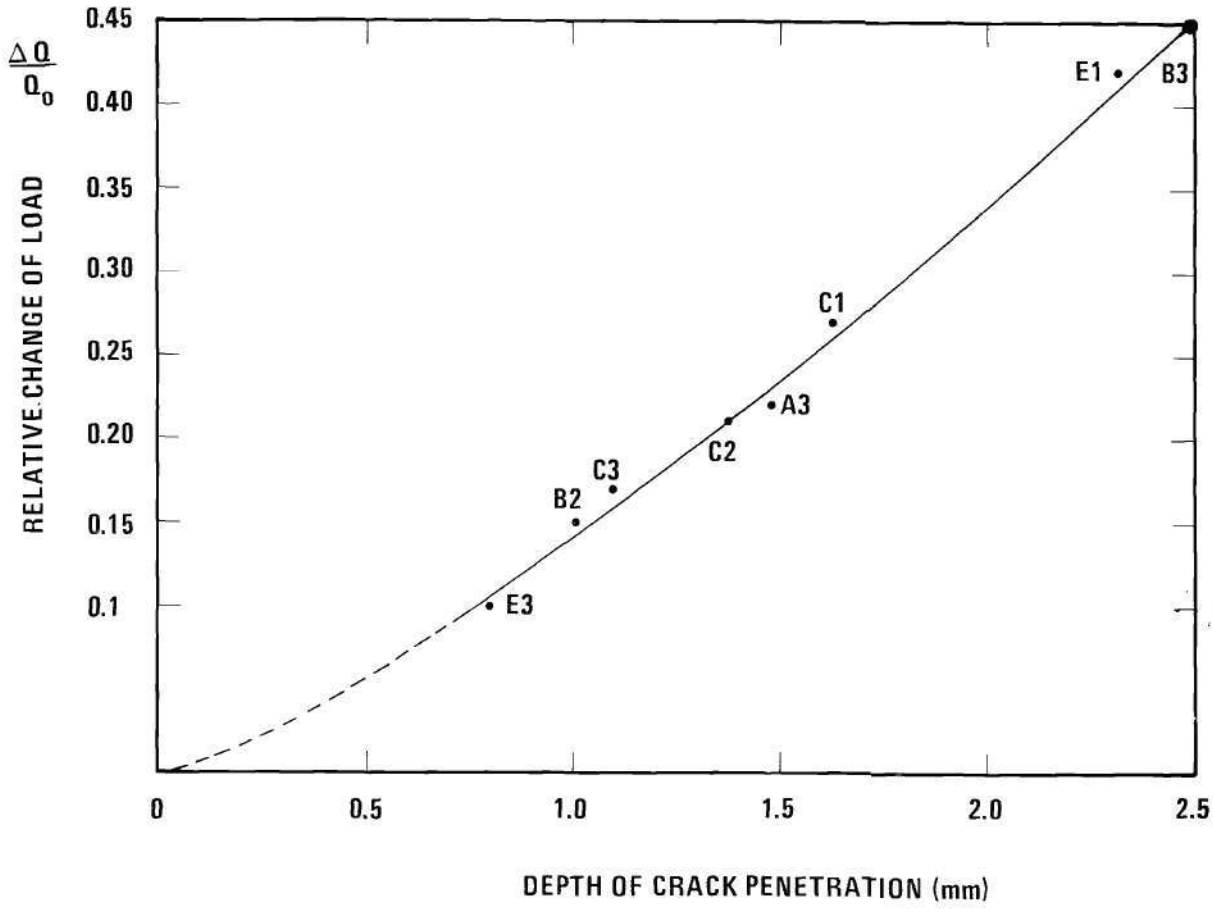

Figure 37. Calibration Curve: Relation Between Relative Change of Load and Depth of Crack Penetration in the Loading System Used in this Work.

The final crack lengths were determined from measurements both on the sides of the specimens and on the fracture surfaces.

The four best charts were selected for the analysis. Actually a slightly different curve was used in each case, similar in shape to the one in Figure 37 but passing through the proper end point. The crack length at the end of each 100 minute interval was obtained from the load at that point. The resulting plots are shown in Figure 38.

The plots in Figure 38 were graphically differentiated with respect to time and the propagation rates vs. time are plotted in Figure 39. The initial parts of the curves in both Figures 38 and 39 are uncertain because of the lack of experimental data for short cracks. Any error in the determination of the onset of cracking would also seriously affect the initial parts of the curves.

All the important data and results pertinent to the kinetics of crack propagation are summarized in Tables 7 and 8 of the Appendix.

The induction period was not investigated. Since the true magnitude of the stress at the root of the notch was uncertain the results would have little meaning. An induction period definitely existed at lower loads and generally decreased with increasing load, varying from almost 100 hours to virtually zero. However, periods shorter than 50 minutes could not be distinguished.

Anodic Polarization Experiments

Potentiodynamic Polarization Curves

The results of the potentiodynamic polarization experiments are presented in Figures 40, 41 and 42 and in Table 10 of the Appendix. The

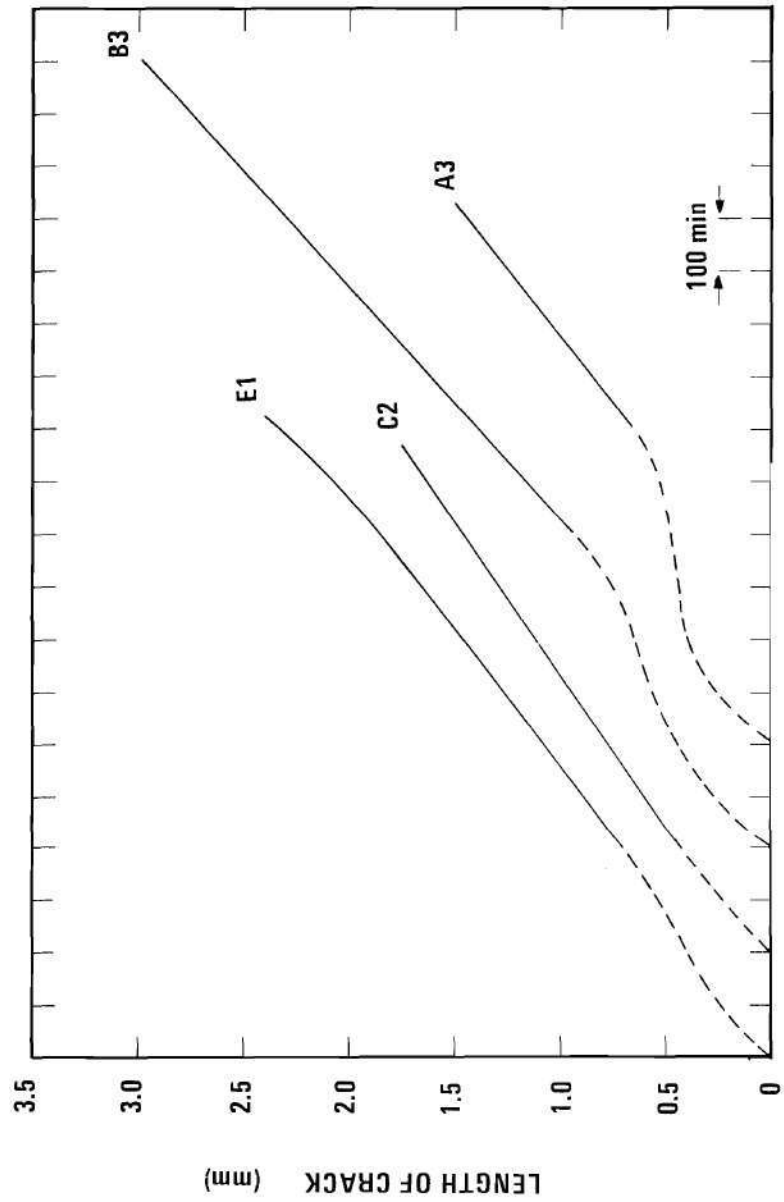

Figure 38. Crack Length as a Function of Propagation Time in Specimens A3, B3, C2, and E1.

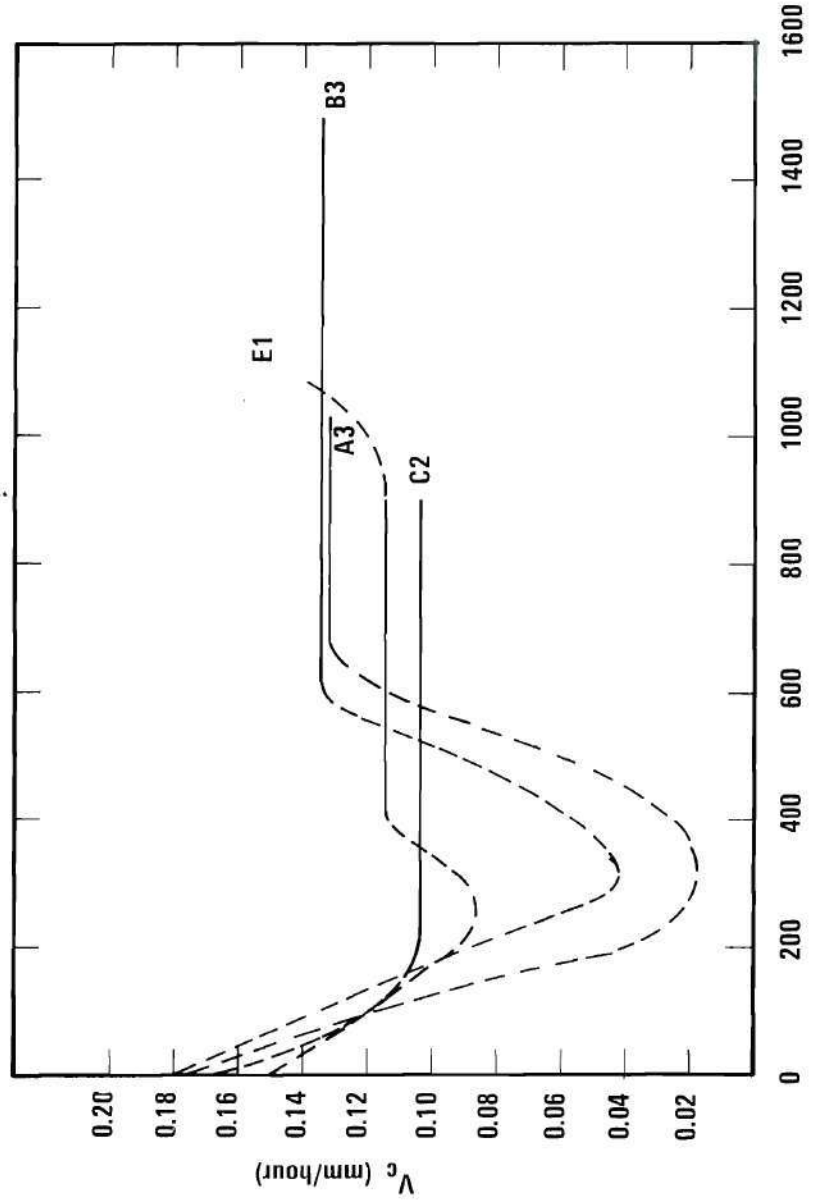

Figure 39. Crack Propagation Rates (v_c) vs. Propagation Time (t_p) in Specimens A3, B3, C2, and E1.

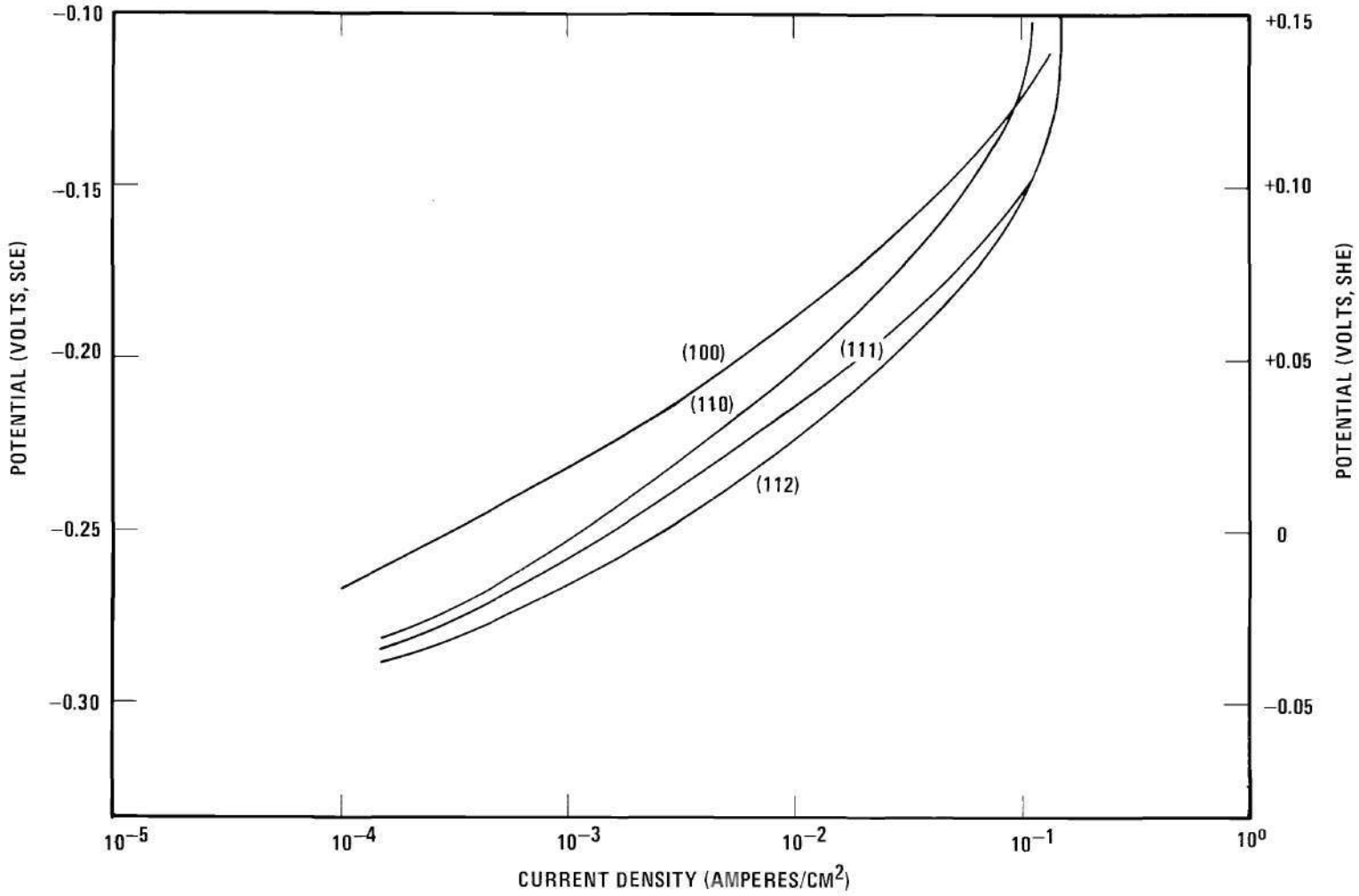

Figure 40. Anodic Polarization Curves for Various Crystal Faces, Series I: Scanning Rate 0.160 volts/minute, Electropolished Specimens.

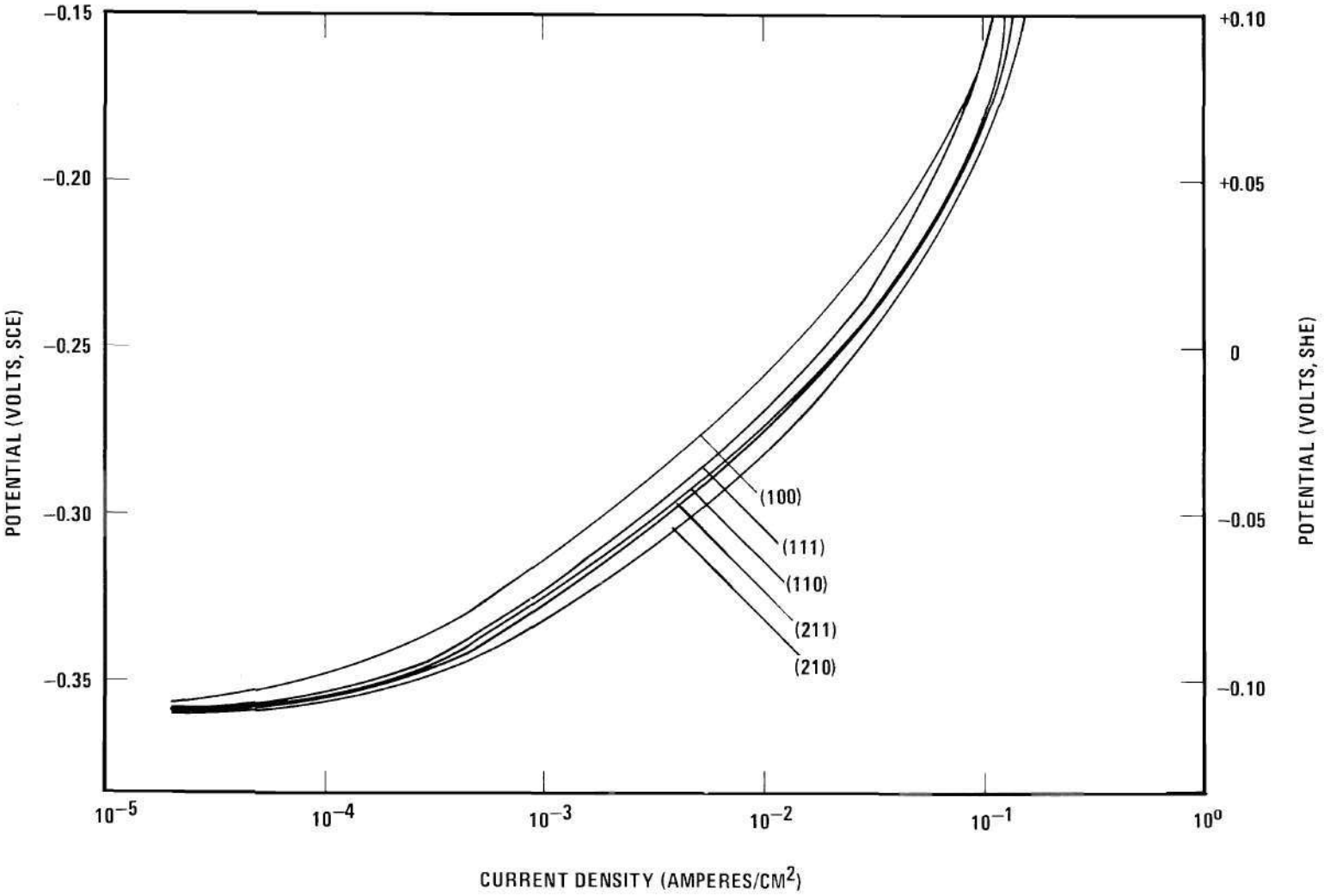

Figure 41. Anodic Polarization Curves for Various Crystal Faces, Series II: Scanning Rate 0.100 volts/minute, Electropolished and Cathodically Activated Specimens.

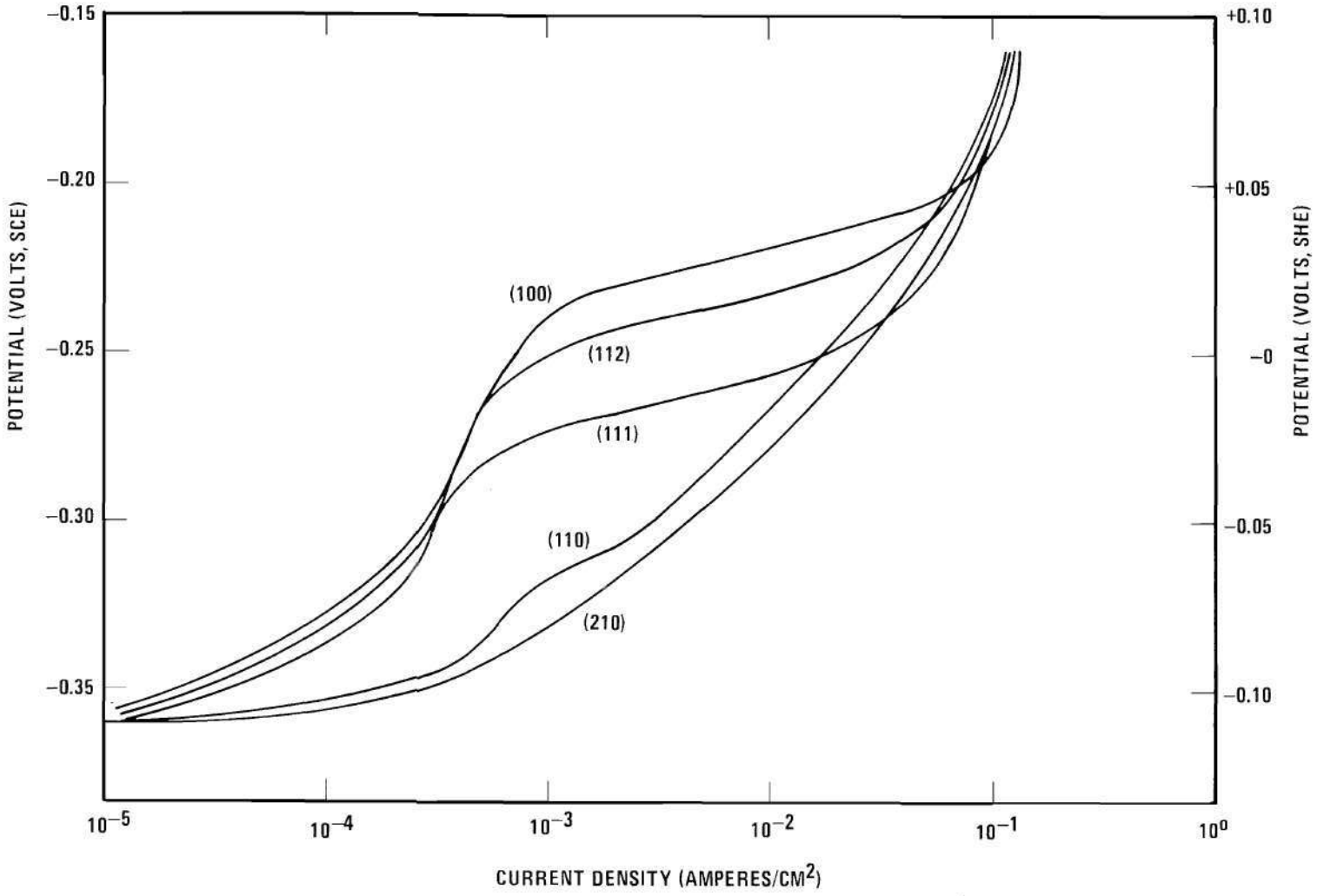

Figure 42. Anodic Polarization Curves for Various Crystal Faces, Series III: Scanning Rate 0.050 volts/minute, Electropolished and Cathodically Activated Specimens.

data from the original charts with linear current scales and switched ranges were transposed into more usual semi-logarithmic plots.

Both the values of the open-circuit potentials and the potentials in the polarization data are accurate to within $\pm$ 1 millivolt throughout the experiments, but only approximate on the absolute scale because no corrections were made for junction potentials, thermal gradients, or IR drops. For a comparison with data from the literature shown in Figure 1 a hydrogen scale is also marked in Figures 40 to 42. These values were obtained by adding 0.250 volts to the potential differences measured against the saturated calomel electrode and are thus only approximate.

The results show the following general features:

a. No differences in open circuit potentials were found on similarly prepared samples.

b. No indication of passivation was observed at potentials between the open-circuit potential and -0.100 volts [SCE].

c. The overpotentials on the various crystal faces increased in the order $\eta_{\{210\}} < \eta_{\{110\}}$, $\eta_{\{211\}} < \eta_{\{100\}}$. The overpotentials on the {111} face were close to those on the {110} and {211} faces.

d. The polarization curves converged to a limiting current density of approximately 0.15 amps/cm^2.

The variations in the experimental procedure produced the following changes in results:

1. The open-circuit potential of electropolished specimens was -0.310 to -0.315 volts [SCE], as measured after 15 minutes of exposure to the solution. The cathodically activated specimens exhibited a potential of -0.360 to -0.363 volts [SCE]. This indicates that a protective film

was removed by activation.

2. Differences in overpotentials on various faces were more pronounced in the first series of experiments (electropolished specimens, faster potential scanning) than in the second series (activated specimens, slower scanning).

3. In the third series (activated specimens, slowest scanning) a significant change in the shape of some of the curves took place (Figure 42).

Other Observations

A surface film was found on the surfaces of the specimens after the experiments. In some cases it could be locally peeled off, in other cases it seemed to be quite adherent. On surfaces that were not polarized to potentials more noble than -0.160 volts [SCE], a microscopic examination revealed a large number of small pits. At more noble potentials large, deep pits developed. Faceting was not observed in the microscopy examination (optical), only slight surface roughening on the {111} oriented surfaces.

CHAPTER V

DISCUSSION OF RESULTS

Interpretation of Experimental Data

Crystallography of Cracking

The examination of the crack traces on the side surfaces of the specimens showed conclusively that the cracking was crystallographic. Crack traces were mostly straight, often symmetrical, not perpendicular to the direction of the maximum tensile stress, and the directions varied with orientations of the specimens. On specimens of the same orientation the angular differences between the directions of the main cracks were almost always within 4 degrees.

The single-surface trace analysis narrowed the possibilities of the cracking plane orientation. Despite the ambiguity of this type of analysis, as discussed in Chapter IV, some conclusions concerning the lowest index planes could be made:

a. The examination of the specimens of the B series proved positively that the cracks did not follow macroscopically any {111} slip plane or any other plane oriented close to {111}. In fact, the results on this series alone limited the possibilities conclusively to the vicinity of the poles which lie on the line from the (001) to the (011) pole in the standard projection.

b. The examination of the specimens of the A and E series made the possibility that cracking occurred on either a {100} or a {110} oriented

plane very unlikely, and pointed to the vicinity of the {210} orientation. Crack traces on some of the surfaces of the C-series specimens, however, were consistent with the {110} orientation of the cracking plane.

Fortunately the cracks in all specimens of the B series penetrated in such a way that a more definite analysis was possible (see Figure 19a). The section parallel to the surface of the narrow side of the specimen B2 shows the pronounced symmetry of the fracture (Figure 18b).

The analysis of the directions of traces on the specimen B2 illustrates the ambiguity of the single-surface method. On the {110} oriented surface of the wide side of the specimens of the B series several {210} planes and one of the {110} planes (as well as other planes with poles on the same lines in the standard projection) make a trace at an angle of $54^{\circ}44'$ with the <111> oriented edges of the specimens. This agrees closely with the observed directions of the traces. On a {112} oriented section (parallel to the narrow side of the specimens) four {210} planes make traces at angles of $67^{\circ}48'$ and two {110} planes traces at angles of $58^{\circ}31'$ with the <111> oriented edges. The measurements on the section showed the angles between approximately 66° and 70°. However, the traces were not quite straight so that the difference could not definitely exclude the {110} orientation.

A more detailed crystallographic analysis, using specific indices in the arbitrary chosen reference system, shows that the {110} plane making a trace consistent with the observed one on the $(1\bar{1}0)$ surface of the side has indices (110) and that this plane intersects the (112) plane of the section in a trace making an angle of 90° with the $[11\bar{1}]$ edge. The $(0\bar{1}1)$ and $(\bar{1}01)$ planes that make traces on the (112) surface at

an angle of $58^{\circ}31'$ make traces on the $(1\bar{1}0)$ side at an angle of $70^{\circ}32'$, inconsistent with the observations. On the other hand, the traces of the (120), (210), $(\bar{1}02)$ and $(0\bar{1}2)$ oriented planes make traces consistent with the observed crack traces on both surfaces.

Even after this analysis an uncertainty remains, because the crack plane, the trace of which is observed on one of the surfaces, is not necessarily responsible for the trace on the other surface. Thus cracking on one plane might produce the observed trace on the side of the specimen, but it might be limited to the surface layer, and the observed trace on the section might be that of another plane. The observed fracture surface irregularities near the sides allowed this interpretation. In view of this it was necessary to make a conclusive two-surface trace analysis on sections through the flat, smooth areas of the fracture surfaces, as described in Chapter IV. The results, summarized in Figure 21, make the identification of the preferred cracking orientation of {210} positive.

Another observation consistent with this conclusion is that the fracture surface of the specimen X4, in which the direction of the maximum tensile stress was close to <210>, was relatively smooth and flat, as shown in Figure 25.

The analysis of the data in Tables 5, 6, and 9 of the Appendix shows that the cracks propagated on those {210} planes that were subjected to the highest normal stresses. On specimen B3 traces of a few subcracks ran in a direction consistent with cracking on {210} planes subjected to stresses considerably lower than the main crack (Figure 14a).

The multiplicity of the {210} planes explains the non-

crystallographic appearance of the fracture surfaces in polycrystalline materials or even in arbitrarily oriented single crystals. Since there are 12 planes in the {210} family in the cubic lattice there is a high probability that several of them will be subjected to stresses high enough to cause cracking. Cracks thus can alternate between several planes much more easily than if the cracking proceeded, for instance, on the {111} planes (4 planes), and the fracture surface will generally be perpendicular to the direction of the maximum tensile stress. The same consideration applies to branching.

The review of the literature on the crystallography of cracking in this system, presented in Chapter II, shows that the often expressed opinion that cracking proceeds, at least locally, on {111} oriented planes, is not supported by any reliable experimental evidence, is contradicted by a substantial amount of evidence, and can be better characterized as a case of wishful thinking. The experimental observations reported in the literature and interpreted as evidence for cracking on slip planes can almost always be attributed to the surface attack on slip steps and dislocations.

It must be emphasized, however, that the experimental evidence of cracking on {210} oriented planes, presented in this work, was obtained only in one specific system and under specific experimental conditions, so that any generalization to other, even similar systems, can be at present only tentative. Reed and Paxton's work on cracking in single crystals of a 20 Cr - 20 Ni alloy (77), in which the cracking plane was positively identified as {100}, seems to indicate that crystallography of cracking may depend on thus far unknown factors.

Surface Attack

The scanning electron micrographs, shown in Figure 35, present further evidence of the often observed attack on slip lines (see Chapter II). They show that the attack is often localized in the form of pits or tunnels. Although it seems likely that the observed trenches developed from pits, such a conclusion cannot be safely made on the basis of this evidence.

There is direct evidence that at least the surface cracks, not connected with the main cracks, develop from the sites of localized surface attack. The scanning electron micrograph presented in Figure 43 shows a small surface crack in an early stage of development. It also shows that since it has formed from individual pits or tunnels its trace may locally follow the direction of the slip steps. The trace of the main crack in this specimen, however, ran in a direction of the arrow in Figure 43, and the surface crack has also a tendency to develop in that direction, as can be seen in the upper left-hand corner of the picture.

The individual pits, such as in Figure 35a, probably result from an attack on either individual dislocations or pile-ups. The trenches, however, may well form directly along the slip steps as a result of dissolution of the highly defective lattice in and at the slip bands, as proposed by Vermilyea (91). The magnitude of the attack is obviously proportional to the amount of yielding that took place in the slip band, as shown in Figure 44. This is a scanning electron micrograph of a tip of the crack on the narrow side of an unnotched specimen in which the crack, initiated at one side, propagated both vertically and horizontally.

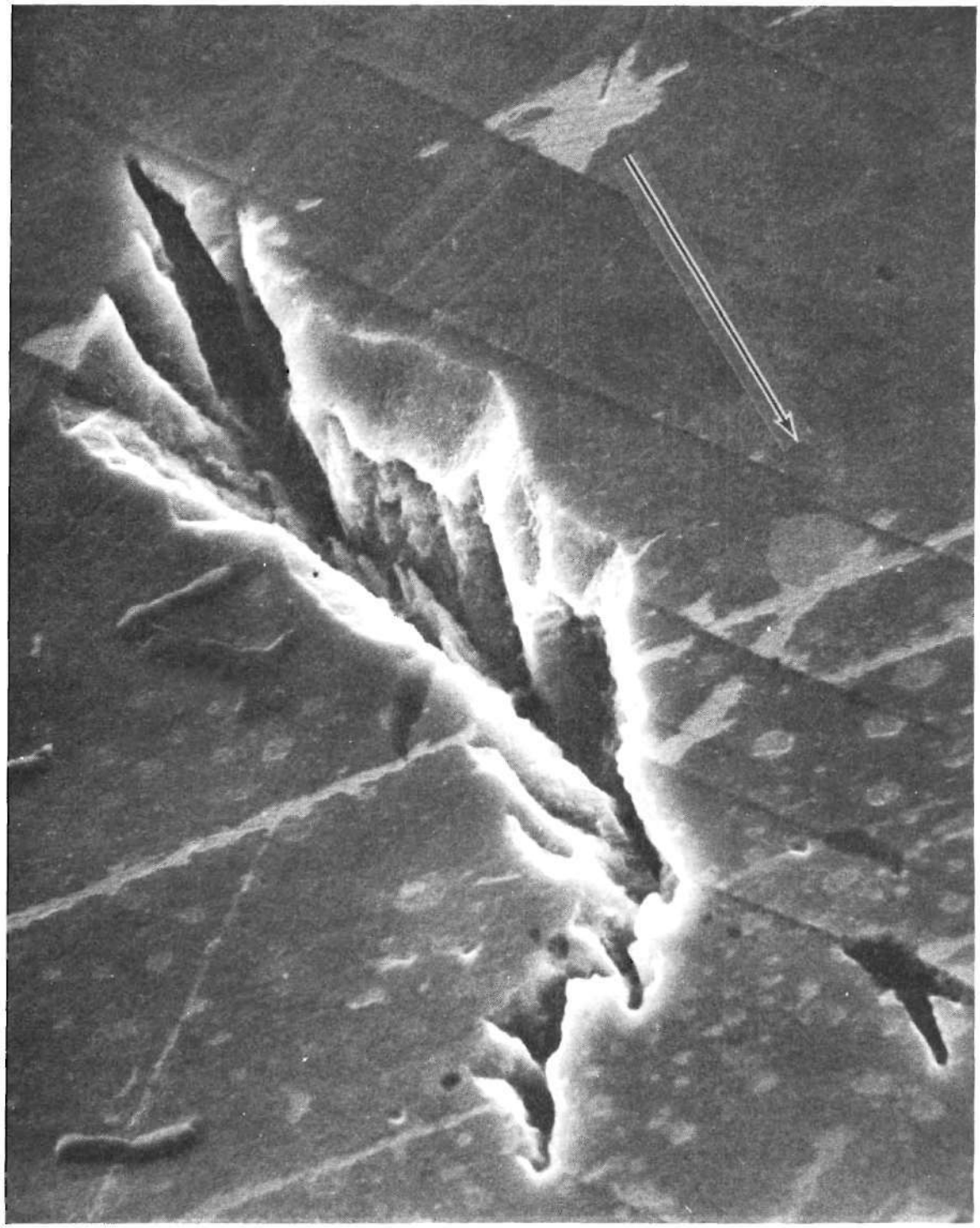

Figure 43. Surface Crack on a Side of Specimen A3. Scanning Electron Micrograph (Magnification 4,400x; the arrow indicates the direction of propagation of the main crack).

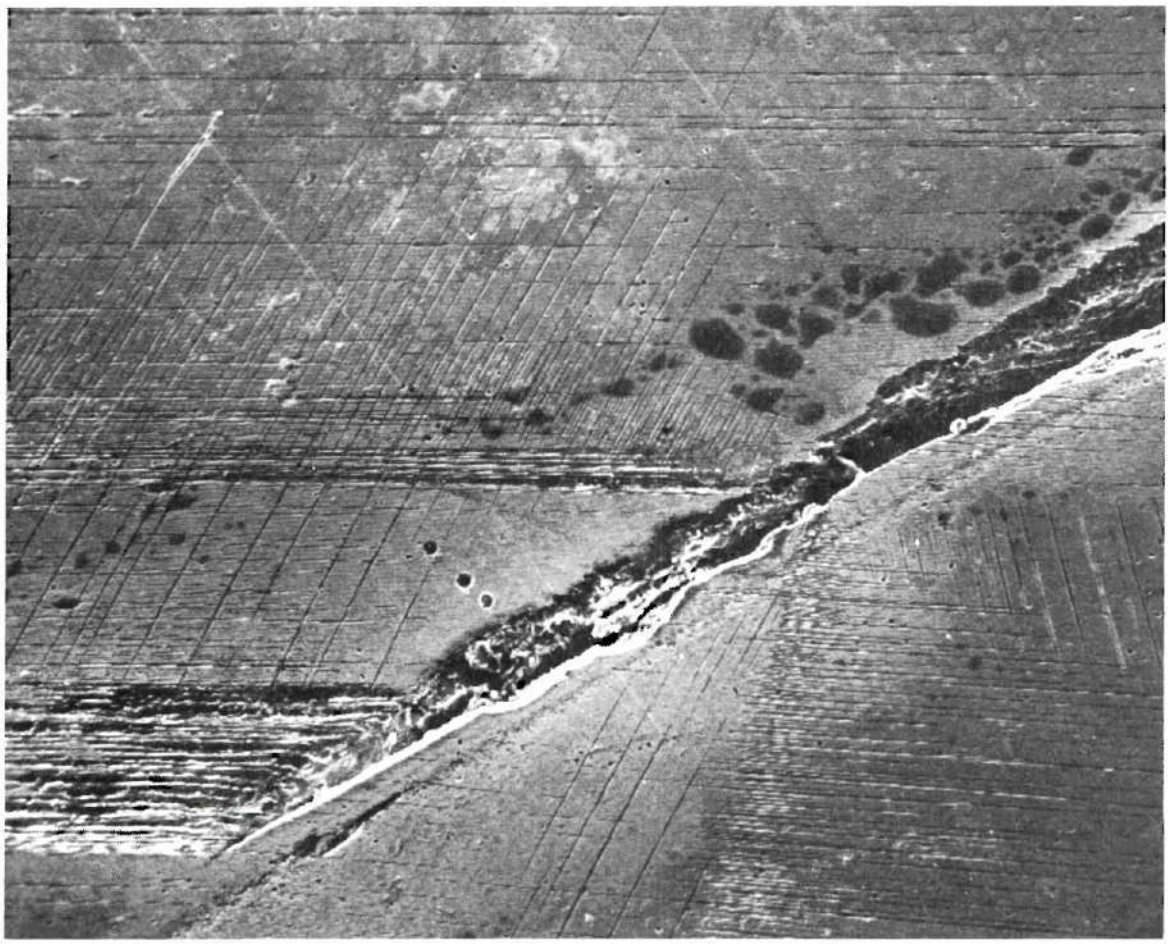

Figure 44. Corrosion Attack on Slip Lines along a Crack. Specimen X2 (unnotched), Narrow Side. Scanning Electron Micrograph (Magnification 190x).

As the crack tip was approaching the side, the cross sectional area decreased, yielding rapidly increased, and the slip steps were strongly corroded.

Kinetics of Crack Propagation

The results of the analyses of crack propagation, presented in Figures 38 and 39, show that after an initial period the cracks propagated at essentially constant rates. In the constant-rate regions the rates in different specimens varied from 0.105 to 0.135 mm/hour. The highest rate was in the specimen B3, in accord with the observed smooth and flat fracture surface of this specimen.

The results imply that the propagation rate was independent of the crack length for cracks ranging up to 3 mm long. The obvious interpretation is that the cracking rate was not limited in this range by the transport of environmental species from the surface of the specimen to the tip of the crack. In view of the small size of the specimens and of relatively simple morphology of cracking, the possibility of transport in the lateral direction makes this conclusion rather meaningless.

More fruitful is the relation between the propagation rate and the applied stress. Figure 9 shows that the nominal applied stress, as calculated from the load and geometry (not taking into account the stress concentration due to the notch effect of the crack), increased to up to 2.7 times the initial value during the crack propagation. The data (Table 7 in the Appendix) show that this nominal stress, at crack lengths corresponding to the constant rate segments, varied from 1860 kg/cm^2 to 4020 kg/cm^2. In this sense the crack propagation rates were independent of applied stress in this given range.

There are the following possibilities in the interpretation of this finding:

a. either the propagation rate was truly independent of the stress at the tip of the crack;

b. or the effective stress at the tip of the crack did not vary in the given range of loads and crack lengths;

c. or some other effects, such as the changing length of the transport path, cancelled the effect of stress.

Of the three alternatives, the third is purely speculative and will not be considered. The first alternative can be most easily understood if the propagation rate is controlled by some process independent of stress and strain, such as a cathodic reaction in a dissolution model. The second alternative implies that yielding relieves the stress to such an extent that the stress at the tip remains essentially at an approximately constant level of the effective yield stress.

The initial parts of the curves in Figures 38 and 39 are unreliable and no conclusion can be based on them. It is interesting to note, however, that the crack lengths corresponding to the minima in propagation rates are between 0.4 and 0.5 mm, which agrees closely with some reports of the apparent limiting depth of some cracks (64, 92, 93). Hines (92) divided the crack development into two stages, the first stage ending at a depth of 0.3 to 0.4 mm, and rationalized this effect in terms of the dissolution model. No other systematic evidence of a two-stage mode of crack development was obtained in the course of this work.

The Threshold Stress

The threshold stress was not systematically investigated in this

work, but some estimates can be made from the data presented in Table 8 of the Appendix:

a. Specimen B1 did not start to crack in 200 hours at the same load at which specimen A2 started to crack after 36 hours. The resolved shear stress in B1, as calculated from the nominal stress, was approximately 270 kg/cm^2. The critical resolved shear stress was approximately 510 kg/cm^2 at room temperature (see Table 3). The results reported by Meyrick and Paxton (94) show that in similar stainless steel crystals the critical resolved shear stress at 155°C was about 70 per cent of the room temperature value. The critical resolved shear stress in the material used in this work can thus be estimated as approximately 360 kg/cm^2. Considering the stress concentration due to the notch some limited, but not extensive yielding must have occurred at the root of the notch of B1. Attacked slip steps were not observed on the surface of B1 after the 200 hours test. The initial nominal stress normal to a possible cracking plane was approximately 600 kg/cm^2.

In specimen A2 both the resolved shear stress on slip planes and the stress normal to the most favorably oriented {210} cracking plane was higher than in specimen B1 by a factor of 1.5 under the same load. The initial nominal resolved shear stress was thus above the estimated critical resolved shear stress. Attacked slip traces were observed in this case. The initial nominal stress normal to the cracking plane was 905 kg/cm^2.

b. In the specimen E2 cracking was interrupted when the crack reached a length of approximately 0.75 mm and later re-initiated at a lower load. The nominal stress analysis (see Table 8 of the Appendix) shows that

propagation resumed at a load corresponding to a nominal resolved shear stress of approximately 500 kg/cm^2 and a normal stress of approximately 1130 kg/cm^2. At two lower loads (see Tables 4 and 8) cracking did not resume in 10 hours on each load.

c. In specimen B3 some subcracks branched from the main crack and made traces consistent with cracking on {210} planes subjected to nominal normal stresses considerably lower than the main crack. One of the subcracks developed at a point where the nominal stress normal to the {210} plane consistent with the trace was only 140 kg/cm^2.

The uncertainty about the true magnitude of stresses at the tips of cracks and notches prevents a reliable quantitative analysis. The results only indicate that cracks can propagate at relatively low normal stresses but that a significant amount of yielding must take place locally if cracking is to start, and that even already initiated cracks do not propagate if sufficient yielding does not take place. A potentially important observation was that the crack in specimen E2 when halted by lowering the load resumed propagation only after a considerable period of time (4 hours) at a load higher than the load at which the crack was inactive. A suggested explanation is that either high acidity or the formation of complexes resulting from dissolution enhanced by yielding are prerequisites for cracking.

Morphology of Cracking

The following outline of crack development in the single crystal specimens tested is proposed as an interpretation of the fractographic evidence:

Cracks are initiated locally at many sites along the root of the

notch. If the {210} plane which is subjected to the highest normal stress contains the direction of the notch a single crack can develop from the beginning and the fracture surface will be relatively smooth and flat. No notched specimen was available in such an orientation. However, cracks in unnotched specimens of suitable orientations can also form fracture surfaces of this type, because in that case there is nothing to force the crack to form along a certain line different from the trace of the cracking plane. The micrograph of the fracture surface of the specimen X4 (Figure 25) shows this result.

If the cracking plane does not contain the direction of the notch many cracks are initiated locally and propagate at first separately from the notch. This results in a stepped surface, the edges of the steps running more or less in the general direction of crack propagation. An example is shown in Figure 24a, which also shows the tendency of the cracks to join and form larger flat areas when they propagate farther from the notch. The ultimate example of this tendency is the case of the B-series specimens, in which the original individual cracks (Figure 28a) developed into two symmetrical cracks that produced the flat surfaces shown in Figures 19a and 28b.

If more than one cracking plane is subjected to a high enough tensile stress either branching may develop or the crack may alternate between the various possible planes. Sub-cracks are probably initiated when the main crack meets an obstacle. Examination of the crack traces showed evidence of increased local yielding at the points of branching. Alternation of the crack between several possible planes in an arbitrarily oriented crystal may explain the very diversified, though locally

symmetrical, fracture surface such as shown in Figure 26.

The substantial difference in morphology of cracking between specimens of the B and C series may be explained as follows. Specimens of both sets share the <111> stress axis and the only difference in orientation is a 90° rotation around this axis, so that the wide side of specimens of one set has the same orientation as the narrow side in the other set. In both orientations two sets of {210} planes are subjected to the same normal stress. The preference for the one observed cracking system in B specimens is probably due to the effect of the notch, the planes of the other system making traces at a larger angle with its direction. In tests on specimens of the C series the loads were higher and apparently forced cracking on both sets of planes alternately. Unfortunately two of the C series specimens could not be examined fractographically.

One of the main difficulties in the interpretation of the fractographs with regard to the mechanisms of cracking is the uncertainty about the direction of crack propagation. Although the general direction is obvious in most cases, the local direction of the advancement of the crack front is not known. For example, in Figure 24a the crack propagated in general from the notch in essentially a vertical direction, but it cannot be positively determined whether locally the crack advanced along the marks seen on the flatter areas or in a direction perpendicular to them.

The origin of these regularly oriented markings is therefore uncertain. Examination at high magnification (Figure 31) shows them to be edges of co-planar strips on the fracture surface. They seem to

indicate that not only the cracking plane but also either the direction of propagation or the direction of the crack front is crystallographically dependent. The complexity is further increased by an observation that the surfaces of the strips exhibit still another set of regularly oriented markings. These are thought to be traces of active slip planes.

Another serious difficulty in stress corrosion fractography is related to the controversial role of dissolution in the formation of the fracture surfaces. The most frequently observed features, such as shown in Figure 29, seem to indicate a cleavage-like fracture, the surface features being later partly obliterated by an electrochemical process. According to the dissolution models the surface features , such as in Figures 29 and 31, would have to result from the dissolution process, which seems improbable. It should be noted, however, that the surface shown in Figure 23a resembles a surface of a single crystal electrode following cathodic deposition (86, 88). The traces of the walls of the ridges on a cross section were found to be consistent with traces of {210} planes, although absolute identification was not possible.

Anodic Polarization Experiments

In the potentiostatic experiments the potential of the tested electrode is maintained at the selected value by flowing the necessary current through the electrode. In potentiodynamic experiments the principle is the same, but the potential is varied in a controlled way through the selected range.

The difference between the zero current potential and the potential of an electrode through which a current is flowing is the overpotential η, which is, in a simple case, a sum of the activation

overpotential η_a and the concentration overpotential η_c (95).

First considering the anodic dissolution from a polarized bare single crystal face and neglecting concentration polarization, the rate of removal of ions from the metal surface, expressed as current density, is given (96) by

$$i = i_o \left[\exp\left(\frac{\alpha z F \eta}{RT}\right) - \exp\left(-\frac{(1-\alpha) z F \eta}{RT}\right)\right]$$

where i is the current density,

i_o is the exchange current density,

α is the transfer coefficient,

η is the overpotential,

z is the charge on the ions,

F is the Faraday's constant.

Of the parameters on the right hand side of the expression only α and i_o may depend on the crystallographic orientation of the surface. The transfer coefficient α is the ratio of the potential difference between the lattice position and the peak of the energy barrier to the total distance between the lattice and solution wells. If the energy barrier is symmetrical then $\alpha = 0.5$ (97). Jenkins (88) found α to vary from 0.46 to 0.50 on various crystal faces of copper in a solution of cupric perchlorate.

For $\eta \gg RT/F$ the second exponential term can be neglected so that

$$\eta = -\frac{RT}{\alpha z F} \ln i_o + \frac{RT}{\alpha z F} \ln i$$

A change in α changes the slope of the anodic polarization curve in the linear (Tafel) region. This effect seems to be insignificant in the

system studied the slopes in Figures 40 to 42 being roughly the same for all the faces studied, approximately 54 millivolts per current density decade. Therefore the product αz is approximately $\alpha z = 1.1$, which is close to the expected value for a divalent metal and a symmetrical barrier.

The orientation dependent parameter is thus the exchange current density, which is given (97) by

$$i_o = A\ n\ \exp(-\frac{\Delta G_a^*}{RT})$$

where A is a constant,

n is the surface density of reactive sites,

ΔG_a^* is the standard free energy of activation of the reactive sites at the zero current potential.

Since ΔG_a^* is prohibitively high for removal of atoms from perfect close-packed atomic planes dissolution is thought to proceed mostly by removal of atoms from sites of high reactivity, such as kinks on surface steps, point defects, points of emergence of dislocations etc. (98). On higher index planes, however, some atoms may be bound loosely enough to make dissolution possible even on a perfect atomic plane. An atom at a kink site on a close-packed plane of a face-centered cubic structure has six nearest neighbors. Considering a simple ball model of perfect atomic planes, a {210} plane has one atom with only six nearest neighbors per each primitive unit cell of the surface, the {110} and {112} planes one atom with seven nearest neighbors, etc. (99). The density of these atoms can be calculated (99) and the binding energy can be estimated as one sixth of the enthalpy of vaporization per each nearest neighbor bond (91).

Using the expression above, the overvoltages, if related to the number of these sites, would be in the order

$$\eta_{\{210\}} \ll \eta_{\{211\}} < \eta_{\{110\}} \ll \eta_{\{100\}} \ll \eta_{\{111\}}$$

The results in Figures 40 to 42 show that the curves for the various faces are in the above order except for the {111} orientation, which exhibits much lower overvoltages than expected. The results are in qualitative agreement with those of Bertocci (87) and Jenkins (88) for copper electrodes. They reported highest overvoltages for the {100} face, lowest for the {321} face, and small differences between orientations other than {100}, the {111} face exhibiting overvoltages not much different from {110} or even {321}.

In view of the positions of the {111} lines Bertocci concluded that not the nucleation but motion of steps was rate controlling, the motion on {100} face being slow and difficult. However, an alternative explanation is possible, in view of the observation in this work that the overpotentials, except for the {111} face, are in the order consistent with the simple model. It is tentatively proposed that the overpotentials are indeed related to the number and binding energies of the atoms, as predicted by the model above, but that the nucleation or motion of steps on the {111} face is, for reasons thus far unknown, much easier than on the {100} plane.

Both Bertocci (87) and Jenkins (88) worked in the range of current densities several orders of magnitude lower than the limiting current density in this work. Even at those conditions Bertocci reported that extensive faceting took place on all faces. Jenkins and Stiegler (100),

working on {100} oriented samples of copper, reported that at current densities of only 15-20 $\mu amps/cm^2$ the removal rate was already higher than that made possible by nucleation of steps at areas surrounding defects and by pitting and concluded that nucleation of reaction sites occurred apparently at random on the crystal surface.

In this work extensive faceting was not found by optical microscopy examination of the specimens after the testing, except for some wrinkling on the {111} faces. The lack of faceting may be due to the high current densities which made random nucleation of reaction sites necessary, or to the presence of a film on the surface. Faceting is usually not observed when the electrode is covered by a film (98). On the other hand, the difference between the first and second set of experiments, the overpotential differences between faces being smaller in the second set when a slower potential scan was used, might have been due to changes in surface geometry caused by removal of a larger amount of material.

The concentration overpotential η_c occurs when the reaction rate or the applied external current is so large that the species that are being oxidized or reduced cannot reach the surface at a sufficiently rapid rate (96). It may be expressed as

$$\eta_c = \frac{RT}{zF} \ln \frac{i_L - i}{i_L}$$

where i_L is the limiting diffusion current density.

In the experiments described the limiting current density was approximately 1.0 to 1.5 x 10^{-1} $amps/cm^2$, which is somewhat lower than the values reported in the literature (see Figure 1). This is probably due

to the differences in experimental technique. The relatively low limiting current in this system may be attributed to the formation of a film on the surface which makes the transport of species difficult.

An explanation for the change of shape of some of the polarization curves in the third series of experiments (Figure 42) was not found. Curves of a shape similar to those on {100}, {112} and {111} oriented surfaces in Figure 42 were reported by Barnartt and Van Rooyen (40). They observed that the bending of curves toward higher currents was accompanied by rapid localized pitting. No difference in the pattern of pits was found in this work on specimens that did and did not exhibit the inflection on the polarization curve. Since the only difference in the experimental procedure between the second and third series was in scanning rate it is likely that the effect is related to the kinetics of surface film formation and that it is more pronounced on specific orientations.

Discussion of Stress Corrosion Models

The results presented in this work do not prove any one model correct and all others wrong. As a matter of fact the individual pieces of evidence could be used in support of several different models. For instance the presence of the corrosion products proves that dissolution takes place inside the crack; the observation that a surface film forms during anodic dissolution may fit the model of dissolution due to film rupture or the brittle film fracture model; the results of the examination of the surface attack support the idea of dissolution on dislocations and on slip steps; the topography of the fracture surface fits best the mechanical fracture models; some of the markings on the fracture

surfaces may be interpreted as indications of tunneling, etc.

It is thus the totality of experimental evidence that has to be considered. An acceptable general model would not have to account for every single detail observed, but it must not be in contradiction with any important, consistent feature.

The most important experimental results of this work are in the field of crystallography of cracking. At present, however, the identification of the cracking plane orientation as {210} is more a negative than a positive argument in a discussion of various models, since a convincing explanation has not been found. The suggestion presented in the course of the following discussion will require further experimental work and analysis.

Dissolution Models

There is hardly any doubt that dissolution takes place inside the cracks. Insoluble corrosion products were found on the fracture surfaces (see Figure 33) and in the interior of cracks (see Figure 43), in agreement with reports in the literature (15, 16). Gas bubbles emerging from the propagating cracks were also observed. The important question is whether the dissolution mechanism can account for the crack propagation rate, crystallography, fracture surface features and other evidence, as presented both here and in the literature.

A dissolution rate, expressed as current density, that would account for the given propagation rate can be calculated from the formula:

$$i = \frac{F.\rho}{A} v_c$$

where i is the current density (amps/cm^2),

F is the Faraday's constant,

ρ is the density of the material (grams/cm ^{3}),

A is the equivalent weight,

v_c is the crack propagation rate (cm/sec).

Taking ρ = 7.85 grams/cm^3, A = 28 and the propagation rate observed in this work $v_c = 3.7 \times 10^{-6}$ cm/sec, the current density is approximately 10^{-1} amps/cm^2, which is close to the limiting current density found in the anodic polarization experiments reported here. The cracking rate is thus at a first glance compatible with the dissolution mechanism.

However, the cracking rate measured in this work was relatively low and values up to two orders of magnitude higher were reported (see Chapter II). (In polycrystalline specimens the measured crack propagation rates may be affected by the proportion between the transgranular and intergranular failure. At present there are no published data on the propagation rate of intergranular stress corrosion cracks in this system.) On the other hand, the reports of anodic polarization experiments show limiting current densities less than one order of magnitude higher at most (see Figure 1). It must be emphasized that the observed rates cannot be higher and are likely to be significantly lower than the true speed of crack advancement, because of the usual tortuous path of the cracks, and that the dissolution would have to account for the highest speeds and not for any average value. The required dissolution rates are thus likely to be considerably higher than those observed in experiments in which concentration polarization was not effectively overcome.

Hoar and West (8) recognized this discrepancy and suggested that the concentration overpotential is reduced by the flow of the electrolyte

to the tip of the crack. This argument is not in accord with observations. Despite the recurring mention in the literature of "yawning" cracks, this is not a consistent feature of stress corrosion. The picture of a crack trace presented in Figure 22 shows no measurable differences of the crack width for a considerable length. Yawning can be expected in cases when the failing part or specimen is highly strained, but cracks propagate even under conditions of a diminishing stress, such as in constant-deformation experiments. Since the dissolution process is continuous no bursts of crack advancement that might produce a "pumping" action are involved. West's experiments on the flow of electrolyte in propagating crevices (42) were made under conditions unrealistically remote from those of stress corrosion.

The surface shown in Figure 22 was lightly polished and etched, so that some rounding of the edges occurred and the crack trace appears wider than the actual width of the crack, which is therefore less than 0.5μ. Inside this hairline crack corrosion products must have plugged the passage. The wedging action, explored by Nielsen (15) and Pickering et al (16), indicates that this plugging can be quite effective. Easy enough passage undoubtedly remains for the transport of the environmental species to the tip of the crack, but a conception of an uninterrupted flow of electrolyte is obviously unrealistic. On the other hand, the chemistry of the environment inside the stress-corrosion cracks may be substantially different from that of the bulk solution in anodic polarization experiments. If the observed polarization is mainly due to the formation of a film on the surface, then a highly acidic environment in the proximity of the tip of the crack may affect the film formation and increase the

limiting current density. Experimental verification of this possibility is needed. Similarly a correlation has not been established between high propagation rates and conditions that produce significant yawning of cracks.

Most dissolution models that have been proposed are based on some form of strain-enhanced dissolution. According to these models, regardless of the details of the mechanisms, the cracks are expected to follow, at least locally, the slip planes because of the attack on either slip steps or the co-planar arrays of dislocations. Accordingly they are in serious contradiction with the crystallographic evidence presented in this work. Although these models do not necessarily predict a macroscopically crystallographic cracking on the {111} planes, they are certainly not in accord with an evidence of a definite preferred plane of another orientation.

The {210} cracking plane does not bisect the angle between two {111} slip planes so that a case cannot be made for a combined effect of two slip systems. Such an explanation would be unrealistic even for a plane such as {110} which bisects the angle since it would assume equal contributions from both systems, otherwise the cracks would be oriented randomly. There is enough evidence (see Figures 16 and 44) that, even in symmetrically loaded single crystal specimens, the amount of yielding was not uniform along the path of the crack and equal on both slip systems, and still the directions of the crack traces were not significantly affected.

The results of the anodic polarization experiments showing the {210} oriented surface to be the most reactive one of those studied

cannot be taken as an argument in favor of crack propagation along that plane. There is no reason why the dissolution in a homogeneous lattice should penetrate along a plane which exhibits higher reactivity when exposed as a free surface. On the contrary, the high reactivity would be expected, in a dissolution model, to widen the crack by lateral dissolution and thus impede the cracking. There is no evidence of any inhomogeneity along the {210} planes that would make them reactive paths, and a model of dissolution on a predetermined path is generally improbable.

There is no evidence at present that a correlation exists between the observed cracking plane and a habit plane of any phase that might form at the crack tip and dissolve. The habit plane of martensite in austenite has been determined mostly as $\{225\}_{\text{austenite}}$ (101). Dissolution of martensite forming in the slip bands would, of course, lead to {111} oriented cracks.

In view of the arguments presented above a conclusion is being made that the present dissolution models are not in accord with the totality of experimental evidence available, unless new evidence and analysis are presented to explain the discrepancies.

Mechanical Models

The crystallographic evidence presented in this work is also in contradiction with the "classical" mechanical model of brittle fracture triggered by electrochemical action. In that model the crack advances in short, fast bursts of cleavage fracture. A cleavage plane in this material is not known because the material does not normally cleave, but a hypothetical cleavage would be expected to follow a plane of low surface energy, in analogy with cleavage in other lattices. The surface

energies of various faces are not exactly known, but it can be safely assumed, on the basis of simple models, that a {210} face in a face-centered cubic material has a relatively high surface energy, if not the highest, because of the high density of broken bonds (102).

The same argument can be tentatively applied to the model of brittle fracture of a hypothetical embrittled zone at the crack tip. It seems unlikely that a high energy plane would be converted into a low energy plane by absorption of some species in the lattice. Any positive evidence in this respect would naturally become an argument in favor of such a mechanism. The model predicts a discontinuous mode of cracking, which would have to be demonstrated conclusively. The absence of such evidence in this work may be due to very small dimensions of the crack-advancement steps.

Analogous to the dissolution model there is no evidence that would link the observed crystallography with the model of cracking along the habit plane of some phase forming at the crack tip. However, it is at least conceivable that such a phase might form in a lattice relationship that would account for the observed cracking plane if the cleavage fracture occurred in the phase itself. There is a chance that such a mechanism might account also for the observation that the direction of crack propagation seemed to be crystallographically dependent as well. At present this model must be considered speculative.

Assuming that either an embrittled zone or precipitates of a brittle phase were induced by absorption of hydrogen at the tip of the crack, the observation that the crack, when halted by lowering the load, required a substantial re-initiation time, would fit the model. The

effect of hydrogen can be expected only if the environment at the crack tip is highly acidic. The acidity might result from oxidation reactions near the tip (61). When the load is decreased the strain induced dissolution would cease and the concentration differences between the proximity of the tip and the bulk of the solution would be removed by diffusion. When a higher load is applied, a period of time is required before a sufficient acidity builds up.

There is little in the evidence presented here that would give serious support or seriously contradict the tunnel model. Some of the fractographic evidence (see Figures 32b and 33) shows features compatible with tunneling. However, these features were not present consistently and there was no evidence of plastic tearing between the ridges. Further, there seems to be little chance of correlation between the tunneling and the observed cracking plane. The model thus does not seem to account for the main mechanism of crack propagation, but it is likely that tunneling plays a role in the initiation of the cracks.

The previously discussed models being found either unacceptable or speculative, the stress sorption model remains to be considered. In spite of the present vagueness of the details of the mechanism - or possibly because of it - the model seems to be in best agreement with the evidence.

The correlation between the observed cracking plane and the cracking in the sorption model is not clear, but there are indications that it may exist. The {210} face, in a simple ball model, is distinguished as a plane with the highest density of broken nearest-neighbor bonds (102). Adsorption can be expected to be strongest on such a plane. If

breaking of atomic bonds at the apex of the crack takes place more or less randomly the walls of the crack nuclei oriented close to {210} may be stabilized by strong adsorption. A fracture proceeding by rupture of bonds in a ductile matrix and resulting in apparently brittle fracture surfaces is possible only if the bonds are considerably weakened by the presence of the environment.

The species adsorbing at the walls and at the apex of the crack do not have to be necessarily of the same type, but they as well may be. The rupture of the weakened bonds would occur only at the apex where the stress is concentrated. Only if an obstacle stops the penetration new cracks would be initiated at the walls behind the tip, forming branches and subcracks.

The specificity of chemisorption is one of the main arguments in favor of sorption cracking (20), but the species responsible for stress corrosion have not been identified. The observation of a re-initiation period required for continuation of cracking seems to indicate that some complexes rather than simple ions may be involved. Similarly to the discussion of the hydrogen model the interpretation may be that the re-initiation period is caused by a necessity of building up a sufficient concentration of complexes which requires a dissolution reaction. In view of the potential dependence of adsorption (62, 63) other compositional changes in the environment at the crack tip may be considered as an alternative explanation.

Based on the stress sorption model the following sequence of events in stress corrosion cracking in this system may be visualized:

1. During the induction period the surface film is disrupted by emerging

dislocations and a surface attack on the slip steps and dislocation pile-ups takes place. The severity of the attack is probably not due to the exposure of the bare metal surface, but to a high concentration of point defects in and at the slip bands (91).

The surface attack is further facilitated if the original protective film is quickly removed. Since the condensate of the vapor of the boiling magnesium chloride solution is highly acidic (103) cracking in specimens exposed to both the liquid and vapor phases will crack above the interface (79, 80, 91), where the film is destroyed. It is suggested that this effect is more significant than a possible build-up of chloride concentration.

2. At points of stress concentration the attack penetrates deeper, either by continuing dissolution along the slip steps or by tunneling and tearing of the walls. The stress concentration may be due to features on the original surface (notches, inhomogeneities etc.) or to the surface attack itself.

3. When either a critical concentration of complexes or another compositional parameter is reached as a result of the dissolution reaction the actual cracking starts by rupture of bonds weakened by adsorption of specific species or complexes. The rupture is induced by the tensile component of the stress and fracture is essentially brittle. However, since the crack advancement depends on the time parameters of the adsorption process and proceeds in atomic steps, the fracture is significantly different from normal cleavage and the Griffith criterion for extension of an unstable crack is hardly applicable.

The tip of an active crack will remain sharp, similarly to the

situation in plastic fracture, as analyzed by Cottrell (104). Following an incremental crack advancement dislocations will be injected into the slip planes from an area immediately behind the tip and will thus widen the slit. As long as the yielding is constant the width of the crack will remain constant. Variation in applied stress will thus affect the crack width, but the effective stress at the apex will remain essentially constant and the crack propagation rate will not be greatly affected. The yielding enhances the dissolution reaction behind the tip so that the environmental conditions for crack propagation are sustained.

The stress-sorption model greatly needs more direct experimental evidence and more detailed knowledge of the basic processes involved. An impartial assessment of all the proposed models, experimental evidence, and arguments shows, however, that the other models are no less speculative and often more in contradiction with evidence. An unbiased effort in a design of critical experiments is needed more than an off-hand rejection of alternatives.

CHAPTER VI

CONCLUSIONS

The results of the present investigation may be summarized in the following conclusions:

1. Cracks in single crystal specimens of type 316 austenitic stainless steel stressed in boiling, aqueous, 45 per cent magnesium chloride solution were crystallographic and propagated along planes oriented close to {210}.

2. The fracture surface features indicated that cracking proceeded in basically a brittle manner. No systematic evidence of a discontinuous mode of crack propagation was found.

3. The solid corrosion products forming inside the cracks and pits were identified as chromium compounds.

4. An induction period was observed before the onset of cracking; the length of this period decreased with increasing load.

5. After an initial period, the cracks in each specimen studied propagated at a constant rate, independent of crack length and nominal stress; the crack propagation rate in the constant-rate period was 0.104 to 0.135 mm/hour.

6. The anodic polarization curves for various crystal faces exhibited overpotentials in the order $\eta_{\{210\}} < \eta_{\{110\}}$, $\eta_{\{211\}} < \eta_{\{100\}}$. The overpotentials on the {111} face were close to those on the {110} and {211} faces.

7. No differences in open-circuit potentials of various crystal

faces were detected.

8. The polarization curves converged to a limiting current density of approximately 0.15 amps/cm^2.

APPENDIX

Table 3. Tension Tests Data and Results.

Specimen Number			1	2	3
Width	1)	cm	0.353	0.363	0.348
Thickness	1)	cm	0.254	0.251	0.259
Cross Section Area	1)	cm^2	0.0897	0.0911	0.0901
Load at Yielding	2)	kg	96.0	94.0	88.5
Yield Stress	2)	kg/cm^2	1070	1032	982
φ			50.5°	48.5°	43.5°
λ			39.5°	41°	47°
$\cos \varphi \cos \lambda$			0.49	0.50	0.495
Critical Resolved Shear Stress		kg/cm^2	524	516	486

1) Central portion of the specimen (see Figure 4a).
2) Easy glide region.
φ ...angle between stress axis and the normal to the active slip plane.
λ ...angle between stress axis and the slip direction.

Table 4. *Stress Corrosion Test Data: Dimensions of Specimens, and Applied Loads.*

Specimen	h (mm)	n (mm)	b (mm)	Q_o (kg)	Q_f (kg)
A1	4.90	0.32	2.28	22.9	ND
A2	4.90	0.34	2.28	18.2	ND
A3	4.92	0.34	2.25	26.9	21.0
B1	5.05	0.51	2.33	18.5	18.5
B2	5.08	0.50	2.32	27.7	23.5
B3	5.10	0.54	2.34	28.0	15.4
B4	5.10	0.54	2.34	28.8	16.4
C1	5.10	0.30	2.28	43.0	34.0
C3	5.00	0.40	2.30	26.8	22.3
E1	4.91	0.26	2.30	28.2	16.3
E2	4.92	0.42	2.31	36.4	ND
E3	5.00	0.40	2.30	28.8	25.9

Specimen E2: Test interrupted at Q = 33 kg by lowering the load to Q = 11.5 kg. Cracking had not resumed in 10 hours at Q = 13.5 kg. Cracking was resumed in 4 hours at Q = 15.9 kg.

Explanation of Symbols:
h depth of the specimen (see Figure 5a);
n depth of the notch (see Figure 5a);
b width of the specimen (see Figure 5a);
Q_o load at the beginning of the test;
Q_f load at the end of the test.
ND not determined.

Table 5. Stress Corrosion Test Data: Crack Parameters

Specimen	Mode of Cracking	α	l_c (mm)
X1	many parallel cracks, no branching	ND	ND
X2	one crack branching into two symmetrical cracks	81°	ND
X3	several parallel cracks	77°	ND
X4	two cracks	86°	ND
A1	one main crack, three subcracks	81°	3.3
A2	one main crack, several subcracks	82°	3.3
A3	one crack	80°	1.5
B1	no cracks	--	--
B2	one crack	57°	1.2
B3	two main parallel cracks, several subcracks	56° (15°)*	3.0
B4	one main crack, several subcracks	60°	3.0
C1	one crack	57°	1.95
C2	two symmetrical cracks	52°	1.75
C3	one crack	54°	1.4
E1	several symmetrical cracks	75°	2.4
E2	two main cracks, several subcracks	72°	2.75
E3	two main cracks, several subcracks	78°	0.8

*subcracks

Explanation of Symbols:

α.. average angle between the trace of the main crack on the specimen side and the edge of the specimen;

l_c..average length of the main crack;

ND..not determined.

Table 6. Stress Corrosion Test Data: Directions of Crack Traces on Two Mutually Perpendicular Surfaces

Specimen	[u v w]	$(h_1k_1l_1)$	α	$(h_2k_2l_2)$	β	Note
B2	[1 1 $\bar{1}$]	(1 $\bar{1}$ 0)	57°	(1 1 2)	69°	sections
B3	[1 1 $\bar{1}$]	(1 $\bar{1}$ 0)	53°	(1 1 2)	61.5°	sections
B4	[1 1 $\bar{1}$]	(1 $\bar{1}$ 0)	59°	(1 1 2)	67°	sections
A2	[1 $\bar{1}$ 0]	(1 1 $\bar{1}$)	81°	(1 1 2)	73°	sections
X4	[0 2 3]	($\bar{1}\bar{3}$ $\bar{3}$ 2)	86°	(1 $\bar{3}$ 2)	89°	original surfaces

Explanation of Symbols:
[u v w]...direction of the specimen edge;
$(h_1k_1l_1)$, $(h_2k_2l_2)$..orientations of the two surfaces;
α ..... angle between the crack trace on $(h_1k_1l_1)$ and the specimen edge;
β ..... angle between the crack trace on $(h_2k_2l_2)$ and the specimen edge.

Table 7. Stress Corrosion Test Data: Kinetic Parameters of Cracking

Specimen	t_i min	t_p min	l_c mm	$\bar{v}_c$ mm/hr	t_{pb} min	l_{cb} mm	σ_b kg/cm^2	t_{pe} min	l_{ce} mm	σ_e kg/cm^2	v_c mm/hr
A1	1100	1920	3.3	0.103	--	--	--	--	--	--	--
A2	2150	1800	3.3	0.110	--	--	--	--	--	--	--
A3	80	1030	1.5	0.087	600	0.65	1866	1030	1.5	2542	0.132
B2	2200	520	1.2	0.138	--	--	--	--	--	--	--
B3	5500	1500	3.0	0.120	600	0.95	1975	1500	3.0	4020	0.135
B4	4800	1510	3.0	0.119	--	--	--	--	--	--	--
C1	3100	1220	1.95	0.096	--	--	--	--	--	--	--
C2	50	970	1.75	0.108	200	0.43	2407	970	1.75	3337	0.104
C3	3700	910	1.4	0.092	--	--	--	--	--	--	--
E1	240	1225	2.4	0.118	400	0.70	1863	1000	1.85	2769	0.115
E2	50	1790	2.75	0.092	--	--	--	--	--	--	--
E3	180	360	0.8	0.137	--	--	--	--	--	--	--

Explanation of symbols:

t_i ... length of the induction period;

t_p ... total length of the crack propagation period;

l_c ... average final length of the main crack;

$\bar{v}_c$ ... average crack propagation rate;

t_{pb} ... time in the propagation period when the constant-rate propagation began;

l_{cb} ... length of the crack at the beginning of the constant-rate stage;

σ_b ... nominal stress at the beginning of the constant-rate stage;

t_{pe} ... time in the propagation period when constant-rate propagation ended (or end of the test);

l_{ce} ... length of the crack at the end of the constant-rate stage;

σ_e ... nominal stress at the end of the constant-rate stage;

v_c ... crack propagation rate in the constant-rate stage.

Table 8. Stress Corrosion Test Data: Nominal Stresses

Specimen	σ_o kg/cm^2	σ_f kg/cm^2	σ_{rss} kg/cm^2	σ_c kg/cm^2
A1	1,252	ND	511	1,126
A2	1,005	ND	410	905
A3	1,491	2,545	609	1,341
B1	1,005	1,005	273	603
B2	1,491	2,079	406	894
B3	1,505	4,023	410	903
B4	1,547	4,795	421	928
C1	1,476	2,452	402	886
C2	2,144	3,333	583	1,287
C3	1,441	2,081	392	865
E1	1,483	3,440	605	1,329
E2	2,039	ND	832	1,835
E3	1,547	2,040	631	1,392

Explanation of Symbols:

σ_o ... nominal highest tensile stress at the root of the notch at the beginning of the test;

σ_f ... nominal highest tensile stress at the tip of the crack at the end of the test;

σ_{rss} .. nominal resolved shear stress on the most favorably oriented slip system at the beginning of the test;

σ_c ... nominal stress normal to the {210} plane, identified as the cracking plane, at the beginning of the test.

Table 8. Stress Corrosion Test Data: Nominal Stress (Continued)

Interrupted Test, Specimen E2: Condition	σ kg/cm^2	σ_{rss} kg/cm^2	σ_c kg/cm^2	Note
Before unloading	2,587	1,056	2,328	propagating crack
Load lowered	907	370	816	no cracking in 10 hours
Load increased	1,065	435	959	no cracking in 10 hours
Load increased	1,254	512	1,129	cracking resumed in 4 hours

Explanation of Symbols:

σ ... nominal highest tensile stress at the tip of the crack;

σ_{rss} .. nominal resolved shear stress on the most favorably oriented slip system, at the tip of the crack;

σ_c ... nominal stress normal to the {210} plane, identified as the cracking plane, at the tip of the crack.

Table 9. Crystallographic Parameters of the {210} Planes in the Specimens for Stress Corrosion Testing (For the Orientation of the Specimens see Table 2)

Specimen Series	Plane Indices	α	β	φ	$\sigma_{\{210\}}/\sigma_{max}$
	$(2\bar{1}0)$, $(\bar{1}20)$	79°06'	74°46'	18°26'	0.900
	$(20\bar{1})$, $(02\bar{1})$	90°	39°14'	50°46'	0.400
	(201), (021)	40°54'	67°48'	50°46'	0.400
A	(120), (210)	30°	22°12'	71°34'	0.100
	$(\bar{1}02)$, $(0\bar{1}2)$	30°	22°12'	71°34'	0.100
	(012), (102)	19°06'	50°46'	71°34'	0.100
	(120), (210)	54°44'	67°48'	39°14'	0.600
	$(\bar{1}02)$, $(0\bar{1}2)$	54°44'	67°48'	39°14'	0.600
	$(20\bar{1})$, $(02\bar{1})$	90°	50°46'	39°14'	0.600
B	(012), (102)	15°48'	39°14'	75°02'	0.067
	(201), (021)	19°28'	22°12'	75°02'	0.067
	$(2\bar{1}0)$, $(\bar{1}20)$	54°44'	15°14'	75°02'	0.067
	$(20\bar{1})$, $(02\bar{1})$	50°46'	90°	39°14'	0.600
	(120), (210)	67°48'	54°44'	39°14'	0.600
	$(\bar{1}02)$, $(0\bar{1}2)$	67°48'	54°44'	39°14'	0.600
C	(012), (102)	39°14'	15°48'	75°02'	0.067
	(201), (021)	22°12'	19°28'	75°02'	0.067
	$(2\bar{1}0)$, $(\bar{1}20)$	15°14'	54°44'	75°02'	0.067
	$(2\bar{1}0)$, $(\bar{1}20)$	74°46'	79°06'	18°26'	0.900
	$(20\bar{1})$, $(02\bar{1})$	39°14'	90°	50°46'	0.400
	(201), (021)	67°48'	40°54'	50°46'	0.400
E	(120), (210)	22°12'	30°	71°34'	0.100
	$(\bar{1}02)$, $(0\bar{1}2)$	22°12'	30°	71°34'	0.100
	(012), (102)	50°46'	19°06'	71°34'	0.100

Table 9. Crystallographic Parameters of the {210} Planes in the Specimens for Stress Corrosion Testing (For the Orientation of the Specimens see Table 2) (Continued).

Explanation of Symbols:

α ... angle between the plane trace on the wide side of the specimen and the edge;

β ... angle between the plane trace on the narrow side of the specimen and the edge;

φ ... angle between the plane normal and the direction of the stress axis;

$\sigma_{\{210\}}/\sigma_{max}$ ... ratio of the stress normal to the plane and the maximum tensile stress.

Table 10. Anodic Polarization Test Data

Experiment Number	Specimen Orientation	E_o volts (SCE)	i_L amps/cm^2	E_L volts (SCE)
1	{100}	-0.310	ND	-0.100
	{110}	-0.310	0.11	
	{111}	-0.312	0.15	
	{211}	-0.315	0.15	
2	{100}	-0.361	0.12	-0.100
	{110}	-0.360	0.13	
	{111}	-0.363	0.11	
	{211}	-0.360	0.14	
	{210}	-0.363	0.15	
3	{100}	-0.362	0.13	-0.160
	{110}	-0.361	0.12	
	{111}	-0.360	0.11	
	{211}	-0.363	0.12	
	{210}	-0.363	0.13	

Explanation of Symbols:

E_o ... open-circuit potential;

i_L ... limiting current density or current density at the end of the test;

E_L ... potential at the end of the test.

BIBLIOGRAPHY

1. Metals Handbook. Eighth Edition, Vol. I, ASM (1964).

2. H. L. Logan. The Stress Corrosion of Metals, Wiley, New York (1966).

3. Proceedings of International Conference on Fundamental Aspects of Stress Corrosion Cracking, Ohio State University, September 1967, NACE (1969).

4. E. H. Dix. Trans. AIME, 137, 11 (1940).

5. R. R. Mears, R. H. Brown, and E. H. Dix. Symposium on Stress Corrosion Cracking of Metals, ASTM-AIME (1945), p. 323.

6. H. L. Logan. J. Res. Nat. Bur. Standards, 48, 99 (1952).

7. T. P. Hoar and J. G. Hines. J. Iron Steel Inst., 182, 124 (1956).

8. T. P. Hoar and J. M. West. Proc. Roy. Soc., A, 268, 304 (1962).

9. D. Tromans and J. Nutting. Corrosion, 21, 143 (1965).

10. C. Edeleanu. J. Iron Steel Inst., 173, 140 (1953).

11. D. A. Vaughan, D. I. Phalen, C. L. Peterson, and W. K. Boyd. Corrosion, 19, 315t (1963).

12. F. H. Keating. Symposium on Internal Stresses in Metals and Alloys, Institute of Metals, London (1948), p. 311.

13. A. J. Forty. Physical Metallurgy of Stress Corrosion Fracture, Interscience, New York (1959), p. 99.

14. C. Edeleanu. ibid., p. 79.

15. N. A. Nielsen, ibid., p. 121.

16. H. W. Pickering, F. H. Beck, and M. G. Fontana. Corrosion, 18, 230t (1962).

17. A. J. Forty and P. Humble. Phil. Mag., 8, 247 (1963).

18. A. J. McEvily and A. P. Bond. J. Electrochem. Soc., 112, 131 (1965).

19. H. H. Uhlig. Physical Metallurgy of Stress Corrosion Fracture, Interscience, New York (1959), p. 1.

20. H. H. Uhlig. International Conference on Fundamental Aspects of Stress Corrosion Cracking, Ref. 3, ante., p. 86.

21. E. G. Coleman, D. Weinstein, and W. Rostoker. Acta Met., 9, 491 (1961).

22. H. W. Pickering and P. R. Swann. Corrosion, 19, 373t (1963).

23. U. R. Evans. Stress Corrosion Cracking and Embrittlement, ed. W. D. Robertson, John Wiley and Sons, New York (1956), p. 158.

24. C. Edeleanu. ibid, p. 135.

25. D. T. Powell and J. C. Scully. Corrosion, 24, 151 (1968).

26. M. A. Scheil. Symposium on Stress Corrosion Cracking of Metals, ASTM-AIME (1945), p. 395.

27. M. Marek and R. F. Hochman. Corrosion, 26, 5 (1970).

28. J. F. Eckel. Corrosion, 18, 270t (1962).

29. J. G. Hines, Corr. Science, 1, 2 (1961).

30. H. L. Logan. Welding J., 37, 463S (1958).

31. D. van Rooyen. Corrosion, 16, 421t (1960).

32. J. G. Hines and T. P. Hoar. J. Appl. Chem., 8, 764 (1958).

33. H. H. Uhlig and E. W. Cook, Jr. J. Electrochem. Soc., 116, 173 (1969).

34. H. H. Lee and H. H. Unlig. J. Electrochem. Soc., 117, 18 (1970).

35. H. Kohl. Corrosion, 23, 39 (1967).

36. H. R. Copson. Physical Metallurgy of Stress Corrosion Fracture, Interscience, New York (1959), p. 247.

37. R. M. Latanision and R. W. Staehle. International Conference on Fundamental Aspects of Stress Corrosion Cracking, Ref. 3, ante., p. 214.

38. T. P. Hoar. Corrosion, 19, 331t (1963).

39. T. P. Hoar and J. G. Hines. Proc. 8th Meeting Int. Comm. Electrochem. Therm. Kin. (CITCE), Madrid 1956, Butterworths, London (1958), p. 273.

40. S. Barnartt and D. van Rooyen. J. Electrochem. Soc., 108, 222 (1961).

41. T. P. Hoar and J. C. Scully. J. Electrochem. Soc., 111, 348 (1964).

42. J. M. West. Nature, 185, 92 (1960).

43. T. P. Hoar. International Conference on Fundamental Aspects of Stress Corrosion Cracking, Ref. 3, ante., p. 98.

44. T. P. Hoar and J. M. West. Nature, 181, 835 (1958).

45. A. R. Despic, R. G. Raicheff, and J. O'M. Bockris. J. Chem. Phys., 49, 926 (1968).

46. E. N. Pugh, J. A. S. Green, and A. J. Sedriks. RIAS Technical Report 69-3, March 1969.

47. J. Bade and R. A. Dodd. International Conference on Fundamental Aspects of Stress Corrosion Cracking, Ref. 3, ante., p. 342.

48. J. J. Heger and E. J. Dulis. Discussion of Reference 10, J. Iron Steel Inst., 175, 390 (1953).

49. H. Nathorst. Discussion of Reference 10, J. Iron Steel Inst., 175, 390 (1953).

50. M. L. Holzworth and M. R. Louthan, Jr. Corrosion, 24, 110, (1968).

51. N. A. Nielsen. Corrosion, 20, 104t (1964).

52. A. Ronnquist. Corrosion et Anticorrosion, 14, 3 (1966).

53. J. S. Armijo and B. E. Wilde. Corrosion, 23, 107 (1967).

54. M. F. Dean, F. H. Beck, and R. W. Staehle. Corrosion, 23, 192 (1967).

55. I. S. McCollough and J. C. Scully. Corrosion Sci., 9, 707 (1969).

56. J. D. Harston and J. C. Scully. Corrosion, 25, 493 (1969).

57. N. A. Nielsen. International Conference on Fundamental Aspects of Stress Corrosion Cracking, Ref. 3, ante., p. 308.

58. A. J. Forty. Recent Advances in Stress Corrosion, ed. A. Bresle, Stockholm (1961), p. 22.

59. M. B. Whiteman and A. R. Troiano. Corrosion, 21, 53 (1965).

60. J. H. Shively, R. F. Hehemann, and A. R. Troiano. Corrosion, 23, 215 (1967).

61. P. R. Rhodes. Corrosion, 25, 462 (1969).

62. I. Rosenfeld and W. Maximtschuk. Z. physik. Chem., 215, 25 (1960).

63. D. N. Staicopolus. J. Electrochem. Soc., 108, 900 (1961).

64. H. L. Logan and R. J. Sherman, Jr. Welding J. (N.Y.), 35, 389s (1956).

65. H. L. Logan. J. Res. Nat. Bur. Standards, 56, 159 (1956).

66. K. W. Leu and J. N. Helle. Corrosion, 14, 249t (1958).

67. J. G. Hines and R. W. Hugill. Physical Metallurgy of Stress Corrosion Fracture, Interscience, New York (1959), p. 193.

68. J. C. Scully and T. P. Hoar. Corrosion, 20, 174t (1964).

69. M. R. Louthan, Jr. Corrosion, 21, 288 (1965).

70. H. L. Logan. Metals Engineering Quarterly, 5, 32 (1965).

71. B. Lehtinen. J. Sci. Instrum., 44, 234 (1967).

72. T. J. Smith and R. W. Staehle. Corrosion, 23, 117 (1967).

73. G. Wassermann. Z. Metallk., 34, 297 (1942).

74. V. V. Skorchelletti and V. A. Titova. J. Appl. Chem. (U.S.S.R.), 26, 41 (1953).

75. R. Bakish and W. D. Robertson. Acta. Met., 4, 342 (1956).

76. R. Bakish. J. Metals, AIME, 9, 494 (1957).

77. R. E. Reed and H. W. Paxton. First International Congress on Metallic Corrosion, 301 (1961).

78. R. W. Staehle, F. H. Beck, and M. G. Fontana. Corrosion, 15, 373t (1959).

79. H. P. Hawkes, F. H. Beck, and M. G. Fontana. Corrosion, 19, 247t (1963).

80. G. H. G. Kraft, J. Z. Amacker, R. K. Saxer, and J. R. Myers. Corrosion, 21, 188 (1965).

81. P. J. Greeley, V. J. Russo, R. K. Saxer, and J. R. Myers. Corrosion, 21, 327 (1965).

82. J. G. Hines and T. P. Hoar. J. Iron Steel Inst., 18, 166 (1956).

83. T. Shimose, A. Takamura, K. Hori and K. Shigomori. Trans. Japan Inst. Metals, 6, 83 (1965).

84. M. Smialowski and M. Rychcik. Corrosion, 23, 218 (1967).

85. R. D. Leggett and H. W. Paxton. Corrosion Sci., 2, 217 (1962).

86. R. Piontelli, G. Poli, and G. Serravalle. Trans. Symp. on Electrode Processes, ed. E. Yeager, John Wiley and Sons, New York (1961), p. 67.

87. U. Bertocci. J. Electrochem. Soc., 113, 604 (1966).

88. L. H. Jenkins. J. Electrochem. Soc., 117, 630 (1970).

89. C. J. Mauvais, R. M. Latanision, and A. W. Ruff, Jr. J. Electrochem. Soc., 117, 902 (1970).

90. I. B. Casale. Corrosion, 23, 314 (1967).

91. D. A. Vermilyea. J. Electrochem. Soc., 115, 162 (1968).

92. J. G. Hines. Corrosion Sci., 1, 21 (1961).

93. H. H. Uhlig and M. Lincoln. J. Electrochem. Soc., 104, 167 (1957).

94. G. Meyrick and H. W. Paxton. Trans. AIME, 230, 1010 (1964).

95. C. W. Davies. Electrochemistry, George Newnes, London (1967).

96. K. J. Vetter. Electrochemical Kinetics. Academic Press, New York (1967).

97. T. P. Hoar. "The Anodic Behavior of Metals," in Modern Aspects of Electrochemistry, Vol. 2, Academic Press, New York (1959), p. 262.

98. D. A. Vermilyea. "Anodic Films," in Electrochemistry and Electrochemical Engineering, Vol. 3, Interscience, New York (1963), p. 211.

99. J. F. Nicholas. An Atlas of Models of Crystal Surfaces, Gordon and Breach, New York (1965).

100. L. H. Jenkins and J. O. Stiegler. J. Electrochemical Soc., 109, 467 (1962).

101. C. M. Wayman. Introduction to Crystallography of Martensitic Transformation, MacMillan, New York (1964).

102. J. K. Mackenzie, A. J. W. Moore, and J. F. Nicholas. J. Phys. Chem. Solids, 23, 185 (1962).

103. M. Marek. Unpublished results.

104. A. H. Cottrell. "Mechanism of Fracture," in Fracture, Proc. of the First Tewksbury Symp., Melbourne 1963, ed. C. J. Osborn, Butterworth (1965), p. 1.

VITA

Miroslav Marek was born in Prague, Czechoslovakia on January 3, 1934. He graduated from the Gymnasium in Prague XVIII in June, 1952. He entered the Czech Technical University in Prague and in May, 1957, he received the Engineering Diploma (Ing., equivalent to M.S. degree) in the School of Mechanical Engineering, majoring in Technology.

After the graduation Mr. Marek joined the faculty of the School of Applied and and Nuclear Physics of the Czech Technical University in Prague in the rank of an Assistant. In 1960 he was promoted to the rank of an Assistant Professor. His teaching and research activity was in the field of physical and nuclear metallurgy. He authored two texts for the students of the School of Applied and Nuclear Physics. In his professional capacity he visited several universities and research institutes in the Soviet Union in 1962 and 1965, and British universities in 1966.

In 1966 Mr. Marek entered the Georgia Institute of Technology for further graduate study in the School of Chemical Engineering, Metallurgy Program. In the first two years of study his research work was in the field of strain-aging of austenitic stainless steels. He co-authored a paper "Strain-aging of 316 Stainless Steel" published in Scripta Metallurgica, vol. 3, 693-698 (1969). In 1968 he was granted the Texaco Corporation fellowship.

Mr. Marek is married to the former Anna Ledecka of Stara Boleslav, Czechoslovakia. He is a member of the American Society for Metals, the

American Institute of Mining, Metallurgical, and Petroleum Engineers, and the Society of Sigma Xi.